Thesis

Simulation of exchange spring recording media thin films

is submitted to the University of Sheffield

for the degree of Doctor of Philosophy

at

Department of Material Science and Engineering

University of Sheffield

by

Lalita Saharan

March 2013

Declaration

This study presented in this PhD thesis has been carried out in a close collaboration with University of Manchester, Manchester, UK, a group led by Prof. Thomas Thomson. The experimental work has been carried out by Dr. Christopher Morrison (Post. Doc.) at the University of Manchester.

The 3D micromagnetic solver code used for this work is written by the group of researchers, who worked under the supervision of Prof. Thomas Schrefl, while at various institutions, including the University of Sheffield.

Lalita Saharan

March 2013

MANCHESTER 1824

The University of Manchester

Prof. T. Thomson
School of Computer Science
The University of Manchester
Oxford Road
Manchester M13 9PL

Tel:+44(0)161 275 4551
thomas.thomson@manchester.ac.uk

Lalita Saharan,
Department of Engineering Materials
Sir Robert Hadfield Building
Mappin Street,
Sheffield, S1 3JD

25 October 2012

Dear Lalita,
I understand that the University of Sheffield rules require you to seek permission from the other co-authors to include published work on which you were a co-author as part of your Ph.D. thesis. I am, of course, delighted to grant such permission in respect of the papers:

"Angle dependence of the switching field of recording media at finite temperatures" L. Saharan, C. Morrison, J.J. Miles, T. Thomson, T. Schrefl and G. Hrkac J. Appl. Phys. 110 (2011) 103906.

"Inter/intra granular exchange and thermal activation in nanoscale granular magnetic materials" C. Morrison, L. Saharan, G. Hrkac, T. Schrefl, Y. Ikeda, K. Takano, J.J. Miles and T. Thomson Appl. Phys. Lett. 99 (2011) 132507.

In these publications, you where responsible for the work to model the experimental results obtained in my group in Manchester as part of our EPSRC funded collaborative research project. Your contribution was key in both publications. It is, of course, not my place to comment of the curiosities of your institution and the apparent lack of willingness to support collaborative PhD projects and encourage students to publish and present their work to the widest possible international audience.

Please do not hesitate to contact me if I can be of any further assistance and I wish you the very best of luck with your thesis submission and viva.

Yours,

Tom Thomson (Prof.)

Prof. Gino Hrkac
Associate Professor in Functional Materials
College of Engineering, Mathematics and Physical Sciences
Harrison Building,
North Park Road
University of Exeter
Exeter, EX4 4QF, UK

THE UNIVERSITY OF WARWICK

Dear Gino,

Regarding your recent communication detailing the requirements for the use of joint papers in Lalita Saharan's thesis, I am happy for the paper entitled "Inter/intra granular exchange and thermal activation in nanoscale granular magnetic materials", co-authored by Lalita, to be used in her thesis.

Regarding Lalita's contribution to this paper, she performed all the micromagnetic simulations presented in the paper, specifically the simulated curves in figure 2, and figure 4.

I am also happy to allow Lalita to use the content of the paper entitled "Angle dependence of the switching field of recording media at finite temperatures" in her thesis. Lalita performed all of the simulations for this paper, the experimental results presented were provided by Prof. Thomson and myself for comparison to simulations.

Yours Sincerely,

Dr Chris Morrison

Department of Physics
The University of Warwick
Coventry CV4 7AL
United Kingdom
Tel: 024 76523965
Email:physicsadmin@warwick.ac.uk
www.warwick.ac.uk/go/physics

IOP Institute of Physics Juno Champion

MIDLANDS PHYSICS ALLIANCE GraduateSchool

SILVER Athena SWAN Charter for Women in Science

Birmingham Science City ideasforlife

Papers

Grain boundaries in granular materials - a fundamental limit for thermal stability

L. Saharan, C. Morrisson, Y. Ikeda, K. Takano, J. J. Miles and T. Thomson, T. Schrefl, and G. Hrkac, accepted in APL.

The importance of interface layers in thin film magnetic multi-layer systems

L. Saharan, C. Morrison, J. J. Miles, T. Thomson, T. Schrefl and G. Hrkac, to be submitted.

Quantifying Exchange Coupling in Segregated Granular Materials

C. Morrison, L. Saharan, Y. Ikeda, K. Takano, G. Hrkac, T. Thomson, submitted

Angle dependence of switching field of recording media at finite temperatures

L. Saharan, C. Morrisson, J. J. Miles, T. Thomson, T. Schrefl, and G. Hrkac, JAP **110,** 103906 (2011).

Inter/Intra granular exchange and thermal activation in nanoscale granular magnetic materials

C.Morrison, L.Saharan, G. Hrkac, T. Schrefl, Y. Ikeda, K. Takano, J. J. Miles and T. Thomson, APL **99,** 132507 (2011).

Magnetic Vortex Core Oscillations in Multi Point Contact Spin Valve Stacks

G.Hrkac, D. Hahn, L. Saharan, T. Schrefl, Joo-Voo Kim, T. Devolder and C. Chappert, IEEE Trans. Magn. **48,** 11(2012).

Conference Presentations

Oral Presentation – Influence of the grain boundary on the switching field of magnetic grains at finite temperatures

12th Joint MMM/Intermag conference, *Chicago, Illinois, USA,* Jan 2013.

Poster Presentation – Switching dynamics of Two-phase media at finite temperature

Intermag conference 2012, *Vancouver, Canad*a, May 2012.

Oral Presentation – Path method vs stochastic thermal field switching in granular media a magnetic grain story lost between LLG and energy space

MATHMOD 2012, *Vienn*a, Feb. 2012.

Oral Presentation – Angle dependence of the switching field of recording media at finite temperature: an extended study

56th Conference of Magnetism and Magnetism Materials, *Scottsdale AZ, USA*, Nov. 2011.

Oral Presentation – Angle dependence of the switching field of recording media at finite temperature

UK & RI Chapter of the IEEE Magnetics Society EGM and Student/RA Workshop, Nov 2010.

Oral Presentation - Angle dependence of the switching field of recording media at finite temperature

55th Conference of Magnetism and Magnetism Materials, A*tlanta GA, USA,* Nov 2010.

Poster Presentation – Finite temperature switching of single phase media

Current Research in Magnetism 2010, organized by IOP magnetism group, *University of Manchester, UK,* Jul 2010.

Poster Presentation – Microwave **assisted spin-torque switching** 11th Joint MMM/Intermag conference, *Washington DC, USA,* Jan 2010.

Oral Presentations – Project meetings, *University of Manchester*.

Oral Presentations – SCAMMD meetings, *University of Sheffield*.

Acknowledgments

I would like to take this opportunity to give my thanks to Prof. Thomas Schrefl to give me the opportunity to do PhD on the interesting project. I would also like to thank my supervisors Dr. Gino Hrkac and Dr. Dan A. Allwood for their support and guidance during the course of my research.

I would also like to thank the Manchester group: Dr. Christoper Morisson, Prof. Thomas Thomson, Prof. Jim Miles and Dr. Josephat Kalezhi for their useful guidance and discussions during this project.

Table of contents

Abbreviations

2DR	two-dimensional readback
BDF	backward differentiation formula
BEM	boundary element method
BPMR	bit patterned magnetic recording
EAMR	energy assisted magnetic recording
EBL	exchange break layer
ECC	exchange coupled composite
FGL	field generation layer
CGR	compound growth rate
FEM	finite element method
FMR	ferromagnetic resonance
GMR	giant magnetoresistance
HAMR	heat assisted magnetic recording
HDD	hard disk drive
LLG	Landau-Lifshitz-Gilbert
LMR	longitudinal magnetic recording
MAMR	microwave assisted magnetic recording
MRAM	magnetic random access memory

MEP	minimum energy path
NEB	nudged elastic band
ODE	ordinary differential equation
PMR	perpendicular magnetic recording
RAMAC	random access memory for accounting and control
RKKY	Ruderman, Kittel, Kasuya and Yosida interaction
SANS-pol	small-angle polarised neutron scattering
SNR	signal-to-noise ratio
SPGMR	scaled preconditioned generalized minimum residual
S-W	Stoner-Wohlfarth
SWR	shingled writing recording
TDMR	two-dimensional magnetic recording
TEM	transmission electron microscopy
UoM	University of Manchester
VSM	vibrating sample magnetometer
WRSN	weighted root square norm

List of symbols

α	angle between the applied field and anisotropy axis
α_G	Gilbert damping parameter
$\alpha_{n,i}$	BDF coefficient
τ	reduced time
$\boldsymbol{\tau}$	measurement time
ε	strain tensor
σ	elastic stress tensor
σ_m	surface magnetic charge density
σ_{noise}	standard deviation of the noise
σ_{signal}	standard deviation of the signal
μ_o	magnetic permeability in vacuum
δ_w	domain wall width
φ_m	magnetic scalar potential
φ	angle between magnetization $\boldsymbol{M}$ and unit vector $\boldsymbol{u}$
$\varphi(r)$	angle between magnetization $\boldsymbol{M}$ and unit vector $\boldsymbol{u}$ as function of r
φ_s	angle between long axis and magnetization direction of sample
ρ_m	volume magnetic charge density

ϕ_d	demagnetization energy density
ϕ_{ex}	exchange energy density
ϕ_G	total magnetic Gibbs free energy density
$\phi_{K,\ cubic}$	cubic anisotropy energy density
$\phi_{K,\ uniaxial}$	uniaxial anisotropy energy density
ϕ_{tot}	total energy density
ϕ_U	internal energy density
ϕ_z	Zeeman energy density
θ	angle between magnetization direction and anisotropy axis
Ω_{int}	internal region
Ω_{ext}	external region
∇E	energy gradient
γ_0	gyromagnetic ratio
atol	absolute error tolerance
A	exchange constant
A_{EBL}	exchange break layer exchange constant
A_h	hard ferromagnet exchange constant

$A(r)$	exchange constant as function of position r
A_s	soft ferromagnet exchange constant
$\boldsymbol{B}$	magnetic flux density
$(\boldsymbol{BH})_{max}$	maximum energy product
$\boldsymbol{B_r}$	remanence
$\boldsymbol{B_r/J_s}$	remanence ratio
$\boldsymbol{B_{in}}$	magnetic flux density inside the magnetic material
$\boldsymbol{B_{out}}$	magnetic flux density outside the magnetic material
D	optimal path
E	energy
E^*	energy barrier as a function of switching field
$E_{anisotropy}$	anisotropy energy
E_b	energy barrier
$E_{exchange}$	exchange energy
$E_{external}$	*Z*eeman energy
E_n	mean norm of the local truncation error at the n-th time step
E_{stray}	magnetostatic field energy
E_{total}	total magnetic Gibbs free energy
f_0	attempt frequency

$f(r)$	scalar function
$f(t, y)$	general function dependent on t and y
$\boldsymbol{G}$	general function
h_n	step-size of the BDF scheme
$\boldsymbol{h_{eff}}$	normalized effective field
$\boldsymbol{H}$	applied field
$\boldsymbol{H_C}$	coercive field
$\boldsymbol{H_d}$	demagnetization field
$\boldsymbol{H_{d,in}}$	demagnetization field inside of the magnetic material
$\boldsymbol{H}_{d,out}$	demagnetization field outside of the magnetic material
$\boldsymbol{H_{eff}}$	effective field
$\boldsymbol{H_{external}}$	external field
$\boldsymbol{H_n}$	nucleation field
$\boldsymbol{H_p}$	pinning field
$\boldsymbol{H_s}$	dipolar field
$\boldsymbol{H_{sw}}$	switching field
$\boldsymbol{H_{write}}$	write field
$\boldsymbol{J}$	Jacobian

$\boldsymbol{J_S}$	magnetic polarization
$\boldsymbol{J_{s,\ EBL}}$	EBL magnetic polarization
$\boldsymbol{J_{s,\ EBL,\ boundary}}$	EBL boundary magnetic polarization
$\boldsymbol{J_{s,\ EBL,\ shell}}$	EBL shell magnetic polarization
$\boldsymbol{J_{s,\ h}}$	hard phase magnetic polarization
$\boldsymbol{J_{s,h,\ boundary}}$	hard phase boundary magnetic polarization
$\boldsymbol{J_{s,h,shell}}$	hard phase shell magnetic polarization
$\boldsymbol{J_{s,soft}}$	soft phase magnetic polarization
$\boldsymbol{J_{s,\ soft,\ boundary}}$	soft phase boundary polarization
$\boldsymbol{J_{s,\ soft,\ shell}}$	soft phase shell magnetic polarization
k_B	Boltzmann constant
K	anisotropy constant
K_0	empirically derived magnetocrystalline anisotropy constant
K_1	empirically derived magnetocrystalline anisotropy constant
K_2	empirically derived magnetocrystalline anisotropy constant
K_3	empirically derived magnetocrystalline anisotropy constant
K_{eff}	effective anisotropy constant
K_{EBL}	EBL magnetocrystalline anisotropy constant
$K_{EBL,\ boundary}$	EBL boundary magnetocrystalline anisotropy constant

$K_{EBL,\ shell}$	EBL shell magnetocrystalline anisotropy constant
K_h	hard ferromagnet anisotropy constant
$K_{h,\ boundary}$	hard phase boundary magnetocrystalline anisotropy constant
$K_{h,\ shell}$	hard phase shell magnetocrystalline anisotropy constant
K_s	soft ferromagnet anisotropy constant
$K_{s,\ boundary}$	soft phase boundary magnetocrystalline anisotropy constant
$K_{s,\ shell}$	soft phase shell magnetocrystalline anisotropy constant
K_u	uniaxial magnetocrystalline anisotropy constant
l_{ex}	exchange length
$\boldsymbol{m}$	magnetic moment
$\boldsymbol{m_{norm}}$	normalized magnetization
m_x	unit magnetization vector component along x-axis
m_y	unit magnetization vector component along y-axis
m_z	unit magnetization vector component along z-axis
$\boldsymbol{M}$	magnetization vector
M_j	*j*th image of the path
$\boldsymbol{M(r)}$	Magnetization as a function of position *r*
M_S	magnetization saturation
n	unit vector pointing outside from the surface

N	number of grains in a bit
N_a	demagnetization factors of the long axis
N_b	demagnetization factors of the short axis
r	position vector
rtol	scalar relative error tolerance
S	entropy per unit volume
t	time
$\boldsymbol{t}$	tangent along the path
t_0	initial time
t_s	thickness of the soft material
T	temperature
u	unit vector
$\boldsymbol{u\,(r)}$	unit vector as function of position r
U	total magnetic scalar potential
U_1	magnetic potential inside and at boundary of the magnetic region
U_2	potential of the whole magnetic system
var_{signal}	variance of signal
var_{noise}	variance of noise
V	volume of the grain

$V_n(t)$	noise signal from the media
$V_s(t)$	signal from the media
y	general vector
y_0	initial position of vector y

Abstract

The aim of this thesis is to investigate and understand the switching behaviour of magnetic grains in high density magnetic recording media, 1Tbit per square inch and above, and by doing so to overcome the discrepancies between simulation and experimental results associated with the quantitative switching field and its applied field angle. This work will bridge the gap between the experiments and simulation results, by considering a realistic micromagnetic model of CoCrPt media thin films to study their magnetization reversal dynamicsat finite temperatures as a function of magnetic structure, interlayer coupling and thermal activation.

The utility of a simplified one-grain model was investigated in describing the switching field of such media at finite temperatures. Together with experiments it is shown that thermal activation modifies the Stoner-Wohlfarth angle dependency of the switching field by reducing the depth of the minimum that occurs at 45 degrees. Whereas inter/intra granular exchange coupling introduces a clear shift in the angle of applied field at which the minimum switching field occurs.

For the first time ever grain interface layers and grain boundaries interactions are explicitly considered in a descriptive micromagnetic model, the overall magnetization switching behaviour of such grains shows a deviation from Stoner-Wohlfarth like behaviour, highlighting their importance on the quantitative and qualitative value of the switching field. The study shows that these layers are essential to understand and predict the magnetization behaviour of such magnetic grains. This work suggests and hypothesis that the presence of such a grain boundary in magnetic grains of recording media might pose a fundamental limit on the diameter that could be achieved in future.

Chapter 1: Introduction

1.1 Aim

The aim of this PhD was to investigate and explain the magnetization dynamics of real recording media thin films by developing a micromagnetic model that can capture switching dynamic and thermal effects. Previous studies treated the magnetic grains as bulk materials in terms of their material properties [1-9]. This study is to bridge the gap between the experimental and theoretical studies by considering more realistic grain structures, which are based on experimental findings [10], where a deviation in the magnetic structure of the grains, from the centre to the boundary of the grain, has been observed.

1.2 Thesis outline

This thesis presents a micromagnetic study of the magnetization dynamics and optimization of CoCrPt–based single and exchange spring perpendicular magnetic recording media in close collaboration with experiments by Prof Thomson's group at the University of Manchester (UoM). One of the aims of the study was to answer the question why there is a qualitative and quantitative discrepancy in the switching field between theoretical/simulation systems and experiments, once the grain size of the magnetic grains approaches the superparamagnetic limit and its implications on magnetic recording media. This complex problem was broken down into small sections to isolate the parameters, which determines the absolute switching field and

results the deviation from the Stoner-Wohlfarth behaviour for single and multi-layer systems. At first a single CoCrPt grain was used and investigated as function of temperature and grain boundary. Then a comparison study, first of a simplified one grain model and more complex multi-layer system with experimental measurements (UoM) done at different temperatures, attempt frequency and lateral dimensions was conducted. These individual effects and studies are discussed in each chapter separately, compared with experimental measurements (UoM). Slowly building step-by-step, chapter-by-chapter, a more complex system is obtained that is summarized in the last chapter to give a complete picture, as outlined below.

Chapter 2 contains brief review of magnetic recording technologies with historical perspectives. This chapter also discusses the challenges faced by the recording industry and proposed alternative technologies to postpone these challenges to increase the areal density in magnetic recording media. Chapter 3 of the thesis provides a brief overview of the computational tools and theory used to calculate magnetization dynamics and temperature effects. This chapter also explains the basic principle of micromagnetics and the important contributing energies: total magnetic Gibbs free energy; exchange energy; magnetostatic energy; and magneto-crystalline anisotropy energy. The Stoner-Wohlfarth model, which gives analytical description of the magnetization behaviour of a single domain particle, is also introduced. The importance of the characteristic length scale in the study of magnetization dynamics in magnetic materials is also explained. The dynamic magnetization regime is modelled using the Landau-Lifshitz-Gilbert equation, which is discussed briefly along with the nudged elastic band method used for the energy barrier calculations. A short introduction to the hybrid finite element and boundary element method (FEM/BEM) is given and it is explained in a simple manner how this

method is used to solve problems in micromagnetics. Basically the method is used to calculate the magnetostatic energy. At the end of the chapter the basic introduction to numerical integration and error control is given.

As the main focus of this PhD was the study of switching field as a function of angle of the applied field at finite temperatures, at first chapter 4 explains how switching field is calculated at an angle of the applied field at a particular temperature value with the help of the Landau-Lifshitz-Gilbert equation and nudged elastic band method. The chapter also presents the importance of the study of thermal effects in magnetization dynamics, which leads to a clear shift in minimum away from the Stoner-Wolfarth model. Latter, the chapter presents the investigation done to understand how structural changes can affect the switching field of the grain boundary study for a single-phase media grain, based on a well-segregated CoCrPt-oxide media, the impact of the grain boundary interaction on the quantitative and qualitative switching field was investigated. The motivation behind this study is a recent study by Lister et. al. [10] on CoCrPt-SiO_2 data storage layers using small-angle polarised neutron scattering (SANS-pol) and tunnelling electron microscopy (TEM) technique. The SANS-pol measurements study the magnetic structure of the storage layer and showed a variation in the magnetic structure of the magnetic grains. In this work he proposed a magnetic core/shell model and pointed out its importance in the micromagnetic study of the recording media.

The findings of chapter 4 were developed further and the model was tested against the behaviour of the real recording media study (UoM). First half of Chapter 5, demonstrate how a simplified one-grain model, representing the single-phase perpendicular recording media, was used to describe the switching field as a function of angle of the applied field at finite temperatures of 150 K, 292 K and 350 K. The

results were compared with vector vibrating sample magnetometer (VSM) measurements on well-segregated, single layer CoCrPt-SiO_x recording media. This demonstrates that thermal activation modifies the Stoner-Wohlfarth angle dependency of the switching field by reducing the depth of the minimum that occurs at 45 degrees. The results and findings of this sub-chapter were published in the Journal of Applied Physics [11]. In second half of Chapter 5, the effect of inter/intra granular exchange coupling and thermal activation on the switching behaviour of nano-scale granular magnetic grains was investigated. It is shown that for larger grains the switching field as a function of angle of the applied field curve shows a shift in the minimum angle. This arises solely due to incoherent reversal induced by inter/intra-granular exchange coupling or incoherency within larger grains, rather than thermal activation. The results and findings of this sub-chapter were published in Applied Physics Letters [12]. Next chapters, shows how more complex exchange spring media systems could be described with our simplified micromagnetic model.

Chapter 6 presents the in-depth study done on exchange spring recording media to understand the importance of the intergranular interface present between the soft/hard phases. The purpose of the study was to model an optimized exchange spring media in line with experiments (UoM). Hence the effect of the material properties of the exchange break layer and soft phase was studied intensively. In addition to this a micromagnetic and associated experimental (UoM) study was conducted on exchange spring recording media to explore the effect of grain boundaries on the switching behaviour and field strength. The study was divided into three cases based on the magnetic structure of the grain. The mapping of the parameter space of the magnetic properties of the magnetic structure was performed to show the importance of the core/shell model for micromagnetic studies. Today

with the continuous focus on scaling of magnetic grains to a diameter less than 6 nm with the purpose to increase the areal density of the hard disk drives, the presence of a core/shell in the grains might pose a fundamental limit on the diameter that can be achieved in future.

The last chapter 7 gives a short summary and outlook of our work, puts it into context with today's technology and possible limitations that might pose a fundamental limit for the present technology discussed here.

Reference

1. M. Benakli, A. F. Torabi, M. L. Mallary, H. Zhou, and H. Neal Bertram, IEEE Trans. Magn. **34**, 4 (2001).
2. N. Honda, K. Ouchi, and S. Iwasaki, IEEE Trans. Magn. **38**, 4 (2002).
3. Kai-Zhong Gao and H. Neal Bertram, IEEE Trans. Magn. **38**, 6 (2002).
4. R. Wood, M. Williams, A. Kavcic, and J. Miles, IEEE Trans. Magn. **45**, 2 (2009).
5. T. Tanaka, A. Kato, Y. Furomoto, A. F. Md Nor, Y. Kanai, and K. Matsuyama, J. Appl. Phys. **111**, 07B711 (2012).
6. Y. Nozaki, A. Kato, K. Noda, Y. Kanai, T. Tanaka, and K. Matsuyama, J. Appl. Phys. **109**, 123912 (2011)
7. D. Suess, J. Magn. Magn. Mater. **308**, 2 (2007).
8. R. H. Victora, and X. Shen, IEEE Trans. Magn. **41**, 2 (2005).
9. J. Zhang, Y. Liu, F. Wang, J. Zhang, R. Zhang, Z. Wang, and X. Xu, J. Appl. Phys. **111**, 073910 (2012).

10. S. J. Lister, M. P. Wismayer, V. Venkataramana, M. A. D. Vries, S. J. Ray, S. L. Lee, T. Thomson, J. Kohlberecher, H. Do, Y. Ikeda, K. Takano, and C. Dewhurst, J. Appl. Phys. **106**, 063908 (2009).
11. L. Saharan, C. Morrison, J. Miles, T. Thomson, T. Schrefl, G. Hrkac, J. Appl. Phys. 110, 103906 (2011).
12. C. Morrison, L. Saharan, G. Hrkac, T. Schrefl, Y. Ikeda, K. Takano, J.J. Miles, and T. Thomson, App. Phys. Lett. **99,** 132507 (2011).

Chapter 2: Magnetic data storage technology

2.1 Abstract

This chapter provides an overview of past, present and future data storage technologies. To begin with, the history of magnetic recording has been revisited briefly. The technological challenges faced by the current perpendicular magnetic recording in terms of signal-to-noise ratio, writing and reading ability at higher areal density regimes is described briefly. Future magnetic recording media that can overcome these challenges such as exchange spring media, bit-patterned media, two-dimensional magnetic recording and writing techniques such as heat assisted magnetic recording and microwave assisted magnetic recording techniques are discussed in detail.

2.2 Introduction

In 1956 IBM introduced the world's first magnetic hard disk drive (HDD) RAMAC (random access memory for accounting and control) with a capacity of 2 kb/in^2 [1]. In the following years there has been a dramatic increase of the areal density in HDDs as shown in figure 2.1. With the help of the present technology HDDs of 325 Tb capacity can be produced in dimensions equivalent to RAMAC [2]. To continue with the trend of increasing the high areal density, the recording industry has transitioned from longitudinal magnetic recording (LMR) to perpendicular magnetic recording (PMR) technology in 2003. It has been realised that the PMR technology is going to meet its fundamental limits in the areal density regime of 1Tb/in^2. Any alternative

magnetic recording technology that addresses the physical limits of PMR is going to be very welcome. This thesis aims to model an exchange spring recording media to enhance the areal density of the HDD beyond 1Tb/in^2.

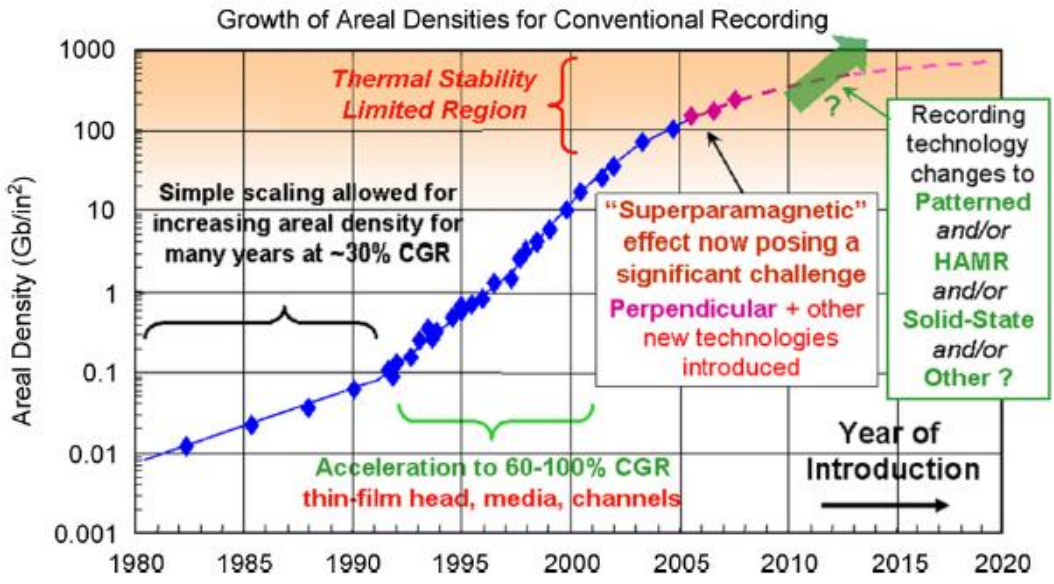

Figure 2.1: The areal density (the number of bits stored per unit area) of the HDD versus the year of introduction of the HDD from year 1980 to 2020. The maximum areal density limit of conventional magnetic recording is expected to be 1 Tb/in^2 [3].

2.3 Conventional Magnetic Recording

The three main components of the magnetic HDD are: a writer; data storage layer and a reader [2]. In this work mainly the data storage layer in addressed. The data storage layer is used to store the information. The information is stored in the form of bits i.e. 0 and 1 which are represented by two opposite magnetization states of the magnetic grains present in the data storage layer.

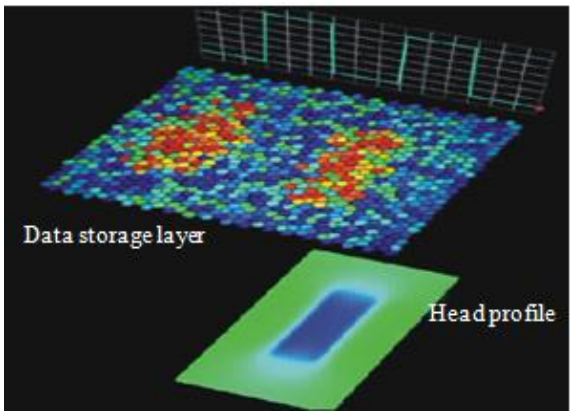

Figure 2.2: The micromagnetic recording process of the HDD. The magnetization of the magnetic bits is changed with respect to the head field profile. The magnetic bits are composed of groups of small magnetic grains. The different colour of grains indicates the different magnetization state: red grains magnetization is pointing opposite to the blue with respect to the plan of recording layer and the rest of the colours shows the intermediate magnetization state [4].

During the recording of the data the head flies over the data storage layer. The magnetization of magnetic bits in the storage layer is altered with the field coming from the head. Later the information stored is read out by detecting the magnetization in the data storage layer with the help of the reader element. The reader sensor is composed a magnetic multilayer system, consisting of a magnetic hard-layer, a spacer layer and a magnetic soft layer and uses the giant magnetoresistance (GMR) effect, which was discovered by Albert Fert and Peter Grünberg who won the Nobel Prize in Physics 2007 [5-7], to detect the change in magnetization in the magnetic media. During the read back process the reader flies over the data storage media and the rate of change of the flux in the storage medium

acts as an induced voltage during read back. Meaning, that the magnetization in soft layer of the reader changes its magnetization in respect to the magnetic hard layer according to the strayfield of the media. The change in magnetization results in a change in resistivity and therefore in a voltage change. A schematic of a micromagnetic recording process of the HDD is shown in figure 2.2.

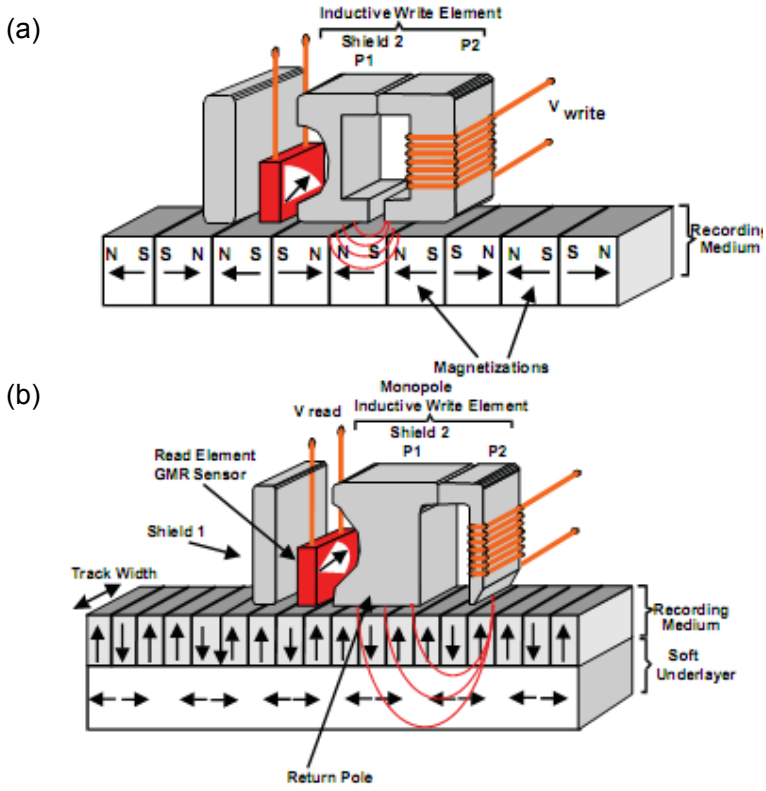

Figure 2.3: Schematic of the (a) longitudinal and (b) perpendicular magnetic recording media [8].

Magnetic bits in the data storage layer consist of a group of small magnetic grains. Based on the orientation of the easy axis of the magnetic grains in the data storage

layer (recording medium), magnetic recording technologies can be divided into two categories i.e. LMR and PMR shown in figure 2.3 along with recording head consist of the reader and writer element. The PMR has an additional soft underlayer below the data storage layer. It acts as a mirror and enhances the available write field making it possible to use the high anisotropy grains resulting into the higher areal density as compared to LMR. The grains of LMR and PMR recording media are shown in figure 2.4. In LMR, the easy axis of the magnetic grains is oriented in the plane of the magnetic thin film (data storage layer), whereas in PMR, the easy axis of magnetic grains is oriented perpendicular to the plane of the thin film [2].

The orientation of the easy axis is an important factor to determine areal density that can be achieved in the media. The disadvantage of the orientation of easy axis of the LMR is that, with the increase in the areal density the grain size decreases, resulting into the decrease of the distance between the magnetic poles of the grain, which in turn leads to increased demagnetizing field. The increased demagnetizing field results into a destabilising effect. Whereas PMR does not faces such destabilising effect as the distance between the magnetic poles remains the same while scaling the bit as explained in figure 2.4.

Currently, HDDs are based on the PMR technology. To increase the areal density of HDDs, there has been a continuous emphasis on the scaling of components of the HDD. However, for a further scale down of the magnetic grains in HDDs, certain issues discussed in the next section needs to be addressed.

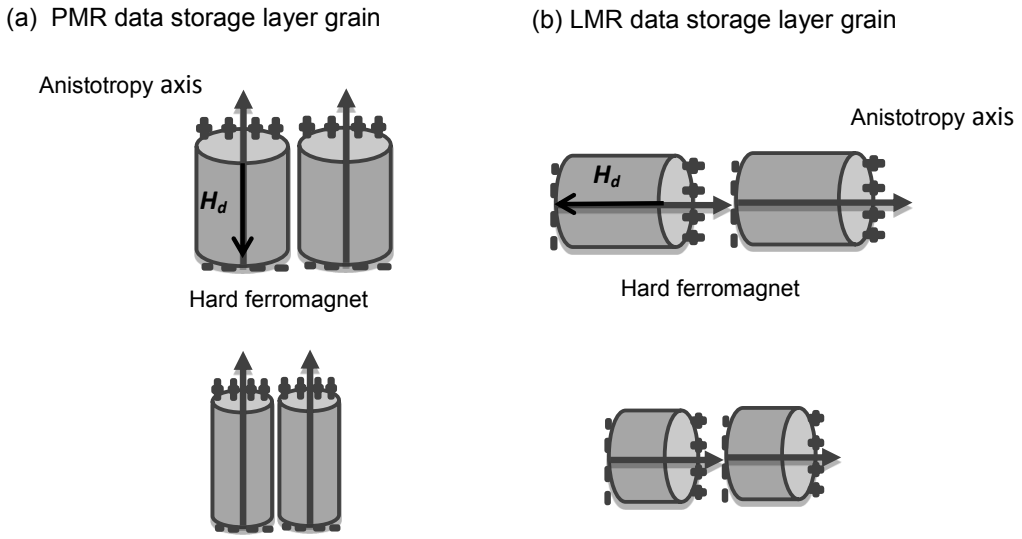

Figure 2.4: Illustrates anisotropy axis orientation of grains and associated demagnetization field H_d effect on the grain at high areal density in PMR and LMR technology. (a) PMR: The easy-axis of the grain is oriented perpendicular to the data storage layer, the distance between the magnetic poles remains the same when the grain size is reduced and hence no increase in H_d. (b) LMR: The easy-axis of the grain is oriented in-the plane of the data storage layer, the distance between the magnetic poles decrease the same when the grain size is reduced leading to increase in H_d *and* destabilised grains.

2.4 Trilemma of magnetic recording

The combination of problems faced during the scaling of magnetic grains in HDDs, while addressing the signal-to-noise ratio, thermal stability and the write-ability issues are known as the magnetic recording trilemma shown in Figure 2.5.

(i) **Signal-to-noise ratio:** The signal to noise ratio is a measure that compares the level of the desired signal to the background noise signal. It is important in evaluating

the performance of magnetic recording media systems. The signal to noise is often measured in the frequency domain, by integrating the power spectra for both the signal from the media and the noise. The signal from the media $V_s(t)$ is periodic (magnetization configuration in patterns of up and down), it has a line spectrum while the noise has a continuous spectrum $V_n(t)$. If the signal is not periodic one has to be careful to choose a measurement interval to be able to resolve the signal. Another technique is the time domain method, where the signal and the noise are measured together and compared with different period sequences. For example: one measures a read-back signal with 60 bits, which is given by connecting three signals that consist of 20 bits. Then one takes another 60 bits signal originating from a different magnetic configuration. Then the difference of the conjugate signals that originate from the different arrangement of the media, is defined as the media noise. Related to this is the auto-correlation SNR and is obtained in the time domain as follows [9-11].

$$SNR = 10\log_{10}\frac{\mathrm{var}_{signal}(V_s(t))}{\mathrm{var}_{noise}(V_n(t))} = 20\log_{10}\frac{\sigma_{signal}(V_s(t))}{\sigma_{noise}(V_n(t))} \tag{2.1}$$

where $\mathrm{var}_{\mathrm{signal}}$, $\mathrm{var}_{\mathrm{noise}}$ and σ_{signal}, σ_{noise} states the variance and standard deviation of the signal and the noise respectively [11]. There are many contributing factors like the distance between the read head and media, temperature, easy axis distribution (randomness) and also the bit size itself, but the dominating factor is the number of grains in a bit N. In principle one can correlate the SNR to the number of grains N approximately by the equation given below [2].

$$SNR = 10\log(N) \tag{2.2}$$

Meaning the larger the number of grains that contribute to a periodic signal the easier it is to distinguish it from the background noise and therefore the higher the *SNR*, and more reliable is the output. To maintain a high *SNR* ratio, the number of grains present inside a bit is required to be large while scaling the bit. Apart from that, decreasing the randomness of the grains can also increase the *SNR*. In the data storage layer, the anisotropy axes of grains are oriented randomly, instead of being in the perpendicular direction. Only grains, which have their c-axis, oriented perpendicular to the storage layer, contribute to the data signal.

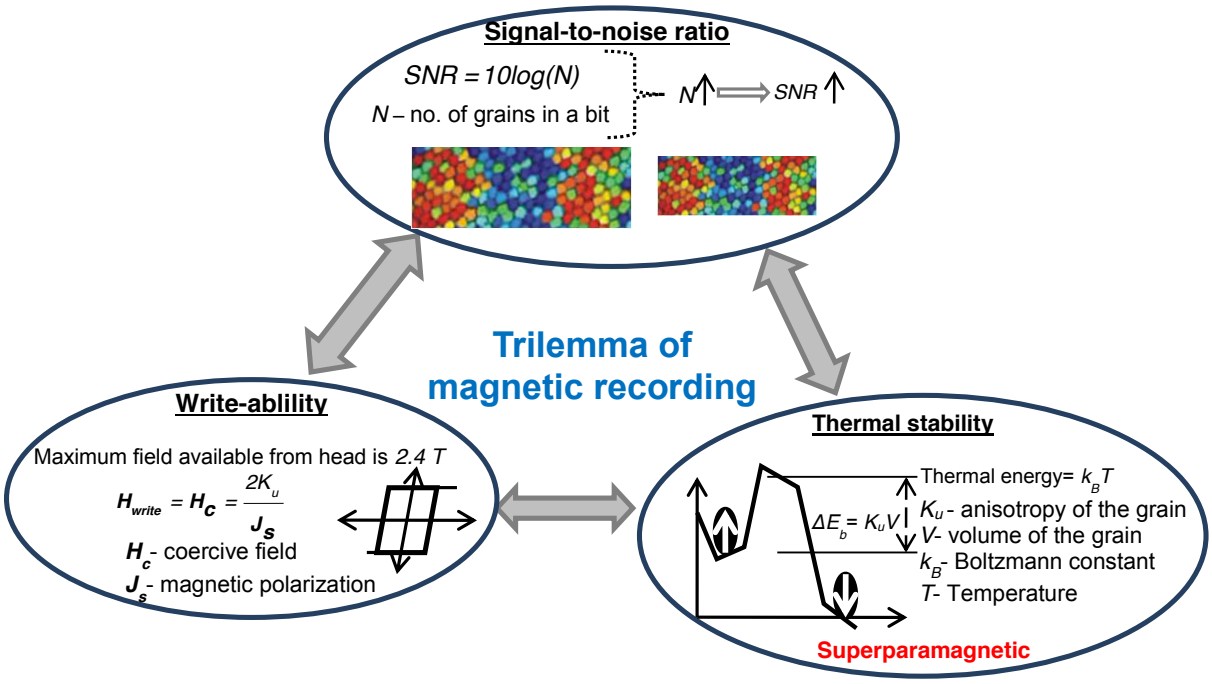

Figure 2.5: Schematic of the trilemma of magnetic recording, it shows the complex interconnection of SNR, thermal stability and write-ability of the grains.

If the orientation of all grains could be controlled to point in the desired direction (i.e. perpendicular to the storage layer in PMR), the signal coming from the storage layer

would be maximised. The reduction in randomness has been realized by changing fabrication processes and by introducing an additional seed layer [1, 2] but the major limiting factor remains the fabrication process. As mentioned before the SNR depends on the number of grains. But if one wants to decrease the bit size and keep a high number of grains (to guarantee a high SNR), one has to decrease the grain size. However the scaling of grains leads to thermal stability and write-ability issues.

(ii) **Thermal stability:** To store the information in grains, their magnetization needs to be switched. To switch the magnetization, the energy barrier between two stable magnetization states must be overcome. The head field supplies the energy needed to overcome the energy barrier. The energy barrier of a given magnetic particle is defined as, $\Delta E_b = K_u V$, where K_u is the magnetocrystalline anisotropy and V is the volume of the grain. While scaling grains, the volume of the grains is reduced. The reduction in the volume results in the reduction of the energy barrier. By scaling the grains in the presence of temperature, a critical point can be defined where thermal activation becomes the dominating factor in the switching process. The grain starts to switch randomly due to thermal excitation. This phenomenon of unwanted switching of grains is known as the superparamagnetic effect.

For industrial purposes this effect is very important as it is used to define the stability of a recording medium. Meaning, if 5% of the magnetic particles of the system will flip their direction due to the thermal activation, the data of the media will be lost [2]. In order to maintain the thermal stability of the media, it is essential to maintain an energy barrier that is higher than the thermal energy $k_B T$. Here k_B is the Boltzmann constant and T is the temperature. The desired ratio between the energy barrier and the thermal energy is $\Delta E_b > 55\ k_B T$ at the operating temperature (340 K) of the HDD [1]. To compensate for the reduced energy barrier due to scaling one has to increase

K_u of the material. However by increasing K_u one can encounter another problem, of write-ability.

(iii) **Write-ability:** The field coming from the magnetic head flying over the storage medium is used to switch the magnetization of the magnetic grains. For a successful write operation, the head field needs to be higher than the coercivity $\boldsymbol{H_c} = 2K_u/\boldsymbol{J_s}$ of the grains, where $\boldsymbol{J_s}$ is the magnetic polarization constant of the data storage layer. Richter et. al. reported that the maximum achievable field from the head is limited to 2.4 T for CoFe alloys [12]. If grains with higher K_u values (materials like FePt) are used to increase the thermal stability, the head field will not be able to switch the magnetization of the grain; hence the write operation will not take place.

To address these problems, new media and writing technologies have been proposed. The most promising writing techniques are heat assisted recording media (HAMR) [13] and microwave assisted recording technology (MAMR) [14]. The proposed media are bit-patterned media [15, 16], shingled writing recording [17] and exchange spring recording media [18]. Among these exchange spring recording media is seen as the best contender to achieve the short-term goals of 4 Tb/in^2 areal density.

2.5 Exchange spring recording media

In exchange spring recording media the conventional hard magnetic grain is replaced with the exchange spring magnetic grain. The exchange spring grain is composed of hard and soft magnets that are exchanged coupled to each other. The soft magnet has a lower anisotropy K_s than the anisotropy of hard magnet K_h for

example in Victoria et. al model K_s = 10 J/m^3 and K_h = 2 MJ/m^3 [19], whereas in Suess et. al. model K_s = 0-0.32 MJ/m^3 and K_h = 2 MJ/m^3 [20]. The soft magnet due to its low anisotropy has a lower switching field than the hard magnet whereas the hard magnet has a higher thermal stability due to its high anisotropy. The combination of these two effects allows designing of a bi/multi- layer magnet with a low switching field and a high thermal stability, rooted on the principles of the exchange spring effect [19].

The exchange spring behaviour of the bilayer system was explained by Fullerton et. al. [18, 11]. This effect depends on intrinsic properties of the soft and hard magnetic layer [21] and also on the thickness of the soft layer. Meaning that there is a critical thickness needed to show an exchange spring effect, which is the domain wall width.

When the thickness of the soft layer is less than the domain wall width, the two layers show the switching characteristics of a single-phase media. Switching of their magnetization takes place at the same time, giving the perfect rectangular hysteresis loop. In this case the magnetic properties of the bilayer system will be the average of the two layers involved. This type of bilayer configuration is not beneficial from the recording point of view [22].

When the thickness of the soft layer is greater than the domain wall width, the bilayer system shows the characteristics of exchange spring switching. When the external field is applied, the soft layer may freely rotate in the field direction. The soft layer starts to switch before the hard layer, at field values less than that of the switching field of the hard magnet. Instead of a continuous switching process over the whole grain, its magnetization gets pinned at the soft/hard interface. This phenomenon results in a twisting of the magnetization of the soft magnet, see figure 2.6 (a).

Figure 2.6 (b) also illustrates the hysteresis i.e. change in the magnetization of the exchange spring grain as function of external applied field. The hysteresis loop shows a two-step reversal process which indicates that magnetization of the soft phase starts to switch first and get pinned at the interface and by increasing the applied field the pinning field is overcome and the magnetization reversal starts to take place in the hard phase.

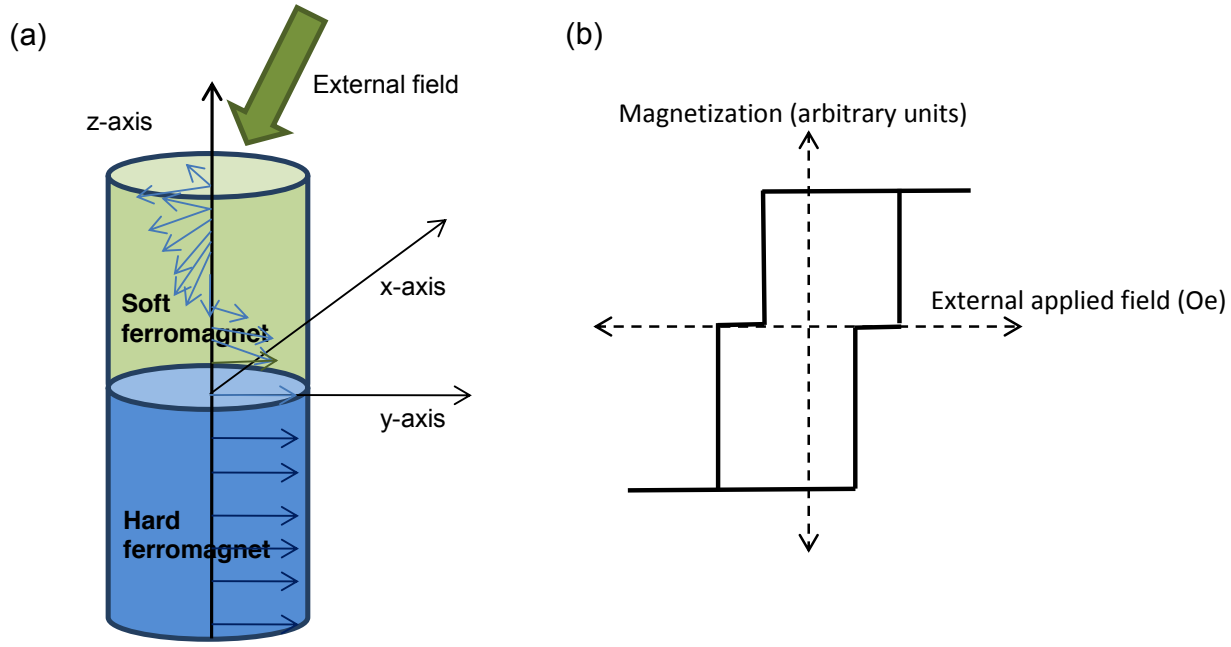

Figure 2.6: (a) Schematic of the exchange spring like switching behaviour of the soft/hard ferromagnetic composite. The soft ferromagnet has a low anisotropy and helps in the switching of the grain at low fields. The hard ferromagnet has a high anisotropy and contributes to the thermal stability of the media [18, 24]. (b) Hysteresis loop for exchange spring bilayer system in the external applied field.

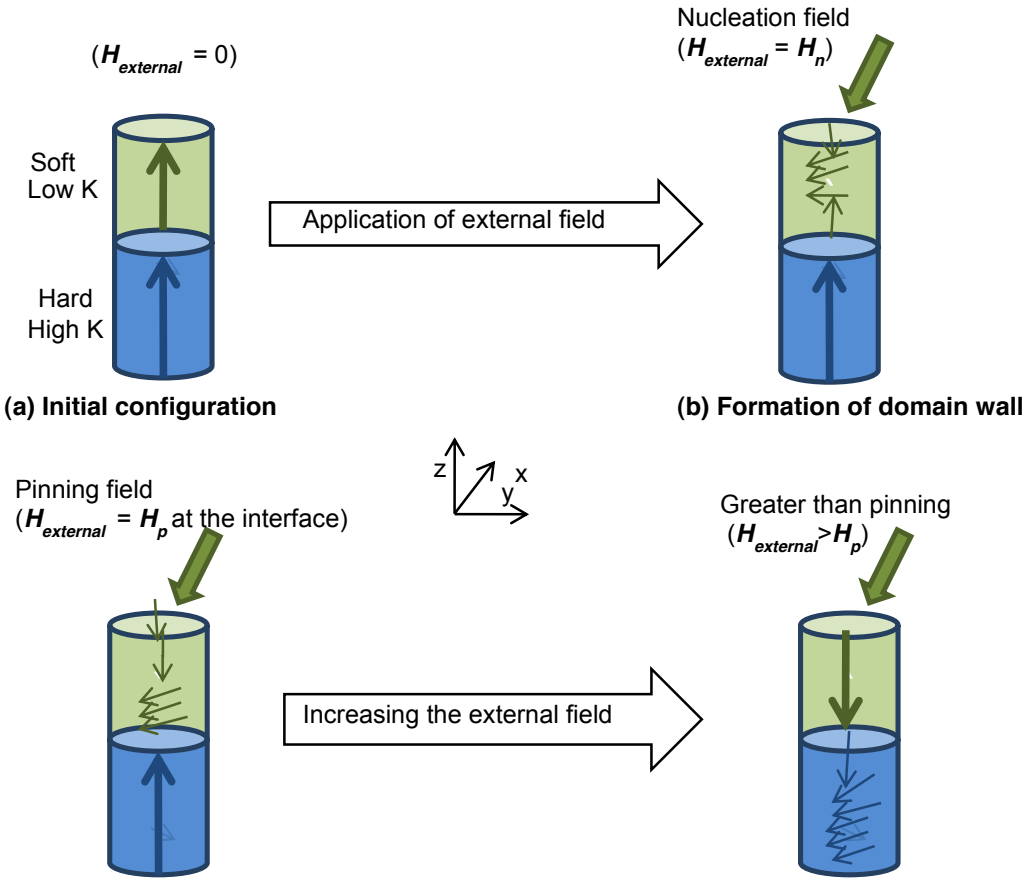

Figure 2.7: The switching process in an exchange spring grain as function of an increasing external field. (a) The initial configuration of the grain. (b) The formation of the domain wall in the soft layer when the external field is equal to the nucleation field. (c) The pinning of the domain wall at the soft/hard interface. (d) The propagation of the domain wall inside the hard layer at higher external field values if the external field is higher than the pinning field.

The domain wall nucleation in the soft layer produces a spring force on the interface, which results in the lower switching field values. The nucleation field $\boldsymbol{H_n}$, to nucleate the domain wall in the soft layer is given by [20, 23]

$$\boldsymbol{H_n} = \frac{2K_s}{\boldsymbol{J_s}} + \frac{2A_s\pi^2}{4t_s^2\boldsymbol{J_s}} \tag{2.3}$$

Where K_s, $\boldsymbol{J_s}$, A_s and t_s, are the anisotropy, magnetic polarization, exchange constant and thickness of the soft material. In the above formula the first terms represent the anisotropy field of the soft layer; the second term represents the energy to form the domain wall. Further increase in the external field makes the domain wall small. The domain wall gets pinned at the hard/soft interface, and propagates into the hard phase when the field is greater than the pinning field.

By assuming that the magnetic polarization and exchange constant are the same for the soft and hard layer, the pinning field $\boldsymbol{H_p}$, is given by [20, 23]

$$\boldsymbol{H_p} = \frac{1}{4}\frac{2\left(K_h - K_s\right)}{\boldsymbol{J_s}} \tag{2.4}$$

Here K_h is the anisotropy constant of the hard magnet. Equation (2.4) indicates that the pinning field at the interface decreases with the increase in the K_s. There is a limit to increase the K_s value, as the nucleation field also increases with the increase in K_s. The approximate optimal value to increase K_s can be calculated, when the nucleation field is equal to the pinning field [20, 23].

By assuming soft layer to be thick the second term of the nucleation field can be neglected, and we have:

$$\frac{2K_s}{\boldsymbol{J_s}} = \frac{1}{4}\frac{2(K_h - K_s)}{\boldsymbol{J_s}} \tag{2.5}$$

$$K_s = \frac{1}{5}K_h \tag{2.6}$$

At field values higher than the pinning field the domain wall propagates into the hard layer and the magnetization of the bilayer system reverses. The coercive field $\boldsymbol{H_c}$ of the bilayer exchange spring system is given by $\boldsymbol{H_c} = max(\boldsymbol{H_n}, \boldsymbol{H_p})$. The complete switching process of the bilayer system is shown in figure 2.7.

2.6 Critical thickness of the soft layer in exchange spring media

Though the domain wall is formed in the soft layer, its critical thickness depends on the hard layer material parameters. The thickness of the soft layer is not given by the typical domain wall width of the soft layer, which is $\delta_W = \pi\sqrt{2A_s/\mu_o M_s^2}$ in the absence of an external field, where M_s is the magnetization saturation. Once a field is applied the domain wall thickness changes with the field. The external field pushes the domain wall towards the hard layer. The domain wall gets pinned at the soft/hard interface. To calculate the domain wall width as a function of the field, let's consider the approximate effective anisotropy strength produced by the field is [22].

$$K_{eff} = \boldsymbol{J_s}\boldsymbol{H_p} \tag{2.7}$$

The field dependent domain wall width δ_w, can be calculated with the help of the domain wall width formula for the hard magnet, which is given by [22]

$$\delta_w = \pi \sqrt{\frac{A_s}{K_{eff}}} \tag{2.8}$$

Using equation (2.7) we have

$$\delta_w = \pi \sqrt{\frac{A_s}{\boldsymbol{J_s H_p}}} \tag{2.9}$$

By replacing $\boldsymbol{H_p}$ with equation (2.4) in the above equation

$$\delta_w = \pi \sqrt{\frac{A_s}{\boldsymbol{J_s}\left(\frac{1}{4}\frac{2(K_h - K_s)}{\boldsymbol{J_s}}\right)}} \tag{2.10}$$

In simple terms

$$\delta_w = \sqrt{2}\pi \sqrt{\frac{A_s}{(K_h - K_s)}} \tag{2.11}$$

By assuming the anisotropy of the soft layer to be zero the domain wall width will become [22]

$$\delta_w = \sqrt{2}\pi \sqrt{\frac{A_s}{K_h}} \tag{2.12}$$

$$\delta_w = \sqrt{2}\pi \sqrt{\frac{A_h}{K_h}} \qquad \text{when } A_h = A_s \tag{2.13}$$

The critical thickness of the soft layer has to be bigger than this value to induce an exchange spring effect in magnetic grains.

The concept of a bilayer system gives the freedom to use materials with a high anisotropy value in the data storage layer. The introduction of exchange spring

magnets in recording layer addresses the problem of SNR, thermal stability and write-ability at higher areal density regimes. This is supported by experimental studies on exchange spring media using the phenomenon of switching field reduction and higher thermal stability [25-27]. From the engineering point of view, the introduction of the exchange spring storage layer in conventional perpendicular media is not a very complex process.

2.7 Bit patterned Magnetic recording media (BPMR)

In novel BPMR media shown in Figure 2.8, the magnetic bit is stored in a highly exchanged coupled and uniformly magnetized single domain island of around 10 nm [28, 29]. Where in the conventional media a group of small grains forms a bit in the novel BPMR it is just a single island that constitutes a bit. The presence of strong exchange coupling in the islands enhances the thermal stability $\Delta E_b = K_u V$ of the bit. This type of structure gives the liberty to use the lower K_u material by ensuring sufficient thermal stability with the increase in the volume of each grain and offers the ease to write with a low field from the head. The bit period in the track of the BPMR medium is highly regular as indicated in figure 2.8.

The islands of the BPMR arrays have less position distribution than conventional granular media, which results in the desired SNR with less transition and track edge noise. The major challenge is to obtain write synchronization, which is achieved when the write field (head field) coincides with the location of pattered islands [30, 31]. Advanced fabrication processes, such as electron beam lithography [32-34], nano-imprinting [28, 33], pattern etching and planarization are required for the fabrication of smaller and denser patterns. This results in a huge expenditure and

increases the complexity and degradation of the device, rooted in the nature of the fabrication process. The new BPMR storage media also require a new head design to write the information [28].

To achieve even higher density recording media advanced BPM islands composed of exchange spring grains can be used [34, 35]. But to achieve high density BPMR very high anisotropy (0.7 MJ/m^3) materials like $L1_0$ FePt has to be used [36]. Although these materials have the advantage of a high thermal stability and the capability to scale the magnetic grains to small sizes (~ 5 nm) one has to be aware that the fields required to switch such systems are beyond conventional recording head fields 2.4 T for CoFe alloys [12]. To be able to induce magnetization reversal in such systems it requires energy assisted writing techniques, which are explained in the next section.

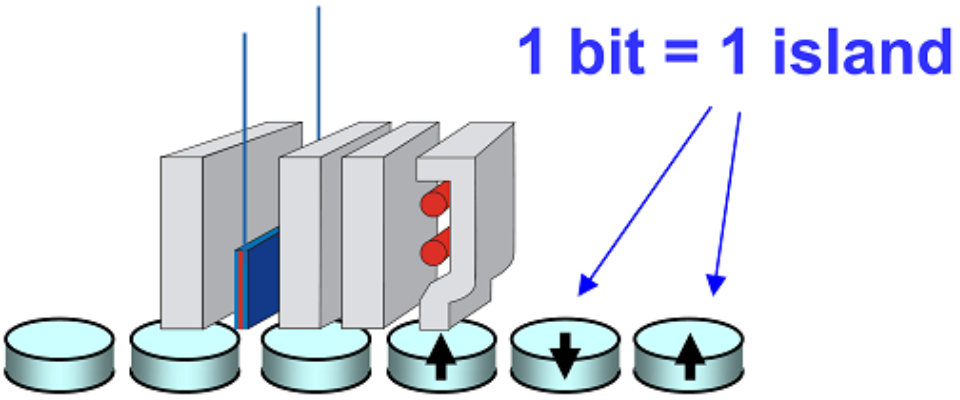

Figure 2.8: Bit patterned magnetic recording media in HDDs [37].

2.8 Energy assisted magnetic recording (EAMR)

In energy assisted magnetic recording the magnetization reversal of the magnetic grain in the data storage medium is triggered with the help of an energy source e.g. heat or microwave effects applied along with the head field.

2.8.1 Heat assisted magnetic recording (HAMR)

HAMR is proposed to solve the problem of writing-ability on smaller grains with a high anisotropy. Figure 2.9 shows a schematic of a HAMR process. The recording medium that has a very high anisotropy for example L0 FePt (0.7 MJ/m^3) [36] is temporarily heated with a laser. Thermal energy induced by the laser beam on the high anisotropy medium reduces the energy barrier and therefore the coercive field. Applying the external field in a particular direction assists in the writing process and the medium is quickly cooled back to the ambient temperature once the write process is complete [28, 38 - 44].

The areal density that can be achieved with HAMR depends on the Curie temperature of the magnetic material used and it is not as restricted by the head field anymore as other technologies. In addition a narrower distribution of grains is possible with this magnetic recording process. The advantages offered by HAMR are small grains, high thermal stability, high SNR, and an enhanced field gradient. In addition by changing from single-phase grains to exchange coupled spring magnets it is possible to even further improve the storage density and the write-ability at more reliable temperatures.

The downside of HAMR technology is its restrictions on the type of high anisotropy magnetic materials (compatibility with the laser integrated in the head system) that can be used with this technology. HAMR also requires a hybrid thermal design to manage and withstand the heat induced in the system. Like BPMR this also involves new physics and new fabrication processes, which demands for high investment and in-depth studies of materials and new designs [45 - 50].

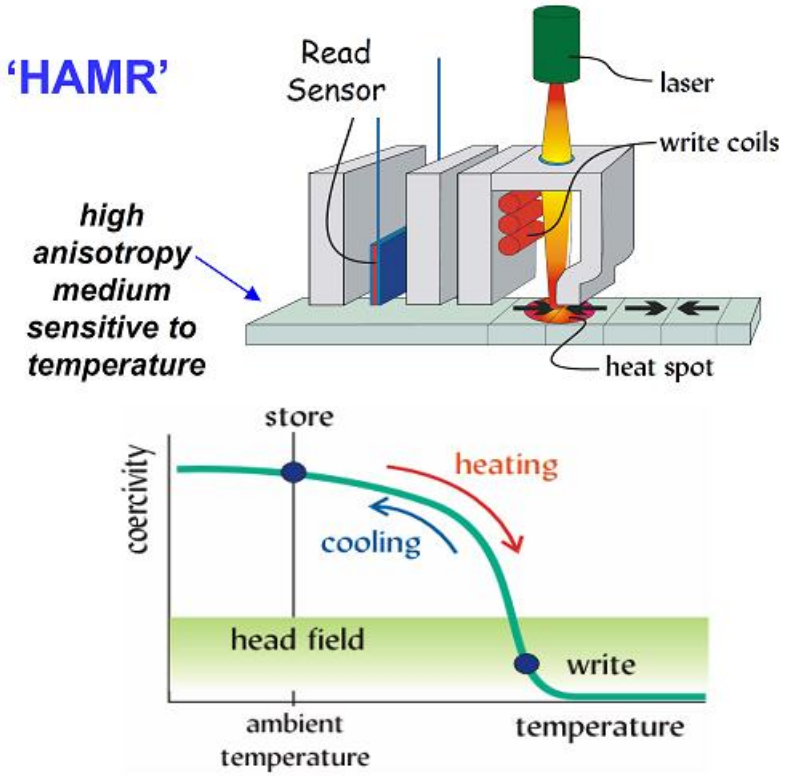

Figure 2.9: **Schematic of writing process and working principle of HAMR. A laser beam is used to heat the storage medium to be able to reverse the magnetization of the grain with the applied head field [37].**

2.8.2 Microwave assisted magnetic recording (MAMR)

MAMR is based on a similar writing technique like HAMR and is proposed to solve the write-ability issue of the recording layer for high anisotropy media with a low head field. The microwave field exerts an additional torque on the magnetization of the grains and together with the head field leads to the reversal of the magnetization at lower applied fields of 2.4 T [12, 51-57]. To produce such a microwave field a microwave oscillator has to be integrated into the write-head design. A schematic of MAMR design is shown in figure 2.10.

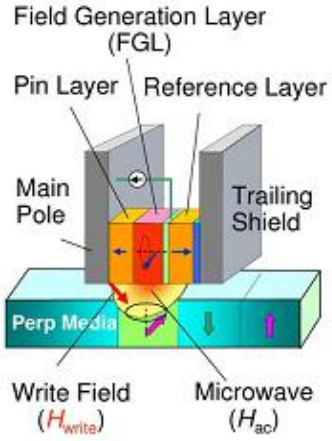

Figure 2.10: Principal of a microwave oscillator on the left and a recording head design with an integrated microwave oscillator on the right [28] © 2009 IEEE.

Despite of being a promising approach, there are practical challenges faced by MAMR. The technology requires a new head design with an integrated oscillator and the microwave signal has to be tuned/optimized for the interaction with the storage layer. To achieve large microwave fields at the data storage layer the flying height of

the head has to be lowered and a larger field generation layer thickness is necessary. The ratio of the field generation layer thickness and flying height should be greater than 1 and the same is true for the ratio of field generation layer width to flying height.

The microwave field that can be produced depends on the value of $2\pi M_s$ at zero flying height and decays strongly with the flying height [58], which makes the matching of the frequency with the media ferromagnetic resonance (FMR) frequency very challenging. The FMR of the media depends on the anisotropy field of the media grains, which may differ in the real media leading to different FMR frequencies for different grains [59-67].

2.9 Two-dimensional magnetic recording (TDMR)

TDMR is an entirely new concept that combines shingled writing recording (SWR) with two-dimensional readback (2DR) technology. The two techniques SWR and 2DR can be used individually to improve the capability and functionality of magnetic recording and when combined together, it promises high gains in areal density on continuous media that avoids the challenges meet by BPMR, HAMR and MAMR [28, 68, 69].

The SWR uses a wide write pole with sharp corner-edges that leads to a high write field as shown in figure 2.11 [67-70]. The SWR write pole writes on a series of heavily overlapped tracks. Due to the overlapping the final resulting tracks are very narrow as compared to the initial written track. On one hand the narrow tracks leads to an increase in the areal density but on the other hand they makes the writing

process highly complicated. As tracks are written sequentially in one cross-track direction the update of the particular point is only possible by recovering all the other tracks of the subsequently written information. After the update is done all the tracks need to be written again, this is challenging aspect for both techniques SWR and TDMR [28].

For the read back processes the 2D waveforms from the storage medium are coded and the signal is processed. For this purpose either an array head, which simultaneously read many tracks or a single head that scan can be used. To get a high read back signal it should have a high SNR in both dimensions.

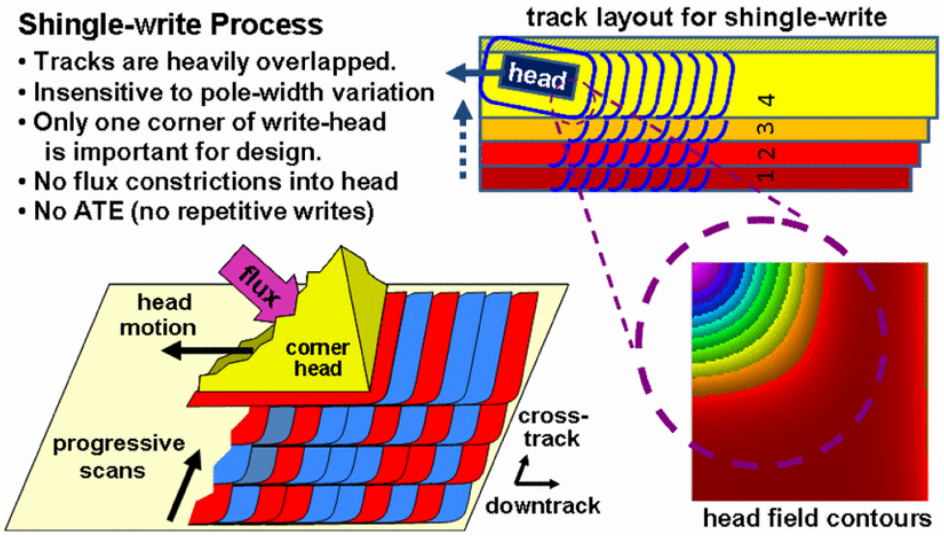

Figure 2.11: A diagram illustrates the Shingled magnetic recording principle where sequentially written tracks are highly overlapped. The schematic also shows the sharp edge corner head [70] © 2009 IEEE].

To achieve a very high density configuration the information has to be stored on only a few grains with a lower limit of at least three grains, to have a strong enough read back signal, so that the signal possessing techniques is able to recognise the information on these grains.

2.10 Summary

This chapter has reviewed the past, present and future magnetic data storage recording technologies. The history of magnetic data storage was discussed briefly ranging from conventional longitudinal magnetic recording to perpendicular magnetic recording and along with that the working principle of data storage technology. The current status and challenges faced by perpendicular magnetic recording to further increase the areal density were discussed in detail and examples of promising solutions to overcome the limitations in writing and scaling of the magnetic grains were underlined. Future data storage technologies that will be realized in the near future such as optimized exchange spring recording media and ones with a longer development timeline such as BPMR, MAMR, HAMR and TDMR including the challenges faced by them have been discussed.

This project studies and takes up the challenges to improve optimized conventional single-phase and exchange spring recording PMR media grains using numerical simulations in close collaboration with experiments.

References

1. A. Moser, K. Takano, D. T Margulies, M. Albrecht, Y. Sonobe, Yoshihiro, S. Sun, E. Fullerton, J. Phys. D: Appl. Phys. **35**, R157 (2002).
2. S. N. Piramanayagam, Appl. Phys. **102**, 011301 (2007).
3. R. Wood, J Magn. Mag. Mat. **321**, 555 (2009).
4. T. Schrefl "Picture of simulation of recording media," report unpublished.
5. A. Fert, P. Grünberg, A. Barthélémy, F. Petroff, W. Zinn, J. Mag. Magn. Mat. **140-144**, 1(1995).
6. A. Fert, Thin Solid Films **517**, 1(2008).
7. S. M. Thompson, J. Appl. Phys. **41**, 093001 (2008).
8. R. Wood, Y. Hsu, and M. Schultz, 'Perpendicular Magnetic Recording Technology', White paper, Hitachi Global Storage Technologies, (2007).
9. H.N. Bertram, H. Zhou, and R. Gustafson, IEEE Trans. Magn. **34**, 4 (1998).
10. J. Moon, IEEE Trans. Magn. **36**, 5 (2000).
11. G. Mian, and T.D. Howell, IEEE Trans Mag. **29,** 3999 (1993).
12. H. J Richter, J. Phys. D: Appl. Phys. **40**, R149 (2007).
13. M. H. Kryder, E. C. Gage, T. W. McDaniel, W.A. Challener, R. E. Rottmayer, G. Ju, Y. T. Hsia, and M. F. Erde, IEEE Trans. Magn. **96**, 1810 (2008).
14. J. G. Zhu, X. Zhu, and Y. Tang, IEEE Trans. Magn. **44**, 1(2008).
15. B. D. Terris and T. Thomson, J. Phys. D: Appl. Phys. **38**, R199 (2005).
16. Y. Shiroishi, K. Fukuda, I. Tagawa, H. Iwasaki, S. Takenoiri, H. Tanaka, H. Mutoh, and N. Yoshikawa, IEEE Trans. Magn. **45**, 10 (2009).
17. T. Thomson, B. Lengsfield, H. Do, and B.D. Terris, J. Appl. Phys. **103**, 07F54 (2008).

18. E. E. Fullerton, J.S. Jiang, M. Grimsditch, C.H. Sowers and S.D. Badar Phys. Rev. B **58**, 12193 (1998).
19. R.H. Victoria, and X. Shen, IEEE trans. Mag. **41**, 10(2005).
20. D. Suess, App. Phys. Lett. **89**, 113105 (2006).
21. E. E. Fullerton, J.S. Jiang, S.D. Badar, J. Magn. Magn. Mater. **200**, 393 (1999).
22. D. Suess, J. Magn. Magn. Mater. **308**, 183 (2007).
23. H. Koronmüller, and D. Goll, Physica B **319,** 122 (2002).
24. E. Goto, N. Hayashi, T. Miyashita and K. Nakagawa, J. Appl. Phys. **36**, 9 (1965).
25. J. P. Wang, W. Shen, and J. Bai, IEEE Trans. Magn. **41,** 10 (2005).
26. J.P. Wang, W. Shen, and S.Y. Hong, IEEE Trans. Magn. **43**, 2 (2007).
27. D. Goll, and S. Macke, App. Phys. Lett. **93**, 152512 (2008).
28. Y. Shiroishi, K. Fukuda, I. Tagawa, H. Iwasaki, S. Takenoiri, H. Tanaka, H. Mutoh, and N. Yoshikawa, IEEE Trans. Magn. **45**, 10 (2009).
29. J. Kalezhi, J. J. Miles, and D. B. Branson, "IEEE Trans. Magn. **45**, 10 (2009).
30. R.L. White, R.M.H. New, and R.F.W. Pease, IEEE Trans. Magn. **33**, 1 (1997).
31. C. T. Rottner, S. Anders, T. Thomson, M. Albrecht, Y. Ikeda, M. E. Best, and B. D. Terris, IEEE Trans. Magn. **38**, 4 (2002).
32. T. R. Albrecht, O. Hellwing, R. Ruiz, M. E. Schabes, B. D. Terris, B.D. and X. Z. Wu, J.P. Liu, E. Fullerton, O. Gutfleisch and D. Sellmyer, Nanoscale Magn. Mater. and Applications (eds.), 237(Springer US, 2009) .
33. Y. Xu, W. Hu, X. Yang, Z. Fan, J. Hwu, K. Wago, D. Kuo, The 23rd International Vacuum Nanoelectronics Conference (IVNC) **P1-15**- 58 (2010).
34. H. J. Richter, A. Y. Dobin, R. T. Lynch, D. Weller, R. M. Brockie, O. Heinonen, K. Z. Gao, K.Z., J. Xue, R. J. M. V. D. Veerdonk, P. Asselin, and M. F. Erden, App. Phys. Lett. **88**, 22 (2006).

35. H. J. Richter, A. Y. Dobin, O. Heinonen, K. Gao, R. Veerdonk, R. Lynch, J. Xue, D. Weller, P. Asselin, M. Erden, and R. Brockie, IEEE Trans. Magn. **42**, 10 (2006).
36. E. Yang, and D. E. Laughlin, J. Appl. Phys. **104**, 023904 (2008).
37. R. Wood and H. Takano, Prospects for Magnetic Recording over the next 10 years, Tech. rep., Hitachi Global Storage Technologies (2006).
38. J. J. M. Ruigrok, R. Coehoorn, S. R. Cumpson, and H. W. Kesteren, J. App. Phys. **87**, 9 (2000).
39. A. Moser, K. Takano, D. T. Margulies, M. Albrecht, Y. Sonobe, Y. Ikeda, S. Sun, and E.E. Fullerton, J. Phys D: App. Phys. **35**, 19(2002).
40. H. Gengnagel, U. Hofmann, Basic Solid state Phys. **29,** 1(1968).
41. T. Sugimoto, T. Katayama, M. Hashimoto, Y. Suzuki, Y. Nishihara, IEEE Translation J. Magn. Japan **183,** 7 (1992).
42. K. Inoue, H. Shima, A. Fujita, K. Ishida, K. Oikawa, K. Fukamichi, Appl. Phys. Lett. **88,** 102503 (2006).
43. R. E. Rottmayer, S. Batra, D. Buechel, W. A. Challener, J. Hohlfed, Y. Kubota, B.L. L. Li, C. Mihalcea, K. Mountfield, K. Pelhos, C. Peng, T. Rausch, M. A. Seigler, D. Weller, and X. M. Yang, IEEE Trans. Magn. **42,** 2417 (2006).
44. http://i.zdnet.com/blogs/hamr-diagram.jpg
45. L. Pan, and D. B. Bogy, Nature Photonics **3**, 4-189 (2009).
46. D. Goll, S. Macke, Appl. Phys. Lett. **93,** 152512 (2008).
47. J. Zhang, R. Ji, J. Xu, J. Ng, B. Xu, S. Hu, H.Yuan, and, S. N. Piramanayagam, IEEE International Magnetic Conference, INTERMAG **GP-09,** 785 (2006).
48. W. A. Challener, C. Mihalcea, C. Peng, and K. Pelhos, Opt. Exp. **13,** 7189 (2005).

49. W. A. Challener, E. Gage, A. Itagi, and C. Peng, Jpn. J. Appl. Phys. **45,** 6632 (2006).
50. M.A. Seigler, W.A. Challener, E. Gage, N. Gokemeijer, G. Ju, B. Lu, K. Pelhos, C. Peng, R.E. Rottmayer, X. Yang, H. Zhou, and T. Rausch, IEEE Trans. Magn. **44,** 119 (2008).
51. C. Thirion, W. Wernsdorfer, and D. Mailly, Nature Mater. **2**, 524 (2003).
52. Y. Nozaki, M. Ohta, S. Taharazako, K. Tateishi, S. Yoshimura, and K. Matsuyama, Appl. Phys. Lett. **91**, 082510 (2007).
53. J. Podbielski and D. Heitmann, Phys. Rev. Lett. **99**, 207202 (2007).
54. G. Woltersdorf and C. H. Back, Phys. Rev. Lett. **99**, 227207 (2007).
55. J. G. Zhu, X. Zhu, and Y. Tang, IEEE Trans. Magn. **44**,125 (2008).
56. S. Okamoto, N. Kikuchi, and O. Kitakami, Intermag 2008, Madrid, Spain, Proc. **HW**-03 (2008).
57. X. Zhu and J.G. Zhu, IEEE Trans. Magn. **42,** 4 (2006).
58. G. Winkler, D. Suess, J. Lee, J. Fidler, M. A. Bashir, J. Dean, A. Goncharov, G. Hrkac, S. Bance, and T. Schrefl, Appl. Phys. Lett. **94**, 232501 (2009).
59. J.H.E. Griffiths, Nature, **158** 670(1946).
60. C. Kittel, Phys. Rev. **71,** 270 (1947).
61. C. Kittel, Phys. Rev. **73**, 155 (1948).
62. C. Thirion, W. Wernsdorfer, D. Mailly, Nature Mate. **2**, 524 (2003).
63. C.K. Goh, Z. M. Yuan, and B. Liu, Appl. Phys. Lett. **94,** 152510 (2009).
64. S. Okamoto, N. Kikuchi, and O. Kitakami, Appl. Phys. Lett. **93,** 102506 (2008).
65. S. Okamoto, N. Kikuchi, O. Kitakami, and M. Igarashi, J. Appl. Phys. **107**, 033904 (2010).

66. R. Wood, M. Williams, A. Kavcic, and J. Miles, IEEE Magn. Trans. **45**, 2-917 (2009).
67. I. Tagawa and M. Williams, INTERMAG 2009, Sacramento. CA, **FA**-**02** (2009).
68. S. Greaves, Y. Kanai, and H. Muraoka, INTERMAG 2009, Sacramento, CA, **FA-03** (2009).
69. S. Greaves, Y. Kanai, and H. Muraoka, IEEE Trans. Magn. **48**, 5 (2012).
70. R. Wood, M. Williams, A. Kavcic, and J. Miles, IEEE Trans. Mag. **45**, 2(2009).

Chapter 3: Micromagnetic theory, nudged elastic band method and basics of finite element modelling

3.1 Abstract

In this chapter a brief introduction on the background of micromagnetics, the nudge elastic band method (NEB) and the basics of finite element modelling is given. The various contributing energies like exchange energy, magneto-crystalline anisotropy energy, magnetostatic energy and Zeeman energy that affect the magnetization dynamics as well as the characteristic length scale for the hard and soft ferromagnetic materials which is important for finite element modelling are discussed. An introduction to the Stoner-Wohlfarth model is also given. The chapter is concluded with a basic introduction into the nudged elastic band method, finite element method (FEM) and numerical integration and error control.

3.2 Introduction

The continuum theory of micromagnetism was developed in 1930 [1] with publications by Landau and Lifshitz [2] and a book by Brown [3]. Important contributions to micromagnetic theory were provided by Dirac in 1928, on the explanation of ferromagnetism [4] and Heisenberg [5] (1928) on the origins of exchange energy. The contribution of Landau and Lifshitz (1935) [2], Akulov (1928-1931) [6], Bloch [7], Becker and Doring (1939) [8], Brown [3, 9-13], Kittel [14-15], Stoner-Wohlfarth [16], and Neel [17-19] led to the development of a descriptive and predictive micromagnetic theory. Micromagnetic theory is a semi-classical theory

with a spin interpretation for the magnetic moment, in order to describe interactive phenomenon like hysteresis loops of ordered spin structures or other magnetization processes. The quantum theory describes the magnetic properties of materials on an atomistic level, whereas the Maxwell's theory gives their description on the macroscopic level. Micromagnetism is the mesoscopic theory of magnetism formed by the combination of these two theories and gives the description of material properties between macro and atomic levels [1, 20-22].

In the early days of micromagnetism was used as a tool to determine domain structures and magnetization reversal mechanism in systems with ideal geometry; for standard energy minimization approaches and classical nucleation theory respectively. The availability of large scale computing facilities has enabled micromagnetism to deal with more realistic geometries and problems [20-22].

This work uses this theory and the nudged elastic band method to study the switching of ferromagnetic materials to explain and understand the magnetization processes within the characteristic range of a few nanometres. Micromagnetics includes chemical as well as physical properties and the micromagnetic simulations give the local distribution of the magnetization as a function of the energies involved. Micromagnetism is a unique technique, which explains the hysteresis effect of the ferromagnetic material at a particular length scale, between the magnetic domain and crystal lattice parameter [1].

In micromagnetism the phenomena taking place during the transition between magnetic domains is described by the continuous magnetization vector of all the existing atomic moments. The calculation starts with the intrinsic magnetic properties namely magnetocrystalline anisotropy, exchange energy, demagnetization energy

and Zeeman energy, which are taken from literature, experiments or first principle calculations. Micromagnetism is widely used to study different magnetic structures and their magnetization reversal behaviour. It provides details of the microscopic processes; hence describes the dynamic response of a magnetic system in an external field and the macroscopic magnetic properties like switching time and switching field [21]. It is successfully used in high-density magnetic recording and magneto-electronic devices industry.

3.3 Basic Principles of Micromagnetics

Basically in micromagnetics atomic moments are replaced by a continuous magnetization vector $\boldsymbol{M}$. The local magnetic moment can be explained by the spontaneous polarization vector $\boldsymbol{J_s}$ [22].

$$\boldsymbol{J_s} = \mu_o \boldsymbol{M} = \mu_o \frac{\boldsymbol{m}}{V} \tag{3.1}$$

Hence the spontaneous magnetic polarization $\boldsymbol{J_s}$ is proportional to the magnetic moment $\boldsymbol{m}$ and is inversely proportional to the volume V. In equation (3.1) μ_o ($4\pi\times10^{-7}$ NA^{-2}) is the magnetic permeability in vacuum. In micromagnetism the magnetization vector is assumed continuous with the position [1]. The magnitude of the magnetization vector is taken as a function of temperature only and is assumed independent of the local fields within the sample. This makes it possible to describe the magnetic state of a system uniquely with the direction cosine of the magnetization vector (the direction cosine refers to the cosine of the angle between the magnetization vector and the unit vector that point to the easy axis direction). In

equilibrium state the direction cosines leads to the minimization of the total Gibbs free energy of the system [1].

In short, micromagnetism calculates the total magnetic Gibbs free energy of the magnetic system and for the time evolution of the magnetization polarization vector $\boldsymbol{J_s}$ the Landau-Lifshitz-Gilbert equation (LLG) is solved [1].

3.4 Total Magnetic Gibbs free energy

The $\boldsymbol{M}$ is calculated by determining the total Gibbs free energy (E_{total}) with other free variables like temperature T, elastic stress tensor (σ) and applied external magnetic field. All contributing energy densities to the total magnetic Gibbs free energy density ϕ_G are derived from condensed matter physics, classical electrodynamics and quantum mechanics and can be written as follows [1].

$$\phi_G = \phi_U - TS - \sigma \cdot \varepsilon - \boldsymbol{J}_s \cdot \boldsymbol{H}_{external} \tag{3.2}$$

Whence ϕ_U, S and ε represent the internal energy density, the entropy per unit volume and the strain tensor respectively. The free energy term contains contributions of all energies like magnetostatic field energy (E_{stray}), magnetic anisotropy energy ($E_{anisotropy}$), which includes shape, stress and magentocrystalline anisotropy), exchange energy ($E_{exchange}$) etc. The total Gibbs free energy can be calculated by integrating the total magnetic Gibbs free energy density over the volume. In terms of the external and internal energy the total magnetic Gibbs free energy (E_{total}) can be written as follows:

$$E_{total} = E_{exchange} + E_{anisotropy} + E_{stray} + E_{external} \tag{3.3}$$

Where $E_{external}$ is the Zeeman energy which arises from the external magnetic field. In the equilibrium state the total Gibbs free energy reaches its minima. Micromagnetism is based on the continuum theoretical expression of the intrinsic energy terms contained in the internal energy. These intrinsic terms are derived by continuation of quantum theoretical expression or symmetry consideration by replacing localized spins with a continuous polarization or magnetization vector. This continuum expression derived takes account of spin interaction with other spins, crystal lattice, and external applied field.

3.5 Heisenberg exchange energy

The continuum expression of exchange energy for a small deviation of the magnetization from the homogeneously magnetized ground state by Landau and Lifshitz (1935) is one of the major breakthroughs in the field of micromagnetism [1]. The exchange energy is very crucial factor in the formation of covalent bond in solids and ferromagnetic coupling. In order to minimize the Heisenberg exchange energy all the dipole moments in the domain lie parallel to each other. In micromagnetic as mentioned before the ***M(r)*** vector should remain uniform. This indicates the divergence and rotor of the magnetization to vanish in order to fulfil the condition. In order to take this into account the exchange energy density (ϕ_{ex}) is given by the following formula [4, 5].

$$\phi_{ex} = \frac{A(r)}{\left| \boldsymbol{M(r)} \right|^2}\left(\left(\nabla \cdot \boldsymbol{M(r)} \right)^2 + \left(\nabla \times \boldsymbol{M(r)} \right)^2 \right) \tag{3.4}$$

Where $A(r) = A$ is the exchange constant and is a function of space. Integration of the above equation (3.4) over the volume of ferromagnetic body gives the exchange energy.

The exchange interactions are mainly of two types: short range and long range. Short-range interactions are the interactions taking place due to small changes in the spin orientations between only nearest neighbours. Long–range interactions take into account interactions between all neighbouring atoms. The indirect exchange interactions known as RKKY- coupling were developed by Zener, Ruderman and Kittel [14-15], Kasuya [23] and Yosida. The RKKY – coupling is based on the interaction between localized spins of d and f orbital electrons and the cloud of delocalized s electrons [1].

3.6 Magnetostatic energy

The total magnetostatic energy has two contributions: the external applied magnetic field $\boldsymbol{H_{external}}$ and the dipolar field $\boldsymbol{H_s}$ that arise from the magnetization. The magnetostatic energy, which results from the external field, is called as Zeeman energy.

3.6.1 Magnetostatic energy due to external field (Zeeman energy)

A change in the magnetization due to an external applied field can result in a change of the domain direction or an enlargement of the domain. This dynamic process results in the reduction of the total overall energy of the system. The Zeeman energy

can be calculated by integrating the Zeeman energy density (ϕ_z) with respect to the volume [22]

$$\phi_z = -\mu_o \boldsymbol{M} \cdot \boldsymbol{H}_{external} \tag{3.5}$$

The above equation indicates that the Zeeman energy reaches its minimum value when the magnetization points parallel to the external field.

3.6.2 Magnetostatic energy due to internal magnetization distribution (stray field)

When the external field is applied the magnetic moments in the magnetic material try to retain their initial orientation and generate a demagnetization field, dipolar field or stray field, which try to oppose the external applied field and leads to the formation of domains inside the magnet. The demagnetization energy density can be written as follows:

$$\phi_d = -\frac{1}{2}\mu_o \boldsymbol{M} \times \boldsymbol{H}_d \tag{3.6}$$

The determination of the demagnetization field $\boldsymbol{H_d}$ produced by the magnet itself can be expressed in terms of scalar potentials with the help of Maxwell's equations.

$$\nabla \times \boldsymbol{H}_d = 0 \tag{3.7}$$

$$\nabla \cdot \boldsymbol{B} = 0 \tag{3.8}$$

as we know

$$\boldsymbol{B} = \mu_0 (\boldsymbol{H}_d + \boldsymbol{M}) \tag{3.9}$$

Equation (3.9) can also be written as

$$\nabla \cdot (\boldsymbol{H}_d + \boldsymbol{M}) = 0 \tag{3.10}$$

Since the curl of any scalar function *f(r)* is zero i.e. $\nabla \times \nabla f(r) = C$, the $\boldsymbol{H_d}$ can be expressed in terms of a magnetic scalar potential φ_m as follows:

$$\boldsymbol{H_d} = -\nabla \varphi_m \tag{3.11}$$

By substituting the value of $\boldsymbol{H_d}$ into equation (3.10) we get

$$\nabla^2 \varphi_m = \nabla \cdot \boldsymbol{M} \tag{3.12}$$

Equation (3.12) is similar to Poisson equation which helps in defining the magnetic scalar potential φ_m in terms of volume magnetic charge density ρ_m and surface charge density σ_m as follows: $\rho_m = -\nabla \cdot \boldsymbol{M}$ in the bulk and $\sigma_m = \boldsymbol{M} \cdot n$ at the surface of the magnetic material. Hence the magnetostatic field can be determined by the equation (3.12) with essential boundary conditions which determines the continuity of the normal component of $\frac{\boldsymbol{B}}{\mu_0} = (\boldsymbol{H_d} + \boldsymbol{M})$ and tangential components of $\boldsymbol{H_d}$ fields at the interface.

$$(\boldsymbol{B_{out}} - \boldsymbol{B_{in}}) . n = 0 \tag{3.13}$$

Where n is the unit vector pointing outside from the surface, $\boldsymbol{B_{out}}$ and $\boldsymbol{B_{in}}$ is the flux density outside and inside of the material respectively. The condition indicates that the perpendicular component of the $\boldsymbol{B}$ is continuous.

$$(\boldsymbol{H_{d,out}} - \boldsymbol{H_{d,in}}) \times n = 0 \tag{3.14}$$

Whence $\boldsymbol{H}_{d,out}$, and $\boldsymbol{H_{d,in}}$ are the demagnetization field outside and inside of the material respectively. The condition indicates that the tangential component of the $\boldsymbol{H_d}$ is continuous. Where n is the unit vector pointing outward from the surface.

3.7 Magnetocrystalline anisotropy energy

Akulov (1928-1931) derived the continuum expression for the magnetocrystalline energy [8]. The term anisotropy here refers to the fact that the saturation

magnetization is approached by different values of large magnetic fields in different crystal orientations and gives rise to terms in the easy and hard magnetic axis. The coupling between the spins moments, orbital's and the crystal fields is the origin of magnetocrystalline energy. In simple words it is the work needed to rotate the magnetization of the ferromagnet in a certain crystallographic direction [22]. The magnetocrystalline anisotropy energy density of a uniaxial and cubic material is illustrated in figure 3.1 and 3.2 respectively.

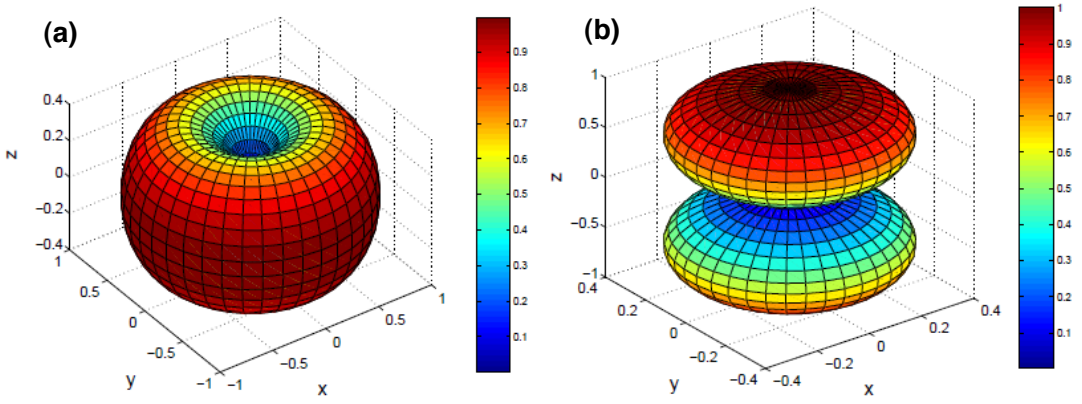

Figure 3.1: The uniaxial anisotropy energy density of an (a) easy axis anisotropy K_1>0, (b) easy plane anisotropy K_1<0 respectively [24].

A uniaxial material has only one easy axis orientation, whereas a cubic material has three c-axis orientations. If the magnetization vector is aligned parallel to the easy axis the energy contribution is zero. Meaning, that the magnetocrystalline energy represents the work that is required in rotating the magnetization away from the easy axis in the magnet.

3.7.1 Uniaxial anisotropy

In case of a uniaxial material the anisotropy energy density is given by equation (3.15). The integration of uniaxial anisotropy energy density over the magnet volume gives the anisotropy energy [22, 24, 25].

$$\phi_{K,\ uniaxial} = K_0 + K_1 sin^2\varphi\,(r) + K_2 sin^4\varphi\,(r) + K_3 sin^6\varphi\,(r) + \cdots\cdots \qquad (3.15)$$

Where K_0, K_1, K_2, K_3 represents the anisotropy constant, which are derived from the experiments and have the dimensions of the energy per unit volume, $\varphi(r)$ denotes the angle between the magnetization vector ***M*** and unit vector ***u*** of the c-axis. The unit vector that is parallel to the easy axis, ***u*** =***u***(r) depends on position r. The angle between the magnetization ***M*** and ***u*** is given by $\varphi = \varphi(r)$. It should be mentioned here that the direction of c-axis can change from one grain to the other. Equation (3.15) by ignoring the higher terms is often written as [24, 25]

$$\phi_{K,\ uniaxial} = K_0 + K_1 sin^2\varphi\,(r) \qquad (3.16)$$

The anisotropic behaviour of the material is described by the constant K_1 that can be negative or positive, if $K_1 > 0$ the anisotropy energy attains two minimum one at $\varphi\,(r) = 0$ and second at $\varphi\,(r) = \pi$. In simple words when $K_1 > 0$ the magnetization of the uniaxial magnetic material lies along the ± z-direction commonly known as easy axis with no preferential orientation as shown in figure 3.1 (a). On the other hand, for the magnetocrystalline anisotropy case shown in figure 3.1 (b) when $K_1 < 0$ the anisotropy energy attains its minima at $\varphi\,(r) = \frac{\pi}{2}$, which means that the any direction in the x-y plane correspond to the easy direction because of this it is referred as easy plane anisotropy [24, 25].

3.7.2 Cubic anisotropy

In the cubic crystals the anisotropy energy density has cubic symmetry contributed by the spin lattice coupling in such materials. The cubic anisotropy density ($\phi_{K,\ cubic}$) is given as [24, 25]

$$\phi_{K,\ cubic} = K_0 + K_1\left(m_x^2 m_y^2 + m_y^2 m_z^2 + m_z^2 m_x^2\right) + K_2(m_x^2 m_y^2 m_z^2 \ldots + \ldots \quad (3.17)$$

Where m_x, m_y and m_z are the component of the unit magnetization vector in the spherical co-ordinates. In a case when higher order terms i.e. K_2 is neglected the cubic material has six minimum along the ± x, ± y and ± z-direction when $K_1 > 0$ as shown in figure 3.2 (a).

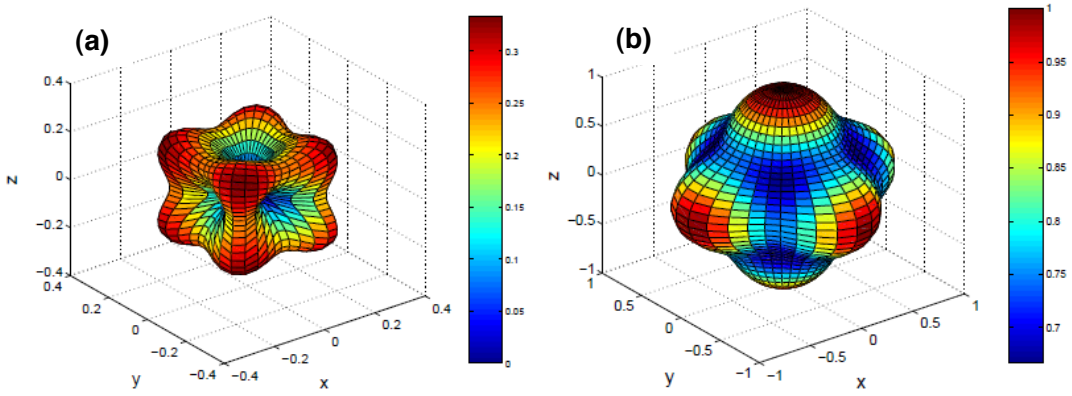

Figure 3.2: The cubic anisotropy energy density of an (a) when K_1>0, (b) K_1<0 respectively [24].

When K_1 < 0 the problem becomes more complex and the system attains eight energy minima's pointing along the vertices of the cube i.e. along the [111] direction

and the co-ordinate axes direction becomes the hard axes, see figure 3.2 (b) [24, 25].

To be more precise the determination of the easy axes requires other additional condition that defines the energy minima described by equation (3.15) and (3.17) [25]. By taking into account the anisotropy constant K_1 and K_2 the energy minima is described for uniaxial and cubic crystal with help of the phase diagram in figure 3.3.

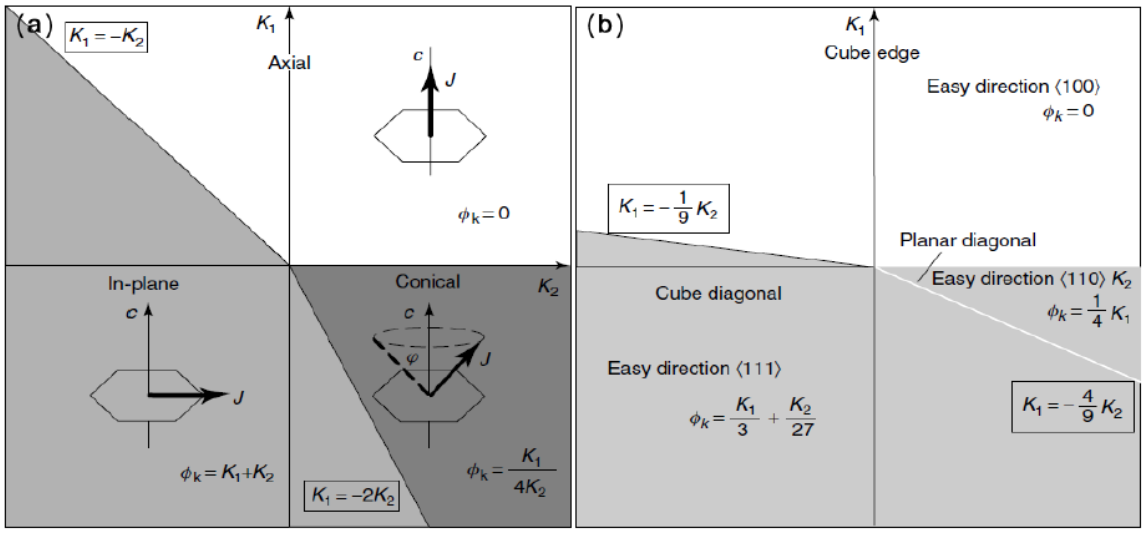

Figure 3.3: Phase diagrams of easy axes direction for (a) uniaxial and (b) cubic crystals [26].

3.7.3 Shape anisotropy

Shape anisotropy can be explained in analogy with the dielectric materials with the magnetization producing fictitious free poles at the surface of the material that results into the demagnetization field $\boldsymbol{H_d}$ with its direction opposite to the magnetization direction of the material as shown in figure 3.4.

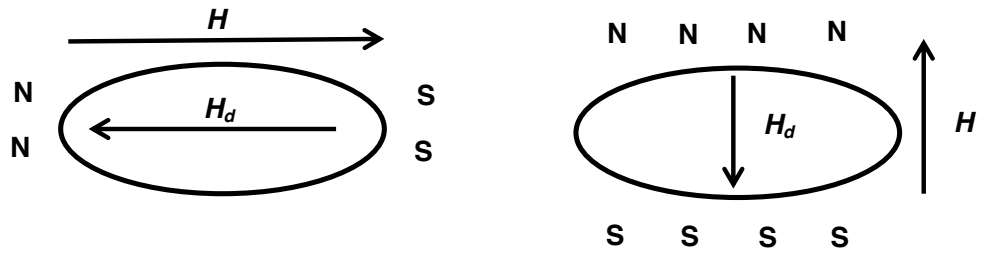

Figure 3.4: Anisotropic shaped sample with magnetic field applied in two different directions (a) parallel to the long axis, the free poles N and S are separated by the large distance resulting into small H_d (b) parallel to the short axis, the free poles N and S are separated by small distance resulting into large H_d [27].

In the figure 3.4 the magnetic field is applied in two different perpendicular directions to the ellipsoid. The energy of the ellipsoid increases with the increase of the demagnetization field. The energy for the ellipsoid of revolution is given as [27]

$$E = -K_{eff} \sin\varphi_s \tag{3.18}$$

Where φ_s is the angle between the long axis and the magnetization direction of the sample. The effective anisotropy expression K_{eff} depends on the demagnetization factors of the long axis N_a and short axis N_b of the sample and the magnetization [27].

$$K_{eff} = \frac{1}{2}\left(N_b - N_a\right)\mu_0 M_s^2 \tag{3.19}$$

The demagnetization factors are geometry dependent and for the sphere $N_a = N_b$, which makes K_{eff} for sphere

$$K_{eff} = 0 \tag{3.20}$$

For the needle shaped geometry the short axis demagnetization factor $N_b << N_a$, after setting $N_a = 1$, K_{eff} is given by equation by equation (3.21) with the help of equation (3.19)

$$K_{eff} = -\mu_0 \frac{M_s^2}{2} \tag{3.21}$$

The interaction between the Heisenberg exchange energy and magnetocrystalline energy defines the domain wall width. The wall width δ_w for the hard ferromagnet is given by [22].

$$\delta_W = \pi \sqrt{\frac{A}{K_h}} \tag{3.22}$$

In the equilibrium state the sum of exchange energy and anisotropy energy is minimised by the domain wall configuration. A smaller transition region indicates a smaller deviation from the easy axis. The domain wall width for a soft magnetic material is given by [22].

$$\delta_W = \pi \sqrt{\frac{2A}{\mu_0 M_s^2}} \tag{3.23}$$

The exchange length l_{ex} (also called the characteristic length) in the soft magnet is given below

$$l_{ex} = \sqrt{\frac{2A}{\mu_0 M_s^2}} \tag{3.24}$$

From equation (3.23) and (3.24) the relation between the domain wall width and exchange length can be written as follows

$$l_{ex} = \pi \delta_W \tag{3.25}$$

3.8 Stoner-Wohlfarth model

Stoner-Wohlfarth model is the simplest analytical model that describes the physics and magnetization of the single domain particle in the presence of the applied field in the absence of thermal effects. In spite of being limited to the coherent magnetization reversal of the single domain particles, Stoner-Wohlfarth model plays vital role in the understanding of the complex magnetization reversal dynamics and is used widely in studying the reversal dynamics in real materials like magnetic data storage [16, 28, 29]. The ellipsoid single domain particle considered by the Stoner-Wohlfarth is shown in figure 3.5. In the figure 3.5, ***H*** is the direction of the applied field, ***M*** is the magnetization direction of the Stoner-Wohlfarth particle, whereas α and *θ* are angle between the applied field and easy axis of the particle and magnetization and easy axis of the particle respectively.

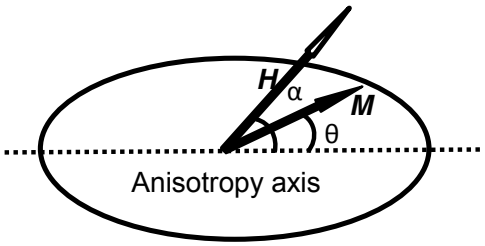

Figure 3.5: Shows a Stoner-Wohlfarth particle. In the schematic α is the angle between the magnetic field and the anisotropy axis and *θ* is the angle between the magnetization direction and the anisotropy axis [16, 28, 29].

Stoner-Wohlfarth work focuses on the finding the equilibrium state of the single domain particle (ellipsoid) shown in figure 3.5 at an angle *θ* where the equilibrium is

obtained, when the gradient of total energy density ϕ_{tot} of the stoner Wohlfarth particle becomes equal to zero i.e. $\frac{d\phi_{tot}}{d\theta} = 0$ The switching of magnetization of the grain, which is an irreversible process of going from one minima to the other minima takes place when the energy minimum is unstable leading to the condition when $\frac{d^2\phi_{tot}}{d^2\theta} = 0$. The Stoner–Wohlfarth normalized switching field $\boldsymbol{H_{sw}}$ is given by equation (3.26) [16, 28, 29].

$$\boldsymbol{H_{sw}} = \frac{1}{\left(\sin^{2/3}\theta + \cos^{2/3}\theta\right)^{3/2}} \tag{3.26}$$

The switching field as a function of applied field angle for the Stoner-Wohlfarth particle is shown in figure 3.6.

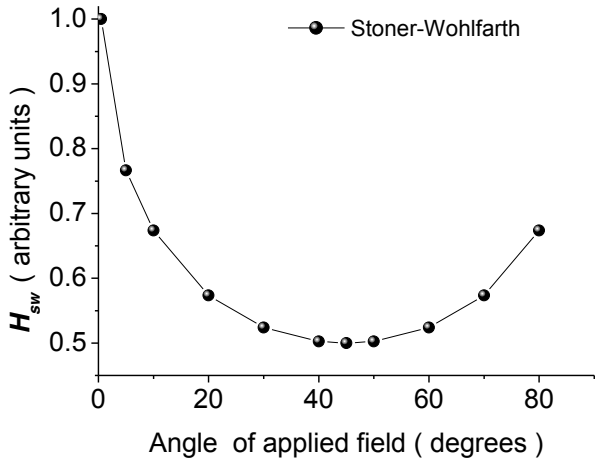

Figure 3.6: Normalized switching field as a function of the applied angle for the Stoner-Wohlfarth particle [16, 28, 29].

As shown in figure 3.6 the switching field first decreases up to 45 degree and then starts to increase afterwards. Hence Stoner-Wohlfarth curve shows the minimum switching field at an angle of 45 degree. Important thing to note here is that the switching field plotted above in figure 3.6 is the minimum critical field which is required to reverse the direction of the magnetization of the grain and is different from the coercive field. Switching of the magnetization of the takes place when the energy landscape is flattest meaning when the first and second derivative of the energy is zero with respect to the angle of the applied field.

3.9 Characteristic length scale

The magnetization behaviour highly depends on the different contributing energy terms. The different energy terms are active over different length scales for example the exchange energy and its associated exchange length, which is determined by the material properties is in the range of a few nano-meter but the magnetostatic energy which is important for the domain wall formation within the material itself remains active on entirely different scales [20]. By keeping this in mind the following characteristic length scale parameters are defined for problems in micromagnetism:

1. The length scale should be small enough that it describes the domain walls properly i.e. the transition of magnetization within the magnetic domain and also captures the exchange interaction of neighbouring spins in the nearest neighbours approximation of the Heisenberg exchange interaction [20-22].

2. The length of the specimen should be larger than the individual magnetic moments. So that the atomistic moments can be replaced by the continuous

function in space rather than a discrete representation by a set of magnetic moments at the atomistic level.

3.10 Static micromagnetics

The Brown's static equation forms the foundation of classical micromagnetics approach to stationary problems [12]. In a ferromagnetic body Browns' equation gives the minimum energy state (i.e. the equilibrium configuration) by minimizing the total energy. Different energies contribute to different effects on the magnetization during the minimization process. Upon minimization, the ferromagnetic exchange energy keeps the magnetic moments parallel to each other and the magneto-crystalline anisotropy aligns the magnetic moments along a preferred crystallographic directions. The minimization of the stray field leads to the formation of magnetic domains whereas the Zeeman energy rotates the magnetization parallel to the applied magnetic field. The total energy E_{total} of the system can be derived by

$$E_{total} = \int_V \left[\phi_{ex} + \phi_K + \phi_d + \phi_z \right] dV \tag{3.27}$$

Where in the equation (3.27) ϕ_K represents the anisotropy energy density of the system. In other form the total energy to be minimized can be written as

$$E_{total} = \int_V \left[\frac{A}{M_s^2} \left(\nabla^2 \boldsymbol{M} \right)^2 + \phi_K - \mu_0 \boldsymbol{M} \left(\boldsymbol{H}_{\boldsymbol{external}} + \frac{H_d}{2} \right) \right] dV \tag{3.28}$$

In the equation above $\boldsymbol{H}_{\boldsymbol{external}}$ represents the external applied field. The effective field of the system is given by the negative functional derivative of the total magnetic Gibbs free energy.

$$\boldsymbol{H_{eff}} = -\frac{\delta E_{total}}{\delta \boldsymbol{M}} \tag{3.29}$$

3.11 Dynamic micromagnetics

In data storage recording where fast switching of the magnetization of the magnetic grain is crucial, the time evolution of the magnetization is described by the LLG equation given below:

$$\frac{\partial \boldsymbol{M}}{\partial \tau} = -\frac{\gamma_0}{\left(1+\alpha_G^2\right)}\left(\boldsymbol{M}\times\boldsymbol{H}_{eff}\right) - \frac{\alpha_G}{\left(1+\alpha_G^2\right)}\frac{\gamma_0}{M_s}\boldsymbol{M}\times\left(\boldsymbol{M}\times\boldsymbol{H}_{eff}\right) \tag{3.30}$$

where γ_0 is the gyromagnetic ratio, α_G is the Gilbert damping parameter and $\boldsymbol{H_{eff}}$ is the local effective field given by equation (3.29). The first term in the equation describes the precessional motion of the magnetization vector. The second term accounts for the energy dissipation of the system, allowing the magnetization to align itself with the effective field.

The LLG equation can be reduced to a dimensionless form as follows [20, 29- 31]

$$\left(1+\alpha_G^2\right)\frac{\partial \boldsymbol{m}_{norm}}{\partial \tau} = -\left(\boldsymbol{m}_{norm}\times h_{eff}\right) - \alpha_G^2\boldsymbol{m}_{norm}\times\left(\boldsymbol{m}_{norm}\times\boldsymbol{h}_{eff}\right) \tag{3.31}$$

Where $\boldsymbol{m_{norm}} = \boldsymbol{M}/M_s$ is the normalized magnetization, $\boldsymbol{h_{eff}} = \boldsymbol{H_{eff}}/M_s$ is the normalized effective field, τ is the reduced time in $(|\gamma_0 / M_s)^{-1}$ with γ_0 being the gyromagnetic ratio. The magnetic field term $\boldsymbol{h_{eff}}$ contains the contribution of all the energies.

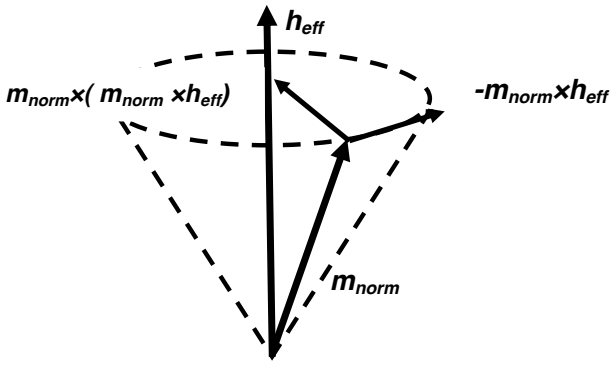

Figure 3.7: Schematic representation of precessional motion of magnetization as in LLG equation [22].

The graphic representation of the equation (3.31) is shown in figure 3.7, where the magnetization component $\boldsymbol{m_{norm}}$ precess along the effective field represented by the prcession term -$\boldsymbol{m_{norm}\times h_{eff}}$. During the precession the loss of the energy takes place which leads to the convergence of the precession of magnetization along the effective field. The higher the damping the faster is the convergence.

3.12 Nudged elastic band method

Thermal stability of nanomagnetic grains used for data storage is one of the physical limitations that have impeded the scaling of HDD. The thermal stability studies are done by calculating a minimum energy path between two stable magnetization states of a particle. This is done by using various approaches: Monte-Carlo, Berkov method of minimization of action [32] and nudged elastic band methods [33, 34]. The Monte-Carlo method is more common in the field of chemistry and the other two methods are used in micromagnetics modelling. In this project the nudged elastic band

method proposed by Henkelman and Jónsson along with the hybrid- finite element and boundary element method (FEM/BEM) [35] was used to study thermal effects in single-phase media and exchange spring media.

Hybrid-FEM/BEM efficiently calculates the total Gibbs free energy at every node of the discretized magnetic microstructure. The Gibbs free energy is integrated over the whole system to obtain the energy of the sample. The total Gibbs free energy defines the local minimum or equilibrium state of the magnetic system in the absence of thermal activation. Once temperature is introduced, the system receives extra energy, which disturbs the above-mentioned equilibrium state; hence it is required to add a term to account for thermal activation. The addition of this extra energy term leads to a shift of the local minima of the energy of the magnetic system. To evaluate the contribution, which arises from thermal effects, the nudged elastic band method is used along with the hybrid FEM/BEM.

The nudged elastic band method calculates the transition rates between the initial and final state of the system. The transition rates are obtained from the energy landscapes of the most probable paths chosen between the two stable magnetization states [34]. The most probable path connecting the two local minima is obtained by initially guessing the point and the path. After the initial guess, the point is moved along the path similar to the tensioning of an elastic band across a mountain. The minimum energy path (MEP) of the system is the path in which the energy gradient points in the direction of the path and its energy remains constant in all the degrees of freedom existing in the perpendicular direction to the path.

3.13 Calculation of the MEP

To calculate the path between the two stable magnetization states the calculation start from a randomly assumed path. The path is then varied in different directions and the energy gradient is determined. The path, in which the direction of the energy gradient point is a minimum, is chosen as the optimal path (*D*) and in mathematical terms is given by equation (3.32) [34].

$$D = -\left\{\nabla E\left(M_j\right) - \left(\nabla E\left(M_j\right)\cdot \boldsymbol{t}\right).\boldsymbol{t}\right\} \quad \text{for } j = 1, \text{n} \tag{3.32}$$

In the above equation M_j is the jth image of the path, ∇E is the energy gradient, and $\boldsymbol{t}$ is the tangent along the path. The property of the optimal path is that the transversal component of its energy gradient is always zero. To find the optimal path during iterations the path images are directed perpendicular to the initial or current path and towards the negative of the energy gradient. In numerical terms M_j is rotated parallel to D in the configuration space. While taking the consecutive images of paths, the distance between paths is kept constant in order to avoid kinks in the path. The equal distance between paths is ensured with the help of the variable method instead of the spring force technique as it results in an overestimation of the saddle point [31].

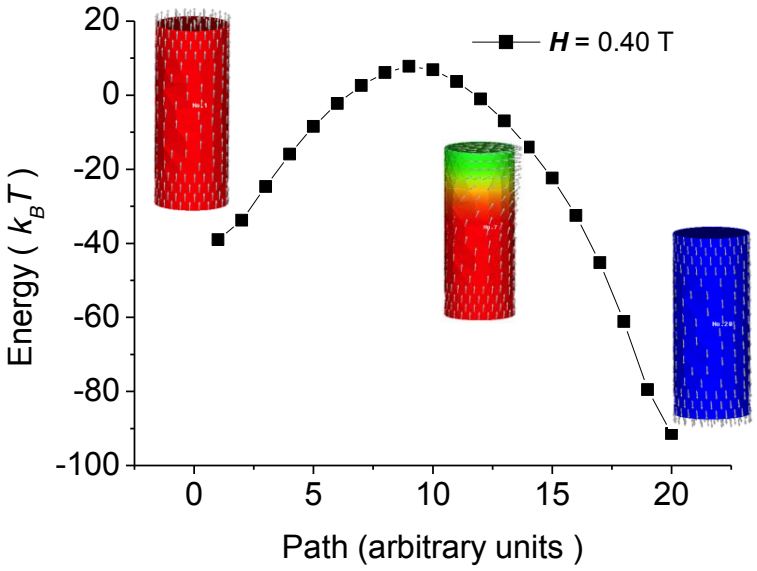

Figure 3.8: Shows the change in minimum energy path and magnetization configuration as a function of energy in units of k_BT for the ferromagnetic grain used in single-phase media, when the external field of 0.40 T is applied [22].

Figure 3.8 shows the minimum energy path obtained for the single-phase media grain in the presence of external field of 0.40 T. Starting from an energy initial configuration grain with all spin pointing up shown by the red coloured grain the NEB finds a minimum energy path shown by black curve to obtain the final magnetization configuration with all spin pointing downwards shown by blue coloured grain in the figure 3.8. The black curve between the initial (blue grain) and final (red grain) configuration is the minimum energy path or optimal path obtained with the help of NEB when the applied field 0.40 T. The energy barrier of the minimum optimal path is calculated and used to study the dynamics of the recording media at finite temperature as described in chapter 4.

3.14 Finite element and Boundary Element method

Since 1970s finite element modelling has become increasingly important in various areas of continuum mechanics, computational fluid dynamics and electromagnetic field computation etc. [36, 37]. The hybrid FEM/BEM approach offers a crucial advantage over the traditional FEM method; it reduces the size of the problem, by mapping the boundary conditions at infinity unto the surface of the problem domain. The main advantage of the hybrid FEM/BEM method is that it uses both the differential and integral equation approaches.

The Hybrid FEM/BEM method uses the finite element approach to solve the problem inside the sample region and BEM method outside the region. The BEM does not require a mesh outside the area of interest and therefore decreases the complexity of the problem when combined with FEM. FEM solves the partial differential equation (from equation 3.27 to 3.31 mentioned in the chapter above) on the irregular-shaped domain and keeps track of the granular microstructure [36, 38]. The hybrid FEM/BEM method is used in the calculation of the reversal dynamics and magnetization of the magnetic samples, which is done by calculating the total Gibbs free energy at every nodal point of the sample. The change in magnetization depends on different field energies namely, anisotropy, exchange, Zeeman and magnetostatic field. The magnetostatic field is calculated from the scalar potential by satisfying the Maxwell's equation from equation 3.6 to 3.14. The Maxwell equation gives the physical condition of the sample and provides the boundary conditions for the system.

3.15 Mesh Generation

First the geometry is discretized into small finite elements. Figure 3.9 shows an example of a regular triangulation of a domain of interest; the domain is divided into a set of connected basic elements.

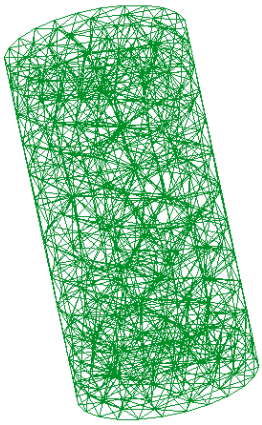

Figure 3.9: Grain sample with a mesh the domain of interest is divided into tetrahedrons (sample is meshed in GID).

In order to generate a mesh in FEM the following conditions defined by Ciarlet [38, 39] have to be taken into account.

- The basis function should have to be one at the point where the vertex of the mesh coincides.
- Every face on the body surface satisfies an essential boundary condition defined by the problem at hand.
- There should be no overlap between different elements of the triangulation.

To generate a mesh that captures all the features of our micromagnetic problem the size of the element or the length of the single mesh element has to be smaller or equal to the calculated exchange length, given be the following formula [38, 40]

$$l_{ex} = \sqrt{\frac{A}{K_1}} \tag{3.33}$$

Where A denotes the exchange constant; K_1 is anisotropy constant. If the anisotropy of the material is zero the following formula is used to calculate the exchange length.

$$l_{ex} = \sqrt{\frac{A\mu_0}{J_s}} \tag{3.34}$$

Where $\boldsymbol{J_s}$ is the magnetic polarization. The value to be entered needs to be little bit smaller than this exchange length value. FEM solves the quasi-static Maxwell's equation on the inner contour of the sample by differential equations and BEM solves them on and outside the artificial boundary with an integral approach, by taking care of the appropriate boundary conditions.

3.16 Magnetostatic field

In micromagnetics the most time consuming part is the calculation of the magnetostatic field. To solve this problem with a FEM/BEM approach first a set of equation with appropriate boundary conditions for the magnetostatic field from Maxwell equations needs to be derived. To do so the problems were separated into two parts, one that deals with the solution of the magnetostatic field inside the magnetic domain and one part that deals with the solution everywhere in space. This poses a problem when the boundary conditions are applied for the Maxwell equations. As outlined below, separation of solution into two parts end up with a

jump at the boundary, which has to be compensated with a boundary integral approach to guarantee the continuity of the field across the boundary, essential BC from Maxwell equations [41, 42].

In hybrid FEM/BEM the magnetic scalar potential U is divided into two parts [42].

$$U = U_1 + U_2 \tag{3.35}$$

Where the potential U_1 is the potential inside (Ω_{int} internal region) and on the boundary of the sample and potential U_2 belongs to the whole system (Ω_{int} and Ω_{ext} are the internal and external regions). The potential U_1 as calculated from the closed boundary condition by BEM [29, 43].

$$\nabla^2 U_1 (r) = \nabla . \boldsymbol{M}(r) \text{ for } \quad r \in \Omega_{int} \tag{3.36}$$

$$U_1 = 0 \text{ for } r \in \Omega_{ext} \tag{3.37}$$

The potential U_1 is zero outside the magnetic sample as it is the solution of the Poisson equation; which holds in and on the surface of the magnetic sample. The potential U_2 satisfies the Laplace equation and is valid all over the system.

$$\nabla^2 U_2(r) = 0 \qquad \text{for } r \in \Omega_{int} \cup \Omega_{ext} \tag{3.38}$$

On the boundary the potential shows a jump [36]. But as solution has to be continues across the boundary (condition from Maxwell equations), the jump was compensated by using a double layer potential approach, as described by Fredkin and Koehler [44].

Once the set of equations are derived, the micromagnetic method uses the Galerkin or Weak formulation to solve the set of partial differential equations [40].

In summary, the hybrid FEM/BEM approach in micromagnetics allows arbitrary geometries and therefore the modelling of real devices, like thin film recording media, permanent magnets, and MRAM.

3.17 Numerical integration and error control

3.17.1 Ordinary differential equations

The femme program uses in this study uses the CVODE package [45, 46] for solving both the LLG equation and for the differential equation defined by the nudged elastic band method

$$\frac{\partial \boldsymbol{M}_j}{\partial t} = D(\boldsymbol{M}_j) \quad \text{for } j=2,\ldots,n-1 \tag{3.39}$$

with $\boldsymbol{M}$ being the magnetization vector and D the optimal path as defined in equation (3.32). As the LLG and the static Maxwell equations are a set of differential equations and are an initial value problem, the LLG, see 3.31, can be expressed in a general form of an ordinary differential equation

$$\frac{\partial y}{\partial t} = f(t, y) \tag{3.40}$$

where y is equivalent to $\boldsymbol{M}$ and t being the time and the initial conditions are given as follows

$$y(t_0) = y_0, \frac{\partial y(t_0)}{\partial t} = \frac{\partial y_0}{\partial t} \tag{3.41}$$

There are different numerical integration methods used to solve ordinary differential equations (ODEs) used by CVODE i.e. Adams method and backward differentiation formula (BDF). The initial value problem is integrated using a backward differentiation formula (BDF) method implemented in a variable-order, variable-step

form. The method orders range from 1 to 5 and the BDF of order k is given by the following multistep equation with *n* being the time index

$$\sum_{i=0}^{k} \alpha_{n,i} y_{n-i} = h_n \frac{\partial y_n}{\partial t} \tag{3.42}$$

with $\boldsymbol{y_n}$ and $d\boldsymbol{y_n}/dt$ being the computed approximations of $\boldsymbol{y_n}(t_n)$ and $d\boldsymbol{y_n}(t_n)/dt$, and the step-size h_n is

$$h_n = t_n - t_{n-1} \tag{3.43}$$

The $\alpha_{n,i}$ are coefficients that are uniquely determined by the order k and the step-size history. Applying the BDF on the differential equation system results in a nonlinear algebraic system that is solved with a Newton-iteration.

$$\boldsymbol{G}(y_n) = F\left(t_n, y_n, h_n^{-1} \sum_{i=0}^{k} \alpha_{n,i} y_{n-1}\right) = 0 \tag{3.44}$$

Where $\boldsymbol{G}$ is a general function. This leads to a linear system for each Newton correction

$$\boldsymbol{J}\left(y_{n(m+1)} - y_{n(m)}\right) = -\boldsymbol{G}\left(y_{n(m)}\right) \tag{3.45}$$

where $y_{n(m)}$ is the m-th approximation to the $\boldsymbol{y_n}$ and $\boldsymbol{J}$ is the Jacobian of the system. Within CVODE the linear system for each Newton-step is solved either with a direct solver or with a Krylov subspace method. Krylov subspace methods have been explored in micromagnetics by Tsiantos et al. [47, 48]. The system (3.45) is solved with a scaled preconditioned generalized minimum residual (SPGMR) method [49].

For details on the finite element micromagnetics as implemented in the femme simulation package see [50, 51].

3.17.2 Error control

While the numerical system is integrating, it estimates a mean norm of the local

truncation error E_n at the n-th time step that has to satisfy the inequality

$$\|E_n\|_{wrsn} < 1 \tag{3.46}$$

and imposes a tolerance on local errors with the weighted root square norm (*wrsn*) with the following definition

$$\|E_n\| = \left[\frac{1}{N} \sum_{i=1}^{N} \left(\frac{E_n^i}{w^i} \right)^2 \right]^{\frac{1}{2}} \tag{3.47}$$

with the superscript *i* denoting the i-th component and w^i the i-th weight

$$w^i = rtol \left| y^i \right| + atol^i \quad \text{or} \quad w^i = rtol \left| y^i \right| + atol \tag{3.48}$$

The scalar relative error tolerance (*rtol*) and the absolute error tolerance (*atol*) are given by the user and permit to define an allowed error per step and thus a control of the magnitude of the error. In our simulations the *rtol* and *atol* was chosen to be *rtol*=*atol* = 1.0 e^{-6}.

All the simulations in the thesis are performed with the same relative and absolute error tolerance and repeated simulations give the same results within the error given above. Concerning the error in respect to discretization size of the finite element mesh and the stopping criteria for the NEB method please refer to the study done by Suess and Dittrich et. al. [50, 52], but the absolute and relative tolerance were $1.0e^{-6}$ and the gradient tolerance was $1.0e^{-3}$ for all of the NEB simulations.

References

1. H. Kronmuller, S. Parkin, Handbook of Micormagnetism, **2** (John Wiley & Sons, 2007).
2. L. D. Landau, and E. M. Lifshitz, Soviet Phys. Z **8**, 153 (1935).
3. W. F. Brown, Micromagnetics, Interscience New York **68** (1963).

4. P. A. M. Dirac, Proceedings of the Royal Soc. **117A**, 610 (1928).
5. W. Heisenberg, Zeitschrift fuer Physik. **49**, 619 (1928).
6. N. S. Akulov, Zeitschrift fuer Physik **67**, 794 (1928).
7. A. Aharoni, international series of monographs on physics, Oxford University Press 2 **109**, (2000).
8. R. Becker, and W. Doring, Ferromagnetisum, J. Springer, Berlin **1** (1939).
9. W. F. Brown, Magnetostatic Principles in Ferromagnetism, **1** (North– Holand Publishing Company, 1962).
10. W. F. Brown, Phys Rev. **130**, 5 (1963).
11. W. F. Brown, IEEE Trans. Magn. **15**, 5 (1979).
12. W. F. Brown, Micromagnetics, **2** (New York: R.E. Krieger, 1978).
13. W. F. Brown, IEEE Trans. Magn.**15**, 5 (1979).
14. C. Kittel, Rev. Mod. Phys. **21**, 541 (1949).
15. C. Kittel, and J. K. Galt, Solid State Phys. **3**, 437 (1956).
16. E.C. Stoner, and E.P. Wohlfarth, Phil. Trans. R. Soc. Lond. A **240,** 599 (1948).
17. L. Neel, Cahiers de Physique **25**, 63 (1944).
18. L. Neel, Annales Uni. Grenoble **22**, 299 (1946).
19. L. Neel, Complete works A **45**, 269 (1978).
20. T. Schrefl, J. Magn. Magn. Mater. **207**, 1-3 (CNRS publications, 1999).
21. J. Fidler, R. W. Chantrell, T. Schrefl, M. Wongsam, and J. Fidler, Encyclopedia of Materials: Science and Technology, Elsevier ed. **1** (2001).
22. T. Schrefl, G. Hrkac, S. Bance, A. Goncharov, J. Fidler and D. Suess, Magn. Mater. Research signpost **3,** 33 (2007).
23. T. Kasuya, Progress of Theoretical Physics, (Kyoto) **16**, 45 (1956).

24. M. D. Aquino, “Nonlinear magnetization dynamics in thin films and nanoparticles” Ph. D. thesis, Universitá Delgi Studi Di Napoli Federico II (2004).
25. L. Jehyun “Inhomogenous magnetization processes in advanced recording media” Vienna University of Technology (2011).
26. H. Kronmüller, M. Fähnle, Micromagnetism and the Microstructure of Ferromagnetic Solids, (Cambridge Uni. Press, 2003).
27. G. Hrkac, PhD thesis “Combing eddy–current and micromagnetic simulations with finite element method,” (2005).
28. C. Tannous, and J. Gieraltowski, Eur. J. Phys. **29**, 475 (2008).
29. J. M. D. Coey, Magnetism and magnetic materials, (Cambridge Uni. Press, 2010).
30. T. Gilbert, IEEE Trans. Magn. **40**, 6 (2004).
31. G. Hrkac, T. Schrefl, S. Bance, D. Allwood, A. Goncharov, J.Dean, and D. Suess, J. Magn. Magn. Mater. **320**, L111 (2008).
32. D. V. Berkov, J. Magn. Magn. Mater. **186**, 1-2 (998).
33. R. Dittrich, T. Schrefl, D. Suess, W. Scholz, H. Forster, and J. Fidler, J. Magn. Magn. Mater. **250,** L12 (2002).
34. R. Dittrich, T. Schrefl, M. Kirschner, D. Suess, G. Hrkac, F. Dorfbauer, O. Ertl, and J. Fidler, IEEE Trans. Magn. **41**, 10 (2005).
35. G. Henkelman, and H. Jónsson, J Chem. Phys. **113**, 22, (2000).
36. R. W. Chantrell, J. Fidler, T. Schrefl, and M. Wongsam, Encyclopaedia of Materials: Science and Technology, K. H. J. Buschow, R. W. Cahn, M. C. Flemings, B. Ilschner, E. J. Kramer, S. Mahajan (eds.), Elsevier, 5651 (2001).
37. J. Fidler and T. Schrefl, J. Phys. D Appl. Phys. **33**, 4 (2000).
38. T. Schrefl, G. Hrkac, S. Bance, A. Goncharov, J. Fidler and D. Suess; Magnetic material: current topics in amorphous wires, hard magnetic alloys, ceramics,

characterization and modelling-Micromagnetism of nanoscale materials, ch. 3 Research signpost (2007).

39. P.G. Ciarlet, The finite element method for elliptic problems, Amersterdam, New York, Oxford: North Holland, (1978).
40. FEMME, Finite element Micromagnetics, ch. 1, User guide-version **4.6**.
41. T. Schrefl, J. Magn. Magn. Mater. **207**, 1-3 (1999).
42. I. S. Grant, and W. R. Philips, "Electromagnetism," Maxwell's equations- ch. 10, second ed. (Wiley Pub., 1990).
43. T. Schrefl, J. Fidler, K. J. K. John, and N. Chapman, IEEE Trans. Mag. **33**, 5 (1997).
44. D.R. Fredkin and T.R. Koehler, IEEE Trans. Magn. **26**, 2 (1990).
45. S. D. Cohen and A. C. Hindmarsh, CVODE User Guide, Lawrence Livermore National Laboratory report UCRL-MA-118618, Sept. (1994).
46. S. D. Cohen and A. C. Hindmarsh, CVODE, Computers in Phys. **10**, 138 (1996).
47. V. Tsiantos, Numerical methods for ordinary differential equations in micromagnetic simulations, Ph.D. Thesis, University of Manchester (2000).
48. V. D. Tsiantos, T. Schrefl, J. Fidler, and A. Bratsos, Applied Numerical Mathematics **39,** 2 (2001).
49. P.N. Brown, A.C, Hindmarsh, and L.R. Petzold, SIAM J. Sci. Comput. (USA) **15**, 1467 (1994).
50. D. Suess, Micromagnetic simulations of antiferro- and ferromagnetic structures for magnetic recording, PhD thesis, Vienna University of Technology (2002).
51. D. Suess, V. Tsiantos, T. Schrefl, J. Fidler, W. Scholz, H. Forster, R. Dittrich, J. Miles, J. Magn. Magn. Mater. **248** (2002).

52. R. Dittrich, "Finite element computation of energy barriers in magnetic systems", Ph.D. thesis, Vienna University of Technology (2003).

Chapter 4: Micromagnetic study of switching field and grain boundary interaction in single-phase media

4.1 Abstract

A finite element micromagnetic [1] study has been undertaken to describe the importance of thermal effects and grain boundary interaction effects in the magnetization reversal dynamics of segregated CoCrPt-oxide perpendicular recording media as function of angle of applied field. First the switching field study for CoCrPt columnar grain was performed as a function of grain thickness in the absence and presence of thermal effects. Quantitative and qualitative comparison of the switching field curves was performed to understand the thermal effect on the magnetization reversal of the grain. At zero temperature the results were similar to the Stoner-Wohlfarth model and the magnetization reversal showed no change with the varying thickness of the grains. The presence of thermal effects led to a large change in the switching field value of the grain while the magnetization reversal curve showed a shift in the minimum with a change in grain thickness. Furthermore as the aim of the research conducted here was to use a simplified one grain model to study absolute switching field values that so far are not captured by conventional micromagnetic approaches, it was decided to incorporate more complex features like the interaction between the magnetic core and the oxide layer surrounding the ferromagnetic grain are included in the single-phase media at room temperature. The grain boundary interactions were found to affects the switching field value of the core/shell grain as compared to the bulk grain significantly.

4.2 Thermal effects and switching field

Micromagnetics simulations were used to study the switching field of nanoscale cylindrical magnetic grains under the influence of an external field at zero and finite temperatures. The Stoner-Wohlfarth model is the theoretical model that describes the switching of single domain particles as a function of applied field angle at zero temperature [2]. At finite temperatures magnetization switching mechanisms have been widely studied experimentally and theoretically [3-6] but are not well understood. Recently, the recording industry has approached the fundamental superparamagnetic limits of magnetic grains in existing storage media, indicating the importance of thermal effects as magnetic grains are scaled to smaller dimensions. Introduction of temperature induces thermal excitation inside the magnetic grains, which causes fluctuations and changes in the magnetization direction. If the thermal effects are too high they may cause the magnetic grain to switch by overcoming the energy barrier and results in an unreliable information storage. Thermal effects are even more important when the magnetic particle is scaled further down, towards 4-8 nm. To get a better understanding of these limits, a thermal stability study was performed with the help of the nudged elastic band (NEB) method. The NEB method provides the information on the energy barrier from which the switching field can be calculated at a particular temperature and measurement time.

4.2.1 Model

To determine the effects of grain thickness and thermal activation on the switching field and magnetization reversal process, a single-phase cylindrical grain with uniform material properties was simulated. The material properties,

magnetocrystalline anisotropy constant K_1, exchange constant A and magnetic polarization J_s of the grain at different temperatures are and its dimensions summarized below in table 4.1.

Diameter (nm)	Height (nm)	K_1 (MJ/m^3)	J_s (T)	A (J/m)
8	6	0.58	0.90	1×10^{-11}
8	11	0.58	0.90	1×10^{-11}
8	16	0.58	0.90	1×10^{-11}

Table 4.1: The material parameters used in the single grain simulations. The material parameters magneto-crystalline anisotropy K_1 and magnetic polarisation J_s were determined from measurements and the exchange constant A were taken from literature [7].

To study the angular dependence of the switching field, the switching field was calculated at different angles of the applied field. The switching field for the grain can be calculated by two methods, discussed below:

4.2.2 Method 1: Switching field at zero temperature

In the first method the angular dependence of the switching field was calculated by solving the Landau-Lifshitz-Gilbert (LLG) equation explained in chapter 3 in section 3.11 at zero temperature. The external field was applied to switch the grain and the equilibrium magnetization state of the system was obtained. The field was increased consecutively until the grain magnetization is fully switched. The external field was ramped till it reaches its maximum at 0.1 ns and was kept constant after that, as

shown in the figure 4.1. Although the field strength was varied, the same field profile was used for all grains. The LLG micromagnetic method gives the equilibrium magnetization state of the system at the applied field. The minimum field required to switch (from $+m_z$ to $-m_z$) and to obtain the equilibrium magnetization state in the same direction i.e. $-m_z$ is called the switching field of the grain.

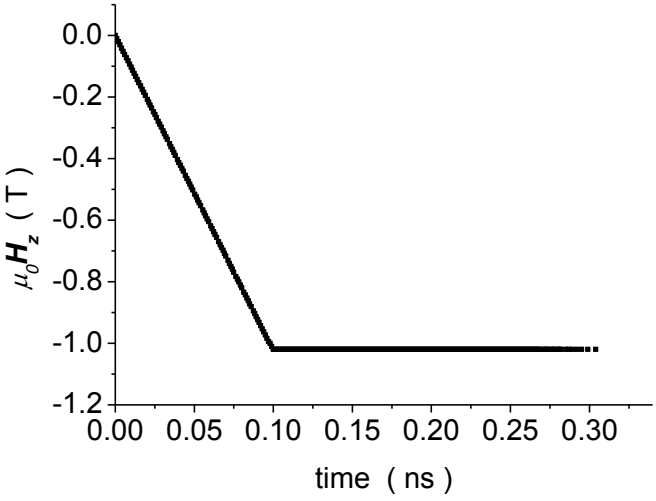

Figure 4.1: The applied field as a function of time for a grain with a diameter of 8 nm and a height of 16 nm (at $T = 0$).

4.2.3 Method 2: Switching field at finite temperatures

The calculation of the switching field at elevated temperatures was a three-step process. In the first step, the LLG micromagnetic model was used to determine the two stable magnetic states in which the projection of the total magnetization onto the easy axis (z-direction) is either positive or negative.

In the second step, the NEB method was used to calculate the energy barrier between the two pre-calculated stable magnetization configurations. The product of the anisotropy and volume of the grain i.e. *KV* defines the grain's energy barrier. To switch its magnetization direction, the magnetic grain needs to overcome the energy barrier between the two magnetization configurations shown in figure 4.2. In the magnetic recording process the field coming from the write head supplies the extra energy required to overcome the energy barrier.

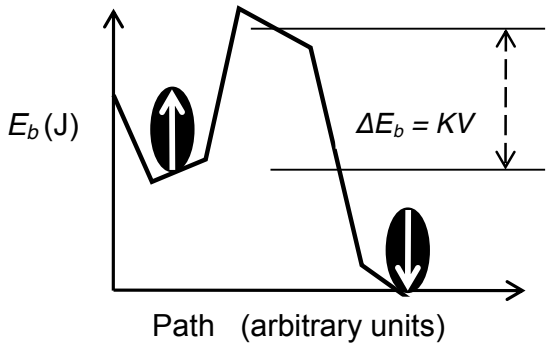

Figure 4.2: Shows the energy barrier between the initial (spin up) and the final (spin down) magnetization configuration.

The thermal stability calculation requires the information of the transition rates between the initial and final magnetization configuration of the magnetic grains. The NEB method [3, 4] initially guesses the minimum energy path (MEP) in the energy landscape between the two stable magnetization states. In order to obtain the MEP the energy is minimized until the energy gradient of the path points along the current path and the energy is constant along the path for any degree of freedom

perpendicular to it. The MEP calculation provides an energy barrier $E_b(\boldsymbol{H})$ of the transition in units of k_BT (k_B = 1.3806503 10^{-23} J K^{-1} is the Boltzmann constant and T is the temperature) between the initial and final magnetic configurations of the grain at any given applied field and field angle. The energy barrier is directly associated with the thermal stability of the system, shown in figure 4.3 is an example curve of energy barrier $E_b(\boldsymbol{H})$ as a function of the external applied field for a cylindrical media grain with aspect ratio 8:11. The curve is used to extract the switching field of the grain as explained briefly in the next paragraph.

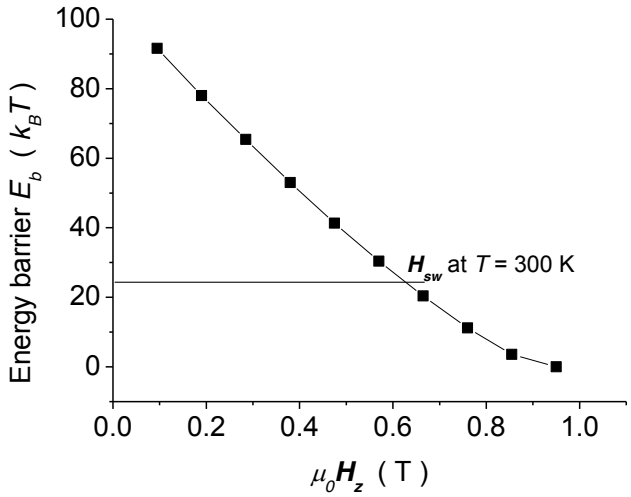

Figure 4.3: An example curve of energy barrier as a function of external applied field. H_{sw} in the graph describes the switching field for an energy barrier value of 25 k_BT.

In the third step, the switching field at temperature T, for a particular applied field angle was calculated from the energy barrier [3]. The switching field value for the grains depends upon the energy barrier, the attempt frequency and the

measurement time for which the field was applied in accordance with the Arrhenius–Neel law.

$$\tau = \frac{1}{f_0} exp^{-\frac{E_b}{k_B T}} \tag{4.1}$$

where τ is the average time required for the grain to switch in the presence of the field in seconds and f_0 is the attempt frequency in Hz. The attempt frequency depends on the material parameters, damping constant, shape and size of the grain, and is normally taken to be in the range of 10^9-10^{12} Hz for the CoCrPt material used here [8-11].

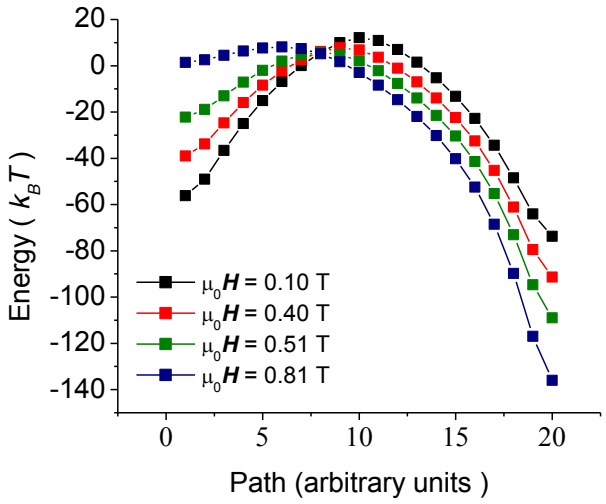

Figure 4.4: The energy along the lowest energy barrier path between the two minima for a grain of 8 nm diameter and 11 nm thick during magnetization reversal at an applied field angle of 20 degrees. The different curves show the change in the energy path for a range of applied field values at T = 292 K.

Using the computed energy barriers at a range of $\boldsymbol{H}$ values we fit a curve $E_b(\boldsymbol{H})$. The switching field at a given temperature T is the value of $\boldsymbol{H} = \boldsymbol{H_{sw}}$ ($\boldsymbol{H_{sw}}$ is the switching field) such that $E_b(\boldsymbol{H_{sw}}) = E^*$, with $E^* = k_B T \ln(\tau f_0)$ where τ is the time for which the field is applied.

Figure 4.4 shows the energy along the minimum energy path between the two stable magnetization states of the single-phase medium with diameter 8 nm and height 11 nm (8:11 aspect ratio) and material parameters from table 4.1. The energy barrier of the grain decreases from 68.30 $k_B T$ to 6.70 $k_B T$ when the field increases from 0.11 T to 0.81 T. For a measurement time of 10 seconds and assuming $f_0 = 10^{10}$ Hz, the critical barrier height is taken as $E^*/k_B T = 25$ as below which the grain becomes superparamagnetic in nature.

4.2.4 Angular dependence of the switching field at zero temperature

In the first step a single-phase grain with a cylindrical geometry is studied with bulk material properties. Grains with the following three thicknesses were considered for the study: 6 nm, 11 nm and 16 nm. The reversal behaviour of the magnetization of the single-phase media was studied as a function of the angle between the easy axis of the grain and the applied magnetic field. The switching field increases with the thickness as expected as the energy barrier of the grain increases with the volume of the grain as shown in the example curve in figure 4.5 for an applied field angle of 0.5 degree. By increasing the thickness of the grain from 6 nm to 11 nm the switching field shows an increase by approximately 6.8 %, while increasing the thickness from 11 nm to 16 nm the increase in the switching field is 4.8 %.

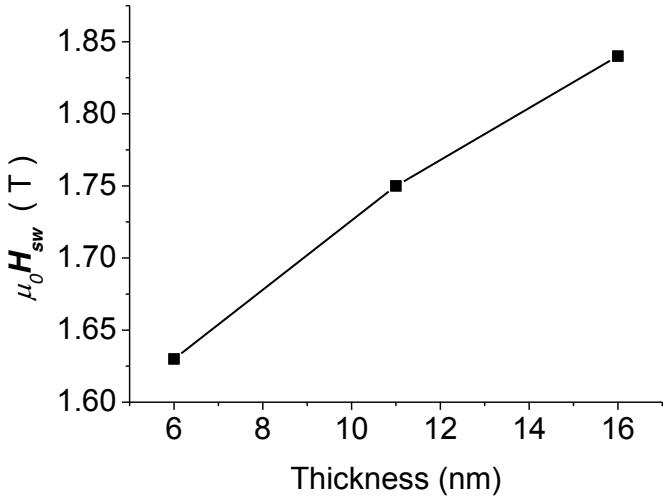

Figure 4.5: The switching field as a function of thickness at the applied field angle of 0.5 degree.

As far as the magnetization switching behaviour of the grain is concerned figure 4.6 (a) and (b) shows the switching field and normalized switching field of the grains with three different thicknesses as a function of applied field angle respectively. The switching field decreases with the decrease in the thickness of the grain. Figure 4.6 (b) also compares the magnetization reversal of the grain with Stoner-Wohlfarth curve. The results show that the switching field for all grains decreases first with the increase in the applied angle to 45 degree and for values above the switching field starts to increase again. The normalized angular dependence of the switching field of the single-phase was found to be similar to the Stoner-Wohlfarth particle as shown in figure 4.6 (b).

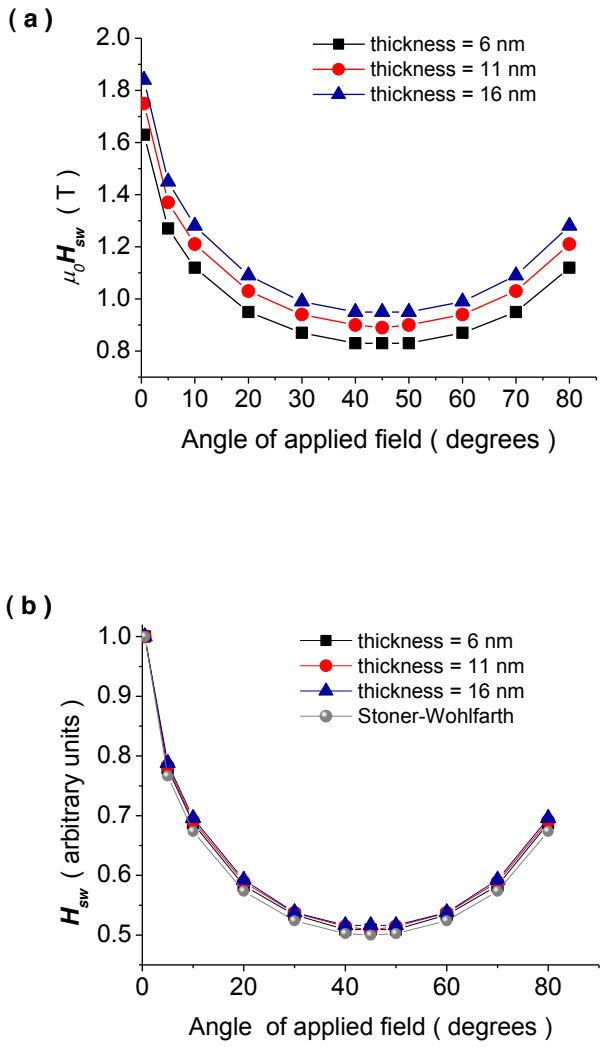

Figure 4.6: The (a) switching field and (b) normalized switching field of the single-phase media CoCrPt grain of constant diameter of 8 nm and variable thickness in the range 6 nm - 16 nm with respect to the change in the angle between the easy axis of the grain and applied magnetic field. The grains show the Stoner-Wohlfarth type switching behaviour irrespective of difference in the total volume of the grains.

The angular dependence of the switching field for all grains with different aspect ratios follows the same trend indicating a similar switching behaviour. The fact that the switching behaviour shows the Stoner-Wohlfarth like switching curve indicates

that the grains behaves like a single domain particle. All grains switches by coherent or uniform magnetization rotation, which is good for their application in recording as shown in figure 4.6.

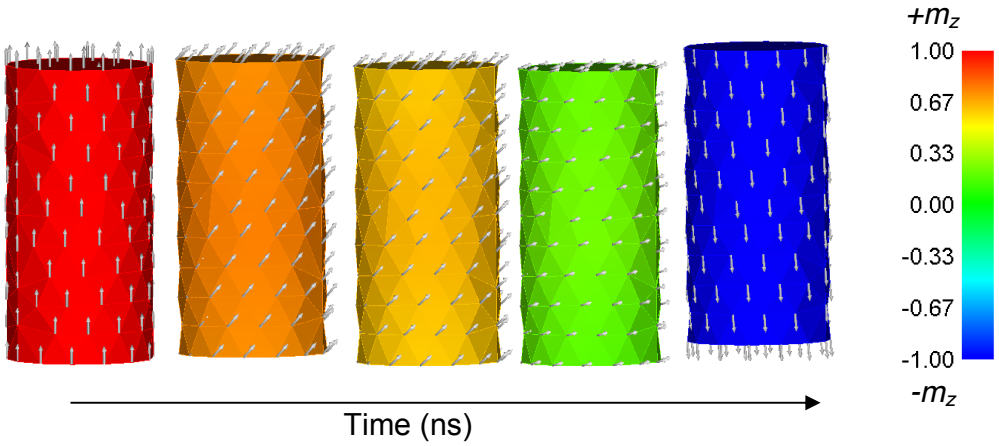

Figure 4.7: The uniform magnetization reversal of the grain with diameter 8 nm and height 16 nm. The different colour represents the different magnetization states of the grain at different time. The colour scale gives the magnetization value of the grain. The red colour shows the initial state of the grain with its magnetization pointing upwards whereas the blue grains represent the final configuration of the grain with its magnetization pointing downwards.

Figure 4.7 shows the magnetization reversal of the magnetic grain with aspect ratio 8:16 in the presence of the external applied field. The different colours of the grains represent different magnetization configuration attained during the reversal process, red and blue colour shows the initial and final configuration of the grain with their spin pointing up and down as shown by the direction of the arrows. The same colour over the whole grain indicates that the grain switches its magnetization through a uniform magnetization reversal process similar to that of a single domain particle.

The fact that the grain switches as a single domain particle is also supported by the magnetization reversal curve of all the grains is similar to Stoner-Wohlfarth (grey colour) in figure 4.6 (b) irrespective of the change in their thickness. An important point to consider here is that these simulations were carried out in the absence of temperature, which is a very important factor to be considered while determining the stability of the real media.

4.2.5 Angular dependence of switching field at room temperature

In order to increase the areal density of the hard disk drives there has been a continuous focus on the reduction of the thickness of the magnetic grains. While scaling the magnetic grains to smaller dimensions the thermal effects start to influence the magnetization behaviour of the magnetic grains at finite temperatures. To study the effect of thermal fluctuation on the varying thickness, the grains with diameter 8 nm and height 6 nm, 11 nm and 16 nm were considered. Figure 4.8 (a) shows the absolute switching field of the considered grains as a function of the applied field angle, whereas figure 4.8 (b) gives the normalized switching field as function of the applied field angle for the same grains, in other words figure 4.8 (b) is the graphical representation of the magnetization reversal process purely at finite temperature regime. The trend of angular dependence of the switching field as a function of applied field angle shown in figure 4.8 indicates the importance of the temperature during the magnetization reversal of the magnetic grains. Due to the presence of thermal effects, the angular dependence of the switching field due to applied field angle has reduced considerably as compared to the switching field of figure 4.6 i.e the $\mu_0 \boldsymbol{H_{sw}}$ for 6 nm in absence of thermal effects at 45 degree is 0.83 T

and in the presence of the thermal activation $\mu_0 \boldsymbol{H_{sw}}$ is 0.17 T, in total the $\boldsymbol{H_{sw}}$ has shown a reduction of 79 %. Due the impact of the thermal activation the angular dependence switching field curve has flattened from the bottom for the grain with a thickness of 6 nm. In the presence of thermal excitation, the grain receives energy from the thermal energy and the external field. As a result of the extra contribution from the thermal activation, the grain switches at lower external field values.

The contribution of the thermal energy helps the grain to switch its magnetization at lower field values, which is accompanied by the lowering of the angular dependence of the switching field curve with an increase in temperature. At room temperature, the grain with a height of 11 nm remains stable with $\mu_0 \boldsymbol{H_{sw}}$ (45°) = 0.48 T, whereas the grain with a thickness of 6 nm starts to switch at field values close to zero with $\mu_0 \boldsymbol{H_{sw}}$ (45°) = 0.17 T. This indicates that the grain with a small volume becomes thermally unstable at higher temperatures. Meaning, the magnetization reversal of small grains is mainly driven by thermal effects. Making small volume grains unstable as compared to the larger volume grains, because of its lower energy barrier, which is a function of volume. Figure 4.9 shows the non-homogenous magnetization reversal of the thicker grain at room temperature. The incoherency in the magnetization reversal in the grains is also indicated by the fact that the normalized switching curve of the grain shows clear deviation from the Stoner-Wohlfarth curve in terms of magnitude though follows the same trend shown in figure 4.8 (b). The shift in the minimum of the normalized curve is approximately 26 % as compared to the Stoner-Wohlfarth model, $\boldsymbol{H_{sw}}$ (0)/$\boldsymbol{H_{sw}}$(45°) = 0.5 whereas for the 6 nm thick grain it is at 0.68.

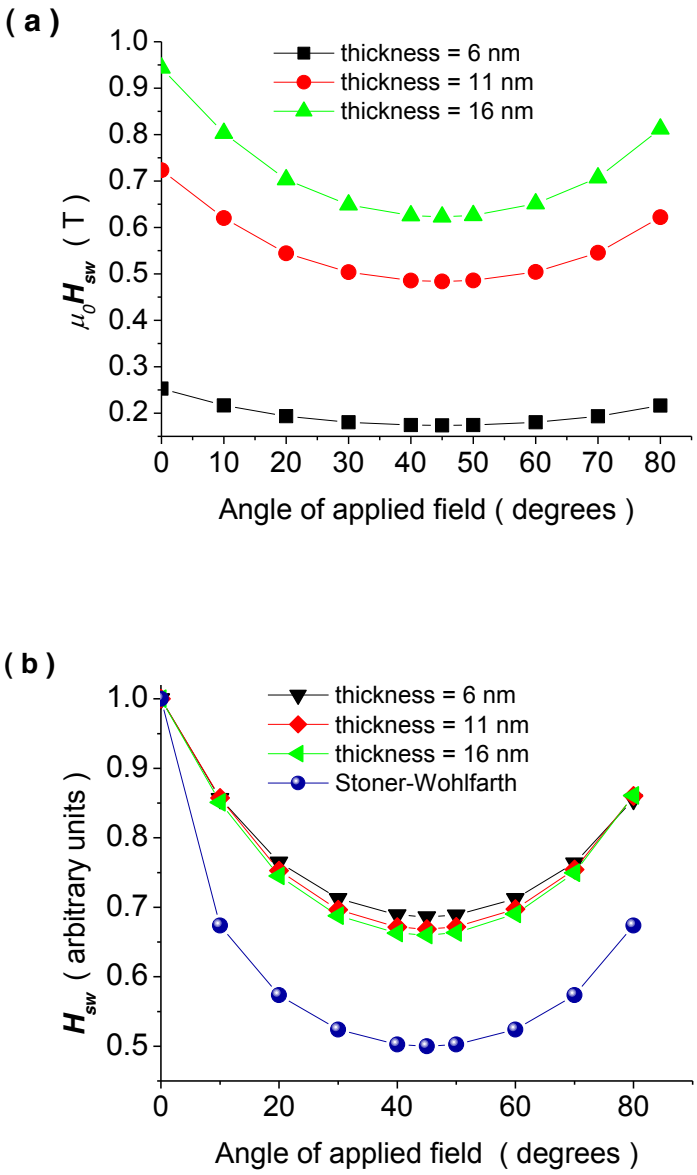

Figure 4.8: The (a) switching field and (b) normalized switching as a function of the applied field angle with f_o = 10^{10} Hz and τ = 10 seconds for the CoCrPt grain with diameter 8 nm and thickness 6 nm, 11 nm, 16 nm at room temperature represented by square circle and triangle respectively.

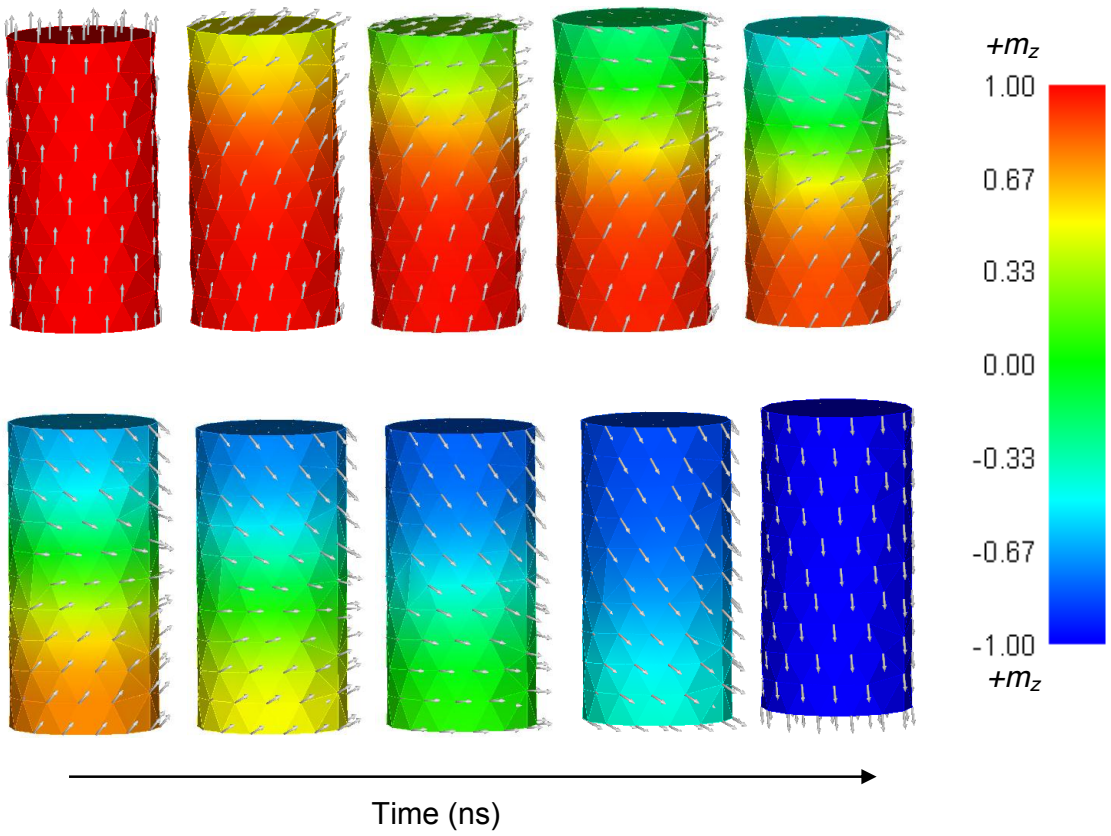

Figure 4.9: The non-uniform magnetization reversal of the grain with diameter 8nm and thickness 16 nm. The different colour represents the different magnetization states of the grain at during the magnetization reversal of the grain. The colour scale gives the magnetization value of the grain. The red colour shows the initial state of the grain with its magnetization pointing upwards whereas the blue grains represent the final configuration of the grain with its magnetization pointing downwards.

The fact that the grain's normalized switching field deviates from the Stoner-Wohlfarth indicates that the grain is not switching its magnetization as a single domain particle, meaning the magnetization reversal is non-uniform in the grain in the finite temperature regime all shown in figure 4.9. The deviation from the uniform or coherent magnetization reversal is explained by the presence of the thermal activation in the system. As the grain thickness decreases from16 nm to 6 nm

thermal activation starts to play role in the magnetization switching process of the grains due to which the grain switches at switching field values. As far as the magnetization reversal of the grains is concerned the difference in the curves with the varying thicknesses in figure 4.8 indicates that the grain's magnetization reversal process as non-homogenous. The results also show that the minima of reversal curves shift downward, meaning the normalized switching field at 45 degree decreases with the increasing grain thickness i.e. for the 6 nm grain at T = 300 K, $\boldsymbol{H_{sw}}$ (0)/$\boldsymbol{H_{sw}}$(45°) = 0.68, for 11 nm $\boldsymbol{H_{sw}}$ (0)/$\boldsymbol{H_{sw}}$(45°) = 0.66 and 16 nm $\boldsymbol{H_{sw}}$ (0)/$\boldsymbol{H_{sw}}$(45°) = 0.66.

The comparison between figure 4.6 and 4.8 indicates that the small grain with an anisotropy value of 0.5 MJ/m^3 is not a good candidate to be considered for a reliable data storage layer i.e. for the 6 nm grain at T = 0 K, $\mu_0\boldsymbol{H_{sw}}$ (10°) = 1.1 T, while at T = 300 K, $\mu_0\boldsymbol{H_{sw}}$ (10°) = 0.22 T, which is a change of 80 % with the addition of temperature. The study done on the grain with the bulk material properties shows that the thermal effect starts to dominate the magnetic system at small dimensions most commonly known as the superparamagnetic effect for example the grain of thickness 6 nm is close to superparamagnetic limit. The superparamagnetic limit is very crucial while modelling magnetic recording media. The instability of grains at smaller dimensions has limited the conventional perpendicular media to achieve higher areal density. For further the scaling it is very important to perform more in-depth studies of the sensitivity of grains switching field value on other factors like grain diameter, attempt frequency and finite temperature range and the interaction at the grain boundaries between the grain and SiO_x present in the real recording media.

4.2.6 Summary

The magnetization reversal in data storage thin films with varying thickness in the absence and presence of temperature is studied. The investigation undertaken show that the path methods approach successfully captures the effect of thermal effects in the system. In the absence of thermal effects the LLG model shows an increase in the switching field of grains with increasing thickness, whereas the normalized curve of the grains is similar to the Stoner-Wohlfarth model, indicating that all the grains are stable and act as single domain particles. Despite of the change in the overall volume due to the variation in thickness all grains switch their magnetization in a similar fashion. But once thermal fluctuations were introduced in the system, the angle dependency of the switching field was modified, deviating from the Stoner-Wohlfarth behaviour (magnitude of the switching field values). These results show that temperature plays an important role in determining the quantitative switching field and its angular dependence as a function of the angle of the applied field. In addition it was observed that at finite temperatures the normalized switching field curve shift its minimum with a change in the thickness of the grain and follows the Stoner-Wohlfarth trend. The smaller grains are found to be thermally unstable. The study indicates that to increase the thermal stability of the grain, high anisotropy materials are required, but their use is limited by the available write field.

Based on the study above the grain with a stable regime was chosen for the further investigation. As the main aim of the research conducted here was to model a simplified one grain model to study the switching behaviour in the regime that so far was captured by the conventional micromagnetic approaches it was decided to incorporate more complex features such as grain boundaries that are based on

interaction matrices between magnetic and non-magnetic systems at the room temperature as explained below in the next sub-chapter. This separate study is very important as Lister's and Thomson's experimental results from the University of Manchester (UoM) were used to validate our model systems in the later chapters and probe to which extend intrinsic effects like grain boundaries influence the switching field and switching mechanism of magnetic grains. This investigation gives a trend in what to expect if irregularities, such as defects, diffusions and impurities are present in magnetic grains, close to the superparamagnetic limit.

4.3 Boundary interaction in the single-phase media

Lister et. al. [12] shows in his study on CoCrPt-SiO_2 data storage layers, using a small angle polarised neutron scattering (SANS-pol) and transmission electron microscopy (TEM) technique, that there is a radial variation of the magnetic material distribution of the individual grains. The study was done to understand the influence of the magnetic structure of such grains on the magnetic properties of the data storage layer. This is important because the magnetic structure of the recording layer determines the characteristic switching behaviour of the recording layer. Nowadays, the length scale of grains in the storage layer is in the range of 7-10 nm. At this length scale, recording behaviour of materials critically depends on the relation between the magnetic and granular structure of the storage layer. Previous micromagnetic studies done on recording media treats the magnetic grain as a bulk material and does not consider irregularities that are present on the boundary of the grains [12-22]. Presented here is a finite temperature micromagnetic study done on the CoCrPt based single-phase media, which focuses on the understanding of the

interaction between the core and the oxide present around the grain and their effect on the magnetization reversal of the magnetic grains.

4.3.1 Model

The perpendicular magnetic layer consists of small magnetic grains with a uniform high anisotropy oriented perpendicular to the platter. In the experiments done at the UoM and therefore in this numerical study, a CoCrPt alloys was used, which gave an anisotropy in the MJ/m^3 regime. This section presents some basic investigations done on CoCrPt alloys, with different magnetic grain geometries. In order to understand the influence of the boundary phase on the switching behaviour of the magnetic grains two types of grains were studied having the following lateral parameters: diameter of 8 nm and thickness of 11 nm.

Figure 4.10: The CoCrPt grain used for the study in case 1. The diameter of the grain is kept constant at 8 nm and the thickness 11 nm. The material parameters are kept constant over the volume of the grain.

Case1: A single-phase material with uniform material properties as shown in figure 4.10. The material properties in this case used are measured by Prof. Thomson's group at the University of Manchester are as follows: magnetocrystalline anisotropy constant K_1 = 0.5 MJ/m^3, exchange constant A = 1×10^{-11} J/m and magnetic polarisation $\boldsymbol{J_s}$ = 0.75 T [23].

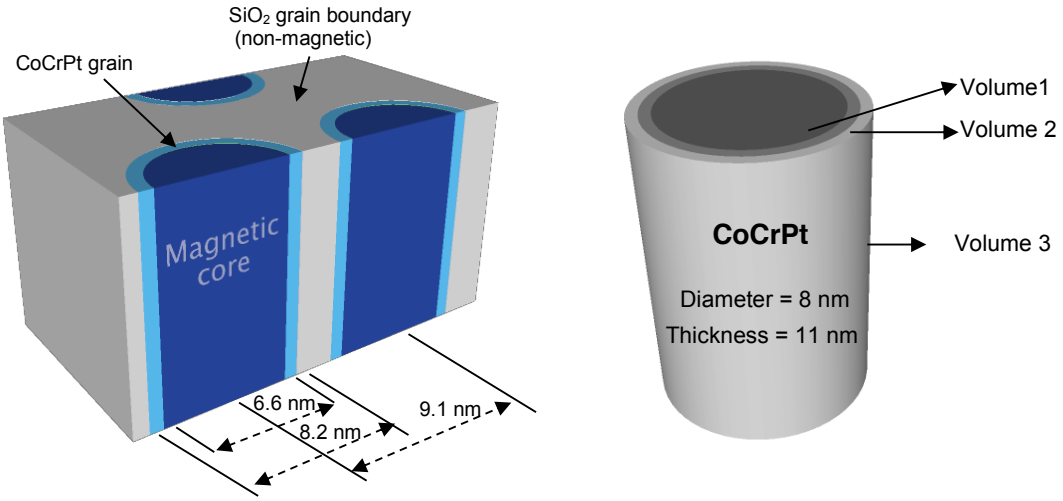

Figure 4.11: (a) sketch of the magnetic structure of the grain proposed by Lister et. al. [12] with the help of SANS-pol technique. (b) micromagnetic model of grain of case 2: divided into three volumes represented by three different colours and has a total radius of 4 nm and thickness 11 nm. Volume 1: is the magnetic core with a radius of 3 nm with magnetic bulk properties. Volume 2: has a lateral expansion of 0.5 nm and have 20 % of the magnetic bulk properties. Volume 3: has a lateral expansion of 0.5 nm and have 10 % of the magnetic bulk properties.

Case 2: The grain structure in this case study is modified according to the results obtained by Lister et. al. on the CoCrPt-SiO_2 recording layer by using the SANS-pol techniques. He showed that the magnetic grains in the data storage layer are surrounded by a non-magnetic oxide (SiO_2) layer and in order to keep account of the interaction between the magnetic core and the oxide layer, material parameters given to the grain are decreased over the boundary of the grain. As in the experiment, the magnetization of magnetic grain is expected to decrease gradually instead of showing a sharp transition from the magnetic state within the boundary to non-magnetic state at the boundary of grain [12].

To study this effect, the volume of the grain is divided into three parts (Volume 1 to 3); the different magnetic properties are indicated by different colours, see figure 4.10. Volume 1 is the magnetic core and has bulk material properties (like in case 1). Volume 2 is the surrounding layer of the core with the following material parameters: K_1 = 0.375 MJ/m^3, A = 0.5 x 10^{-11} J/m and $\boldsymbol{J_s}$ = 0.56 T. Whereas the outer volume (volume 3) has the following material parameters: K_1 = 0.125 MJ/m^3, A = 0.5 x 10^{-11} J/m and $\boldsymbol{J_s}$ = 0.14 T [23].

The anisotropy of the grain is reduced at the boundary of the grain as shown in figure 4.12, which accounts for crystal distortions in the CoCrPt grain boundary. The diffusion of the non-magnetic SiO_2 into the CoCrPt grain at the boundary is accounted by varying the magnetic polarization as shown in figure 4.13. The exchange constant is kept constant at 0.5 x 10^{-11} J/m at the shell and boundary of the ferromagnetic grain.

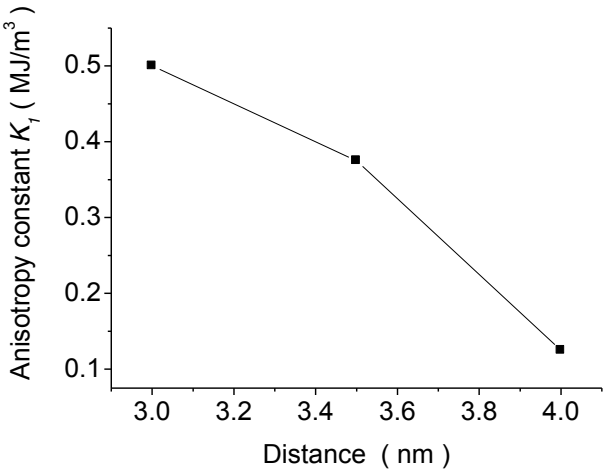

Figure 4.12: The anisotropy constant as a function of distance from the centre to boundary of the grain of case 2.

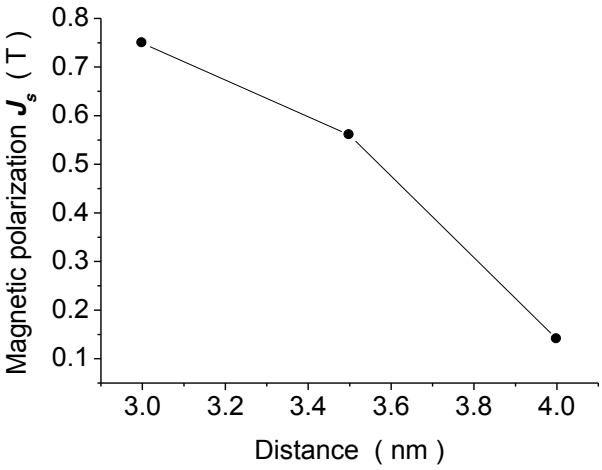

Figure 4.13: The magnetic polarisation as a function of distance from the centre to boundary of the grain of case 2.

4.3.2 Results and discussions

The basic aim of the study is to consider the interaction between the core of the magnetic grain and the outer boundaries, as it approaches the non-magnetic grain boundaries. Initially the effect of applied external field angles with respect to the switching field in order to get a better insight into the magnetization reversal process of the grains was studied.

Figure 4.14 (a) show a comparison of the angular dependence of the switching field of the grain with bulk property bulk grain (case 1) and the core/shell grain with variable magnetic properties (case 2). The comparison shows that the core/shell grain switches at lower applied magnetic field values as compared to the grain with bulk magnetic properties i.e. for the bulk grain $\mu_0 \boldsymbol{H_{sw}}$ (5°) = 0.59 T, and for the core/shell grain $\mu_0 \boldsymbol{H_{sw}}$ (5°) = 0.51 T, which is a change of 13 %. The reduced switching field can be explained by two effects: first by the fact that the total anisotropy of the grain has been reduced due to the boundary effects and second the outer shell of the grain supports the switching of the whole grain by posing as a nucleation site for reversal.

Concerning, the normalized switching field curves of the two models as shown in Figure 4.14 (b) it is observed that for the single-phase media the boundary interaction shows only a slight change in the gradient of the curve after the minimum angle of 45 degree i.e. 22 % change in gradient ($d\boldsymbol{H_{SW}}/d\theta$) between the two curves between the angle interval of 50 degree to 60 degree, meaning that the grain boundary only has a small effect on the magnetization reversal behaviour.

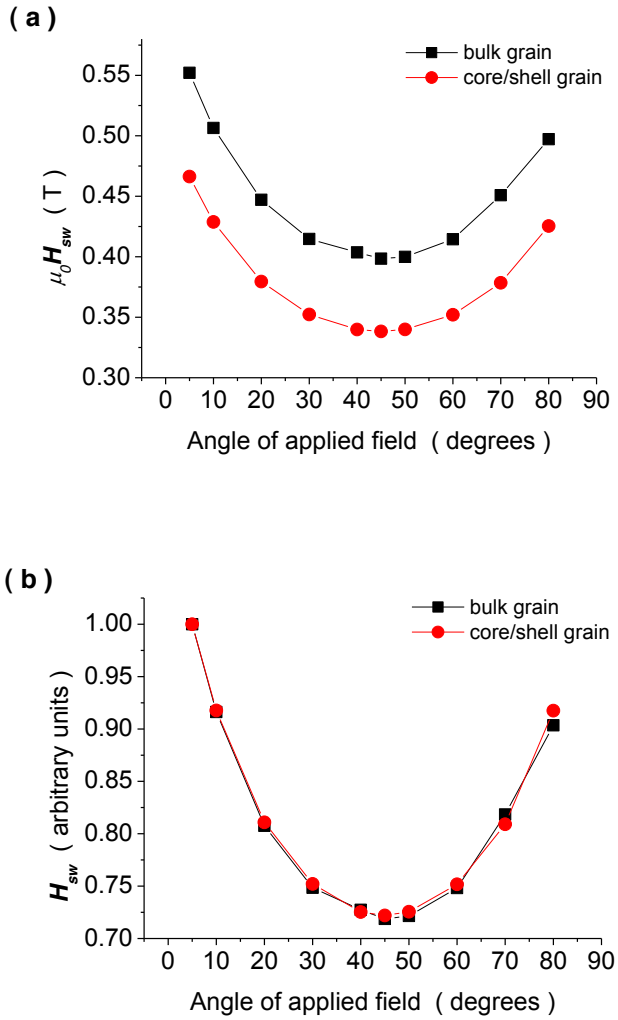

Figure 4.14: (a) The switching field and (b) normalized switching field as function of applied field angle of the CoCrPt single-phase grain with bulk magnetic properties and the variable magnetic properties at the boundary of the single-phase grain. The switching field is calculated with an f_0 of 10^{10} Hz and a τ of 10 seconds.

But this 22 % change in gradient in this simplified model indicates the presence of incoherency in the system, which will be more pronounced in a more complex model that will be studied in the coming chapters. It will be shown that this incoherency will be the driving factor of the shift in the minimum angle. Because magnetic recording

media consists of a large number of grains with different magnetic structures (morphological and chemical composition) that deviate from bulk properties, makes studies like the angular dependence of the switching field an important part for the development of high density recording media

4.3.3 Summary

A theoretical study on single-phase grains used in conventional PMR storage media was performed to understand the angular switching distribution of the grain as a function of angle of applied field was performed. To bridge the gap between the experimental and the theoretical studies, a grain with a varying magnetic structure is studied which includes the interaction between the magnetic core of the grain and the non-magnetic oxide surrounding the grain. It is shown that by including a grain boundary in our model, the switching field is decreased i.e. for the bulk grain $\mu_0 \boldsymbol{H_{sw}}$ (5°) = 0.59 T, and for the core/shell grain $\mu_0 \boldsymbol{H_{sw}}$ (5°) = 0.51 T, which is a change of 13 %, which is explained by the gradual change in anisotropy and magnetic polarisation. Such a grain boundary model is a better representation of the experimentally found grains with a varying chemical and morphological composition. The reduction of the switching field shown by the core/shell model emphasises the importance of the core/shell in real recording media. It shows that to further increase the areal density of recording media a more in depth study of core/shell grains needs to be performed, to get a better understanding of the magnetization reversal process and switching fields of magnetic grains in recording media. In that respect, this study done here is used as a starting and argumental point for our grain studies shown in this work. One should understand this simple theoretical experiment as a proof of

concept study that has two implications; one that grain boundaries are imminent and intrinsic and second that for grain sizes close to the superparamagnetic limit this effect might pose a fundamental limit in scaling for magnetic grains and therefore will give guidelines in magnetic grain density for future magnetic recording media systems such as HAMR.

References

1. T. Schrefl, G. Hrkac, G. Bance, D. Suess, O. Ertl, and J. Fidler, Handbook of Magnetism and Advanced Magn. Mater. **2,** 765 (Wiley, New York, 2007).
2. E.C. Stoner, and E.P. Wohlfarth, Phil. Trans. R. Soc. Lond. A **240,** 599 (1948).
3. R. Dittrich, T. Schrefl, D. Suess, W. Scholz, H. Forster, and J. Fidler, J. Magn. Magn. Mater. **250**, L12 (2002).
4. D. V. Berkov, J. Magn. Magn. Mater. **186**, 199 (1998).
5. W. Scholz, T. Schrefl, and J. Fidler, J. Magn. Magn. Mater. **233**, 296 (2001).
6. G. Hrkac, T. Schrefl, J. Dean, A. Goncharov, S. Bance, D. Suess, and J. Fidler, J. Apl. Phys. **105**, 053901 (2009).
7. C. Morrison, L. Saharan, G. Hrkac, T. Schrefl, Y. Ikeda, K. Takano, J.J. Miles, and T. Thomson, App. Phys. Lett. **99** (2011).
8. T. Schrefl, H. Foster, D. Suess, W. Scholz, V. Tsiantos, and J. Fodler, Advances in Solid state Phys. **41,** 623 (2001).
9. W. F. Brown, Phys. Rev. **130**, 1677 (1963).
10. H. B. Braun, J. Appl. Phys. **76**, 6310 (1994).
11. A. Moser, K. Takano, D. T. Margulies, M. Albrecht, Y. Sonobe, Y. Ikeda, S. Sun, and E. E. Fullerton, J. Phys. D: Appl. Phys. **35**, R157 (2002).

12. S. J. Lister, M. P. Wismayer, V. Venkataramana, M. A. De Vries, S.J. Ray, S.L. Lee, T. Thomson, J. Kohlberecher, H. D, Y. Lkeda, K. Takano, and C. Dewhurst, J. Appl. Phys. **106**, 063908 (2009).
13. J. Lee, M. Fuger, J. Fidler, D. Suess, T. Schrefl, amd O. Shimizu, Journal of Magn. Magn. Mater. **322**, 24 (2010).
14. D. Makarov, J. Lee, C. Brombacher, C. Schubert, M. Fuger, D. Suess, Appl. Phys. Lett. **96**, 6 (2010).
15. M. Benakli, A. F. Torabi, M. L. Mallary, H. Zhou, and H. Neal Bertram, IEEE Trans. Magn. **34**, 4 (2001).
16. N. Honda, K. Ouchi, and S. Iwasaki, IEEE Trans. Magn. **38**, 4 (2002).
17. K. Z. Gao and H. Neal Bertram, IEEE Trans. Magn. **38**, 6 (2002).
18. R. Wood, M. Williams, A. Kavcic, and J. Miles, IEEE Trans. Magn. **45**, 2 (2009).
19. T. Tanaka, A. Kato, Y. Furomoto, A. F. Md Nor, Y. Kanai, and K. Matsuyama, J. Appl. Phys. **111**, 07B711 (2012).
20. Y. Nozaki, A. Kato, K. Noda, Y. Kanai, T. Tanaka, and K. Matsuyama, J. Appl. Phys. **109**, 123912 (2011)
21. D. Suess, J. Magn. Magn. Mater. **308**, 2 (2007).
22. R. H. Victora, and Xiao Shen, IEEE Trans. Magn. **41**, 2 (2005).
23. T. Thomson, “Material parameter” University of Manchester, private communication, (2009).

Chapter 5: Angle dependence of switching field of recording media at finite temperatures

5.1 Abstract

Through simulations and experiments done by Prof. Thomson's group at the University of Manchester (UoM), an in depth angular dependence study of the switching field was conducted on the two key contributing factors to the reversal behaviour of nanoscale granular magnetic grains – thermal activation and inter/intra granular exchange coupling. At first the use of simplified CoCrPt based one grain model to describe the switching field as a function of applied field angle of CoCrPt perpendicular recording media thin films at finite temperatures of 150 K, 292 K and 350 K was investigated. The effect of grain diameter, attempt frequency and the thermal activation on the switching field of the grain was studied followed by the effect of inter/intra exchange coupling on the switching behaviour of the grain was investigated. For an ideal, non-interacting granular system, the minimum switching field occurs at 45 degrees from the easy axis of the grains. Through this comparison study it was shown that exchange coupling of either an inter or intra granular nature leads to a reduction in the switching minimum angle, whereas thermal activation leads to changes in the depth of the switching minimum but does not change the angle at which the minimum occurs. In the granular CoCrPt-oxide thin films studies here this reduction in the angle at which the minimum switching field occurs can be associated with increased intergranular coupling, provided that individual grains can be considered coherent. (The results and findings in this chapter were published in the Journal of Applied physics [1] and Applied Physics Letters [2])

5.2 Simplified single grain model to investigate real media thin film

An ongoing focus of research in magnetic recording is to increase the areal density of perpendicular media whilst maintaining the thermal stability and high signal to noise ratio [3]. In order to deal with the stability issue the main focus is to produce highly thermally stable small grains with diameter less than 8 nm. The most commonly used ferromagnetic materials for the data storage layers are CoCr based alloys, which have been used in both longitudinal and perpendicular recording media [4-6]. Although recently FePt-alloys that promise highly thermal stable grains of up to 3 nm in diameter have been proposed to be used in data storage layers [3, 7-8]. Apart from the stability factor related to the FePt grains there are write-ability issues associated with them and leaves the CoCrPt as a material of choice as recording media even today.

One way to understand the limitations and properties of a material for its application in data storage is to study their magnetization dynamics. A lot of theoretical and experimental study has been done to understand the reversal mechanisms of the grains in recording media layers. In experiments, the whole data storage layer is studied [9-12], whereas for the theoretical studies various simplified models representing the part of data storage have been used to understand the magnetization dynamics of such layers [12-16].

This chapter presents a numerical study of a single grain CoCrPt based model together with experiments, done by Prof. Thomson's group at the University of Manchester [1] and compare the results to investigate if such a model, within the experimental and fabrication constraints, can be used to describe the data storage layer at finite temperatures. In order to take thermal activation into account the

nudged elastic band method (NEB) along with the hybrid finite and boundary element method (FEM/BEM) is used [17-19]. The change in the material properties of the CoCrPt grain with variation in temperature has been taken care of by measuring the magnetic anisotropy and the magnetic saturation magnetization for the grain experimentally. Here the effect of the grain diameter, attempt frequency and thermal activation of a CoCrPt grain on the switching field as a function of applied field angle at temperatures of 150 K - 350 K has been studied. The simulation results show good agreement with experiments (UoM) [1] for a temperature range of 292 K - 350 K, but the results deviate from their experimental values at a lower temperature of 150 K. This deviation can have several sources of origin; one being a possible defect or dislocation close to the grain boundary, which is more pronounced at lower temperatures another possibility might be an exchange effect with neighboring grains. In order to extract the information on the reversal behaviour the results have been normalized with the zero degree switching field value including a correction for the easy axis orientation distribution of the grains in the real data storage layer.

5.2.1 Model

In this chapter a micromagnetic model [17, 18] along with the NEB method [19] is used to study switching behaviour of magnetic recording media grains. To simulate the effect of grain diameter, attempt frequency, and thermal activation on the switching field and magnetization reversal process, a single-phase cylindrical grain with uniform material properties is used.

	Diameter (nm)	Height (nm)	K_1 (MJ/m^3)	J_s (T)	A (J/m)
T = 150 K	7.5	11	0.73	0.98	1×10^{-11}
T = 292 K	7.5	11	0.58	0.90	1×10^{-11}
	7.8	11	0.58	0.90	1×10^{-11}
	8	11	0.58	0.90	1×10^{-11}
	8.3	11	0.58	0.90	1×10^{-11}
T = 350 K	7.5	11	0.54	0.87	1×10^{-11}

Table 5.1: The material parameters in the temperature range of 150 K - 350 K experimentally derived by Prof Thomson's group at the University of Manchester University, have been used for the modelling of the simplified CoCrPt based one-grain cylindrical model [1, 2].

The material properties, magnetocrystalline anisotropy constant K_1, exchange constant A and magnetic polarization J_s of the grain at different temperatures are given in table 5.1 and were measured by the Prof. Thomson's group at the University of Manchester [1]. The lateral parameters of the grain are as follows: height 11nm and diameter 7.5 nm, 7.8 nm, 8 nm and 8.3 nm. We neglect the slight dependence of the exchange constant A on the temperature range 150 K - 350 K investigated here.

5.2.2 Switching field as function of grain diameter

Practically, the data storage thin films are composed of lots of grains, the geometry of the grains is found to be non-uniform and also have a grain size distribution. In order to understand the effect of the change in the grain diameter on the switching field of the grain, the grain diameter is varied whereas the height of the grain is kept constant at 11 nm. The four different value of average diameter used in simulating

the one-grain model are 8.3 nm, 8.0 nm, 7.8 nm and 7.5 nm. The variation in the average diameter of the grain also indicates an overall change in the volume of the grain. The volume of the grain is directly proportional to the energy barrier of the grain, which is a determining factor for the thermal stability and switching field of the grain. The switching field as a function of the grain diameter for the different angle of applied field is shown in figure 5.1 (a). The result shows that the angular dependence curve for small diameter (7.5 nm) grains have the lowest switching field of 0.45 T as compared to the switching fields of 0.47 T, 0.48 T and 0.50 T for the grains with comparatively larger diameter of 7.8 nm, 8.0 nm and 8.3 nm respectively at applied field angle of 45 degrees, see figure 5.1 (a).

As mentioned above, the volume of the grain is proportional to the energy barrier, which is proportional to the switching field, hence it can be concluded that the switching field value decreases with a decrease in the diameter of the grain. An interesting observation is that there is no change in the gradient of the switching field curve, meaning the grains have symmetric switching field behaviour with applied field angle with a minimum at 45 degree for all grain diameter cases. This indicates a coherent reversal mechanism or Stoner-Wohlfarth like switching behaviour [20]. It can only be considered Stoner-Wohlfarth like as the minimum at 45 degrees occurs at 0.67x$\boldsymbol{H_{sw}}$(0), which is shallower than the predicted Stoner-Wohlfarth value of 0.5x$\boldsymbol{H_{sw}}$(0), see figure 5.1 (b).

Although one can see a change in the switching field as function of grain diameter, see figure 5.2 this effect could be explained in two ways: either only due to an increase in volume (and energy barrier) or only due to a change in the magnetization reversal behaviour. The possibility of these two effects takes place at the same time is also present there.

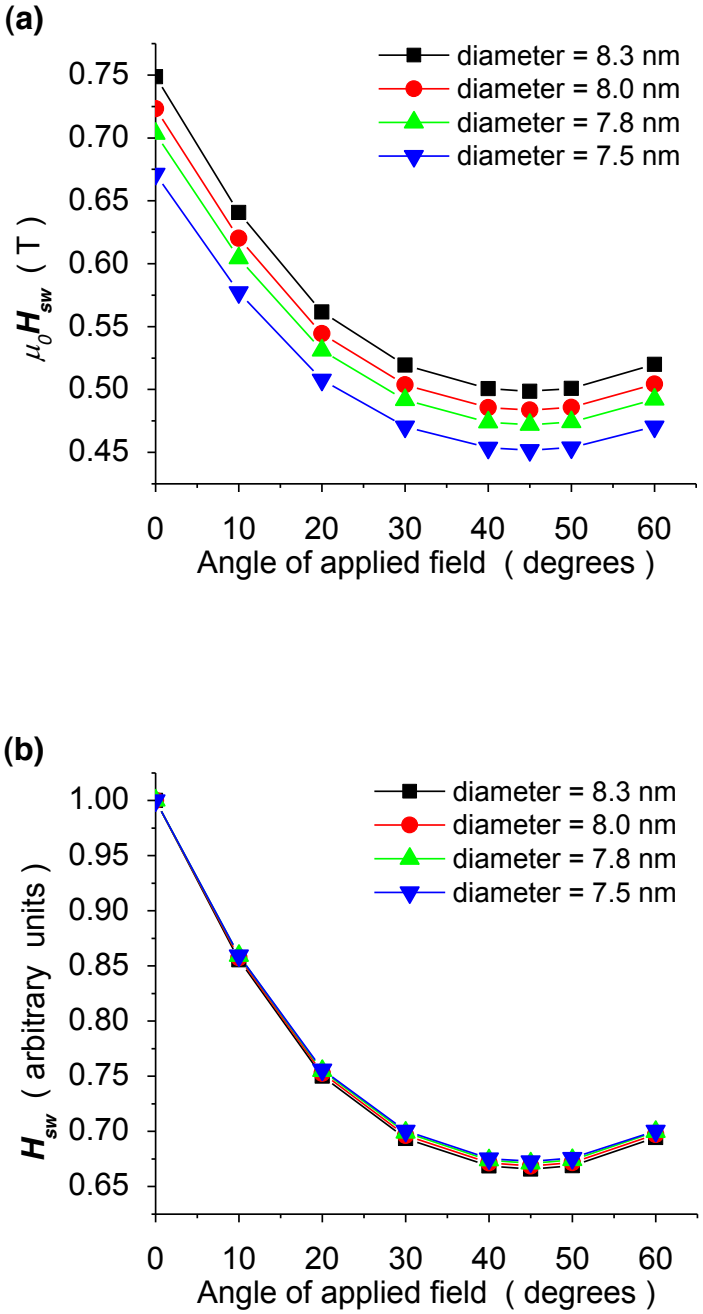

Figure 5.1: (a) The switching field as a function of the applied field angle with $f_o = 10^{10}$ Hz and τ = 10 seconds for the CoCrPt grain for height 11 nm and diameter 8.3 nm (black curve), 8.0 nm (red curve), 7.8 nm (green curve) and 7.5 nm (blue curve) at 292 K. (b) Normalized switching field as a function of applied field angle for the same grains [1].

To clarify this we normalize the switching field as function of applied field angle and also investigate the reversal behaviour. The normalized data shows that the angle dependence of the grain is the same for the diameters, indicating homogenous magnetization rotation with no change in the reversal mechanism of the grain with change in the diameter, see figure 5.1 (b).The grain diameter study of the 11 nm grain shows a change in the switching field values (figure 5.1 (a)) but no change in the magnetization reversal process (normalized curves, figure 5.1 (b)), meaning that the changes in the switching field are only due to the change in volume as the grain reverses by homogenous rotation. As shown in Figure 5.2 the switching field varies directly proportional with the grain diameter at 0 degree of applied field angle.

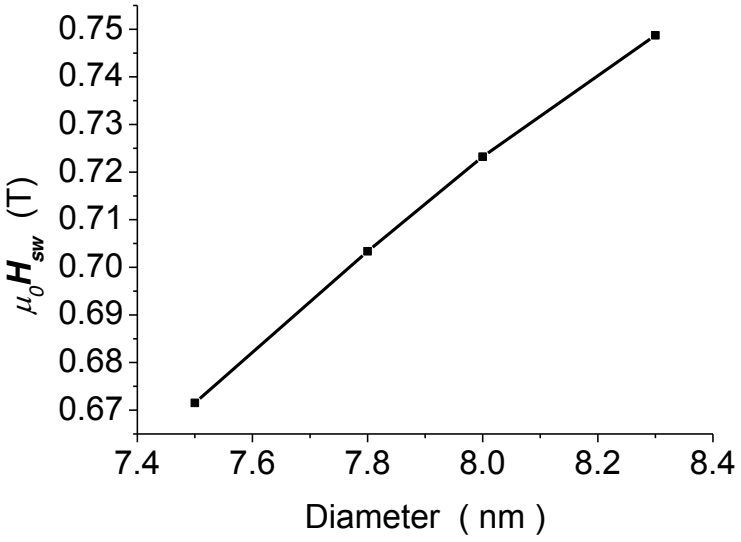

Figure 5.2: The switching field as a function of grain diameter at of 0 degree of applied field angle with $f_o = 10^{10}$ Hz and $\tau = 10$ seconds for the CoCrPt grain for height 11 nm and at 292 K.

5.2.3 Switching field as function of attempt frequency

Experimentally the value of the attempt frequency with which the grains magnetization is reversed is difficult to determine. The theoretical study done for the CoCrPt material considers an attempt frequency in the range of 10^9 Hz - 10^{12} Hz when studied at finite temperatures [21-24]. The value of the switching field is expected to depend on the attempt frequency in accordance with the Arrhenius-Neel law (see equation 4.1). In order to understand the effect of the changing attempt frequency from the modeling point of view, a switching field study as function of the attempt frequency is conducted. For this case a single-phase grain is chosen with a diameter 8 nm and height 11 nm at the finite temperature value of 292 K. To quantify the change the attempt frequency f_0 is varied in the following range of 10^9 Hz – 10^{12} Hz as shown in figure 5.3 (a) and 53 (b). Figure 5.3 (a) shows the quantitative switching field of the single-phase media grain as a function of the angle of the applied field.

The comparison of the switching field values with different attempt frequencies indicates that the attempt frequency has a large impact on the switching field values. The result shows that the attempt frequency is inversely proportional to the switching field of the grain, meaning a larger value of the attempt frequency results into a smaller switching field i.e. for $f_0 = 10^{12}$ Hz the switching field = 0.77 T, while for $f_0 = 10^9$ Hz the switching field = 0.66 T at 0 degree of applied field angle, see inset figure 5.3.

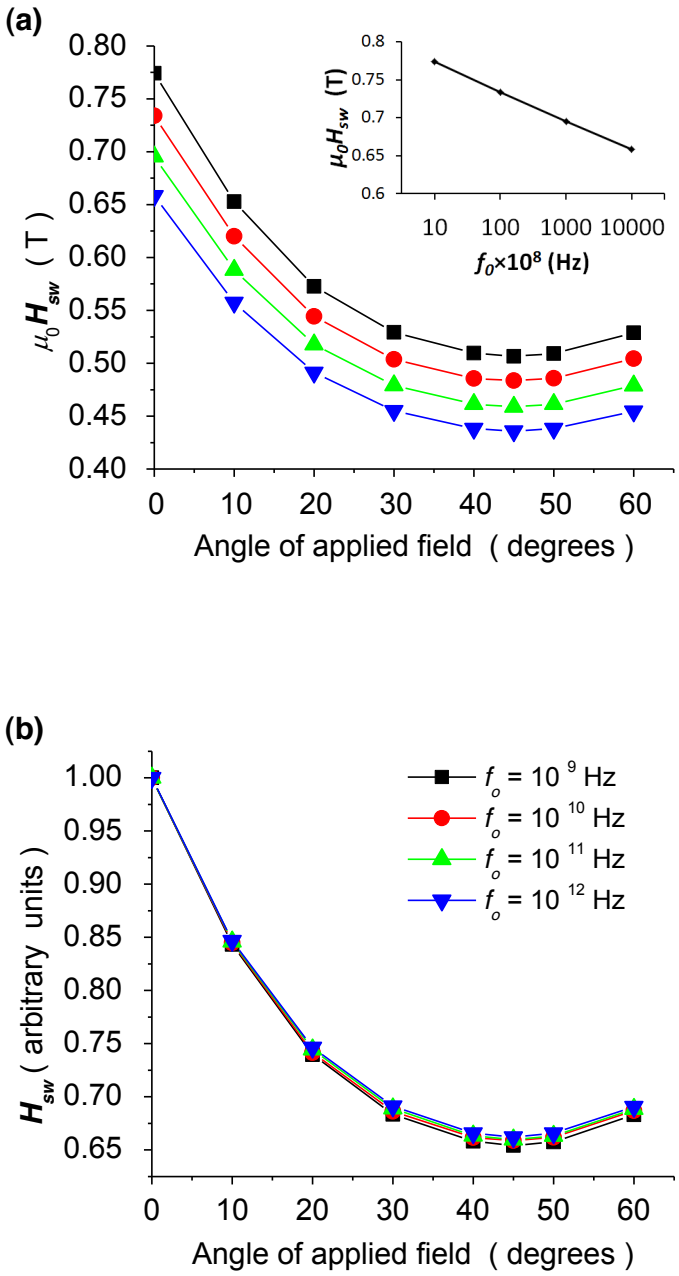

Figure 5.3: (a) The H_{sw} and (b) normalized H_{sw} as a function of angle of applied field with varying attempt frequency for a CoCrPt grain with diameter 8 nm and height 11 nm at 292 K and τ = 10 seconds. The different colors black, red, green and blue of the curves represents the attempt frequency 10^9 Hz, 10^{10} Hz, 10^{11} Hz and 10^{12} Hz respectively [1]. Inset: switching field at 0 degree as function of f_0.

This result shows nicely that the switching process at elevated temperatures is a function of probability, meaning that the larger the perturbation of the magnetization is the more likely it is that it can overcome the energy barrier. On the other hand as seen in Figure 5.3 (b) the normalized switching field as a function of the angle of applied field, the attempt frequency has a little impact on the reversal process.

Later in the chapter while comparing simulated results with experiments done by (UoM) the attempt frequency of 10^{11} Hz has been used. The choice of the value of the attempt frequency is not going to affect the conclusions of the study conducted as demonstrated by figure 5.3 (b).

5.2.4 Experiments and simulations

After the attempt frequency and grain diameter study the micromagnetic simulation results were compared with experiments (UoM) to validate the simplified one-grain model. In the experiments a Microsense DMS model 10 vector vibrating sample magnetometer (VSM) is used to measure the switching field as a function of applied field angle at finite temperature ranging from 150 K-350 K and τ = 10 seconds for a CoCrPt thin film [1]. As mentioned in the previous section, the material parameters like magnetocrystalline anisotropy and volume magnetization were determined from experimental measurements (UoM) [1].

To investigate the magnetization of the grains the lateral dimensions of the grains are extrapolated to be used in micromagnetic model from the experimentally measured magnetization of the thin film.

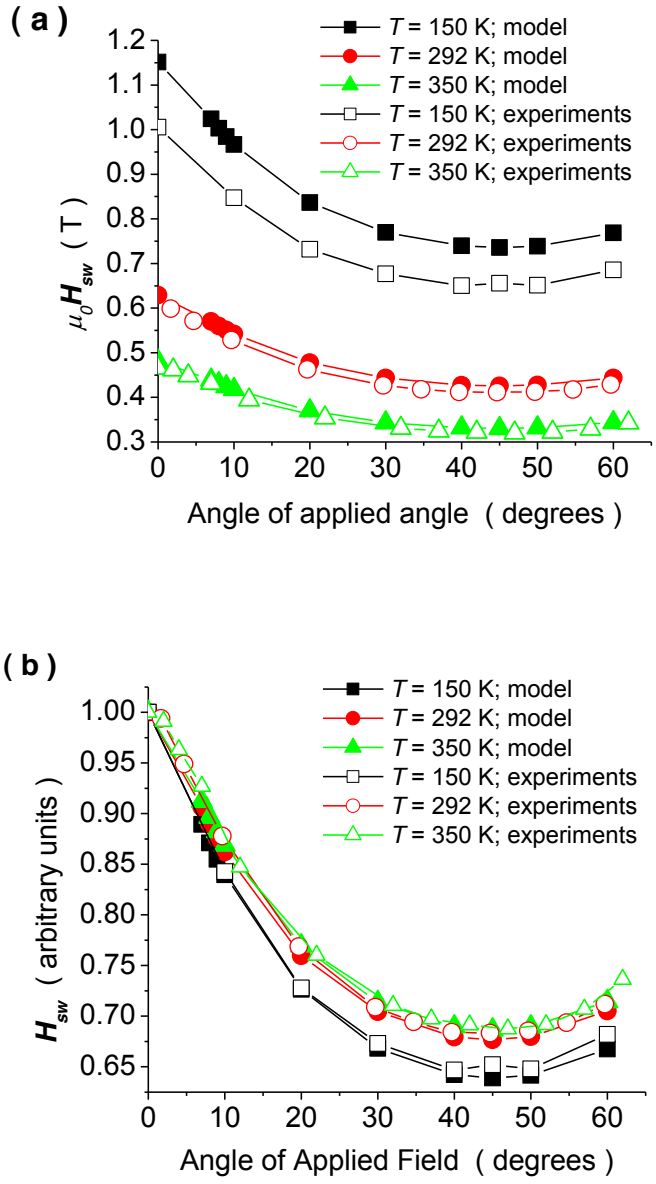

Figure 5.4: (a) Switching fields as a function of angle of applied field at T = 150 K (black curve), 292 K (red curve) and 350 K (green curve). (b) Normalized switching field as a function of angle. The bold shows the simulations results of simplified CoCrPt one-grain with diameter 7.5 nm and height 11 nm with $f_o = 10^{11}$ Hz and τ = 10 seconds and hollow curve shows the experimentally measured results by Prof. Thomson's group at University of Manchester [1].

Based on the measurements from UoM, a packing density of 0.8 is assumed, which would give an average grain diameter of 8 nm [1]. As shown by Lister et al. [11], the total volume of the grain in the real thin film is greater than the magnetic volume of the grain. The grain in the recording layer has been reported to have grain boundary regions. The boundary regions of the grain have a saturation magnetization close to zero as shown by Lister et. al. [12]. This reduction in the magnetization saturation is due to the interaction between the non-magnetic SiO_2 with the magnetic CoCrPt.

To account for the non-magnetic boundary layer the diameter of the grain used to compare with the experiments (UoM) is reduced by 0.5 nm for the theoretical study, which is consistent with the findings of Lister et al [11,12]. Meaning that the grain with 7.5 nm diameter is used to compare with experimental results (UoM).

Figure 5.4 shows the comparison of the switching field value as function of the angle of applied field for the CoCrPt simplified one-grain model simulation of diameter of 7.5 nm and height 11 nm and the experimental switching field (UoM) of the CoCrPt thin film at the finite temperature range of 150 K - 350 K. To calculate the switching field values of micromagnetic model the attempt frequency of 10^{11} Hz and measurement time 10 seconds were considered. As shown in figure 5.3 (a) the simplified one-grain micromagnetic model shows good agreement with the experiments (UoM) at temperature 292 K and 350 K. At the low temperature of 150 K the micormagnetic model shows deviation from the experimental values (UoM) i.e. for T = 150 K, $\mu_0 \boldsymbol{H_{sw}}$(experiments) = 1 T and $\mu_0 \boldsymbol{H_{sw}}$(model) = 1.2 T, which is a difference of 16 % at 0 degree of applied field angle as shown in figure 5.5 [1].

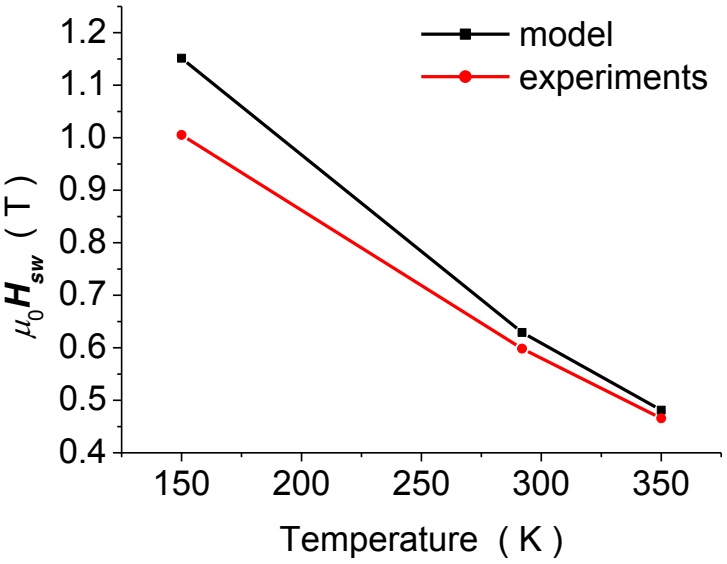

Figure 5.5: Switching fields as a function of temperature for 0 degree of applied field angle for simplified CoCrPt one-grain with diameter 7.5 nm and height 11 nm with f_o = 10^{11} Hz and τ = 10 seconds, model (black curve) experimentally measured results (red curve) by Prof. Thomson's group at University of Manchester.

The trend of angular dependence of the switching field curves in figure 5.3 shows that with the increase in temperature the thermal activation starts to play an important role in the switching of the grains. Due to the presence of thermal effects, the gradient of the angular dependence of the switching field curves is reduced by 0.01 T/degree between the temperature ranges from 150 K to 350 K. For homogenous rotation without thermal activation, one would expect a decrease of the normalized switching field to 0.5.

As known from previous studies, see previous chapter 4 on thermal effects, in case of thermal excitation, the grain receives energy from thermal activation and the

external field. Meaning that due to thermal activation, the grain switching takes place at lower external field values compared to simulations that do not include temperature effects. This implies that the applied field and thermal activation lower the total energy barrier for the transition between the initial and final state and therefore are equivalent and inter-exchangeable as both represent a form of energy/momentum transfer. The reduction in switching field is more pronounced at field angles close to zero or close to 90 degrees. For example in figure 5.4 (a) at T= 150 K for model the switching field reduced by 0.18 T from 0 degree to 10 degree whereas the reduction in switching field from angle 40 degree to 50 degree is 0.00085 T.

To be able to extract the reversal mechanism of the grain and compare it with different data sets, the absolute switching curves were normalized with the switching field values at zero degrees. It should be mentioned here that there is a 3 degrees easy axis distribution in the experimental CoCrPt film. In order to include this into the numerical results the switching field was normalized by the switching field computed for 3 degrees. By comparing experimental (UoM) and simulation results the model successfully reproduces the flattening of the angular dependence of the switching field curve with an increase in the temperature. Despite the discrepancies at low temperatures, the model is successful in determining the reversal behaviour of the grain in the temperature regime of 150 K - 350 K as shown in Figure 5.4 (b).

5.2.5 Summary

The study presented here has shown that a simplified single grain model at finite temperatures can be used to simulate a CoCrPt recording layer, as its comparison

with experiments (UoM) shows. The good agreement is a result of a deterministic approach to investigate the influence of the attempt frequency and the diameter of the grain on the switching field and switching mechanism. Both play an important role. For the latter, it means that to determine the average grain size in the thin film from experiments the effective magnetic volume of the grain has to be taken into account instead of the total physical volume.

Furthermore, the magnetization reversal process of the grain is found to be independent of the grain diameter and the attempt frequency for the grains studied here, which reverses by homogenous rotation. The chosen range of grain size and attempt frequency of the grain only affect the switching field value of the grain. Our study of the attempt frequency shows that the best agreement with experiments is achieved by considering an attempt frequency value of 10^{11} Hz in our models for CoCrPt, which is in the theoretical predicted range of 10^{9} Hz - 10^{12} Hz for a CoCrPt system. Concerning the thermal activation it is observed in simulations and confirmed by experiments (UoM) that the increase in thermal activation leads to a reduction in the depth of the minimum of the switching field curves. It should be mentioned here that only good agreement with experiments at 292 to 350 K could be achieved. The discrepancies at 150 K are an indication that there might be a morphological change either in the lattice structure or a presence of defects that have greater implications at lower temperature.

The important message here is that a well-designed one grain model can be used to explore material parameters, which are not easily accessible by experiments and also can give a more in depth understanding of the magnetization dynamics of magnetic grains. This approach can be used in the design of future magnetic recording film structures giving important parameters like absolute switching field

values and angular switching mechanism, which are important for the design of magnetic recording heads.

In the next sub-chapter the previous investigation was extended to study the effect of the inter/intra exchange coupling in recording media. Inter/intra granular exchange coupling, which produces a clear shift in the magnetic reversal behaviour of magnets grains, is investigated however the origin of such observed behaviour in real materials is still part of a controversial debate.

5.3 Inter/Intra Granular Exchange and thermal effects in granular magnetic recording media

There is a significant ongoing debate within the community concerning origin of magnetic reversal mechanisms in granular materials. There are two key contributing factors to the reversal behaviour of these materials – inter/intra granular exchange coupling and thermal activation. Identifying these factors is important for a complete understanding of the physical origins of the reversal process. This is of significance in two key technologically important areas of research – permanent magnets and perpendicular magnetic recording media. Research into permanent magnets has traditionally focused on improving the maximum energy product $(\boldsymbol{BH})_{max}$ [25-27], but recently has shifted towards minimizing the rare earth content of these materials, due to the scarcity of rare earth metals.

For the purposes of this sub-chapter a well segregated granular CoCrPt-oxide perpendicular magnetic recording media is chosen for the study, which provides an ideal platform to study reversal in granular magnets through both simulations and through experiments (UoM). This class of materials remains the focus of intensive research as methods are found to provide improved thermal stability without

compromising write-ability in recording applications. Previous research has shown that the switching behaviour of two-phase granular exchange coupled (ECC) recording media [28, 29] deviates from a coherent, Stoner-Wohlfarth (S-W) type behaviour [20], towards a Kondorsky-like 1/cos(θ) model, which describes magnetization reversal as a function of domain wall movement and rotation [30] shown in figure 5.6, the difference being revealed through the angular dependence of switching field [9].

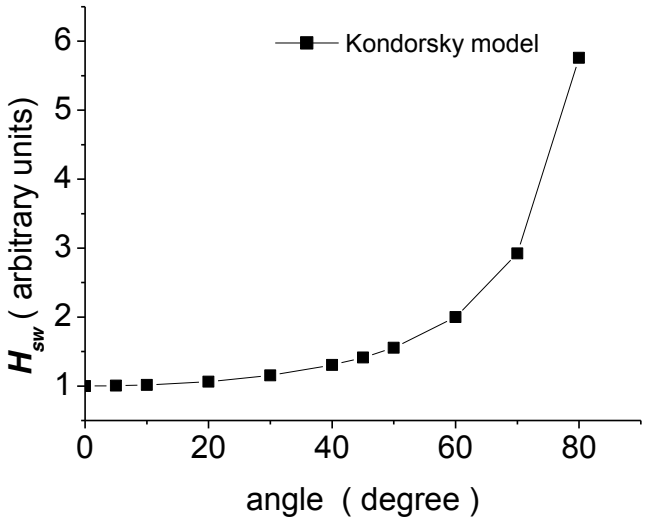

Figure 5.6: Kondorsky switching as a function of angle of applied field with respect to the easy axis of the grain [9].

Previously it has been speculated that this apparent incoherency arises from an increased degree of lateral intergranular exchange coupling, rather than from the intragranular exchange spring [9]. However the presence of incoherency in magnetic grains indicated by a decrease in the depth of the Stoner-Wohlfarth minimum can

also have its origin from thermal activation [31]. In order to understand precisely the contributions to the observed effect, it is critical to have an understanding of the coupling mechanisms that arise in the native CoCrPt-oxide granular layer. This chapter reports a systematic study of the angle dependence of reversal in CoCrPt-oxide thin films as a function of film thickness (11 nm and 16 nm) and temperature (150 K, 292 K and 350 K). The measurements (UoM) were compared to the predictions of a finite temperature micromagnetic model of a single, isolated CoCrPt grain, which allows to explore the degree to which inter/intra granular coupling contributes to switching behaviour.

5.3.1 Model and experimental set up

To have an ideal platform for the study of the magnetization reversal, a CoCrPt-oxide based perpendicular magnetic recording media as a model system is used, on which micromagnetic study was conducted in line with experiments done by UoM [2]. Together with simulation and experiments (UoM), here a systematic study of angular dependence of the switching field as a function of data storage layer film thickness at the finite temperature range of 150 K – 350 K is presented. The simulations results of simplified and isolated CoCrPt based single grain model are compared directly with the experimental measurements (UoM). This comparison gives an opportunity to explore the contribution of the inter/intra granular coupling in the magnetization reversal of these grains.

In the experimental study (UoM), the samples used are a well-segregated perpendicular granular media. The sample was deposited on the 65 mm diameter and 0.6 mm thick glass substrate via dc magnetron sputtering (UoM) [2]. Initially,

followed by a Ru seed layer, a CoFe-based soft underlayer is deposited on the glass substrate. On the top of the Ru seed layer a CoCrPt-oxide based granular segregated recording layer of the thickness 11 nm and 16 nm is deposited. In the end the media is capped with a protective layer and a lubricant. The DMS model 10 vector vibrating sample magnetometer (VSM) is used to measure the switching field as a function of applied field angle at finite temperature ranging from 150 K - 350 K and τ = 10 seconds for a CoCrPt thin film by Prof. Thomson's group at the University of Manchester [2].

	Diameter (nm)	Height (nm)	K_1 (MJ/m^3)	J_s (T)	A (J/m)
T = 150 K	7.5	11	0.73	0.98	1×10^{-11}
	7.5	16	0.73	0.98	1×10^{-11}
T = 292 K	7.5	11	0.58	0.90	1×10^{-11}
	7.5	16	0.58	0.90	1×10^{-11}
T = 350 K	7.5	11	0.54	0.87	1×10^{-11}
	7.5	16	0.54	0.87	1×10^{-11}

Table 5.2: The material parameters derived experimentally by Prof Thomson's group at the University of Manchester in the temperature range of 150 K - 350 K [2], have been used for the modelling of the simplified CoCrPt based one-grain cylindrical model of nominal diameter 7.5 nm and height 11 nm and 16 nm [2].

To conduct the finite temperature micromagnetic [17-28] study of the above experimental sample (UoM) and to study the magnetization reversal in the absence of coupling effects resulting in the thin film, a simplified and isolated CoCrPt based media grain which was cylindrical in geometry having uniform material properties was considered. The material properties, magnetocrystalline anisotropy constant K_1,

exchange constant A and magnetic polarization $\boldsymbol{J_s}$ of the grain at different temperatures given in table 5.2 were measured by the Prof. Thomson's group at the University of Manchester [2].

In table 5.2 the material and lateral parameters for the 11 and 16nm grains. The 11 nm grain parameters, although discussed in the previous sub-chapter were included here for better comparison with the 16 nm grains. The lateral parameters of the cylindrical grain are as follows: diameter 7.5 nm and height 11 nm and 16 nm. The switching field of these grains is calculated at the three different temperatures 150 K, 292 K, 350 K. For the simplification of the study, at first the slight dependence of the exchange constant A on the temperature range 150 K - 350 K was neglected. Later to probe the effect of the intragranular exchange coupling on the switching of the grain the exchange constant A is varied in the range of 0.25×10^{-11} J/m - 1×10^{-11} J/m [2].

5.3.2 Switching behaviour of magnetic recording media grains

Due to the fabrication process there is a grain size distribution in the recording layer. It is important to understand and study the effect of the variation in the CoCrPt-oxide media film thickness on the magnetization switching behaviour of the grain to be able to predict switching fields of such media. Therefore the switching field of the isolated and simplified micromagnetic grain is calculated for thickness and temperature range as discussed in the previous sub-chapter. The experimental measurements (UoM) were carried out for film thickness of 11 nm and 16 nm at 150 K, 292 K and 350 K. The switching field was calculated over the range of applied field angle from 0

degree to 60 degree, where angle 0 degree is the direction of the easy axis of the cylindrical grain, which was perpendicular to the plane of the thin film [2].

The exploration of the extent to which the switching behaviour of these CoCrPt-oxide media varies from the ideal case through normalization of switching field

as a function of applied field angle, using the value of switching field H_{sw} at 0 degree applied field angle along the easy axis as a normalization parameter. While normalization of the simulated data the 3 degree granular dispersion along the easy axes found from x-ray measurements has been incorporated with the help of a Gaussian normalization function. Characterizing the reversal using switching field H_{sw} eliminates the mean field effects of magnetostatic interactions as the net moment, and hence net magnetostatic field contribution, is zero.

Figure 5.4 (b) and 5.7 shows the normalized switching field curves as a function of applied field angle at 150 K, 292 K and 350 K, for film thicknesses of (a) 11 nm and (b) 16 nm respectively. As seen from the figure 5.4 (b) and 5.7 the simulated results shows good agreement with the experimental thin film measurements (UoM) on 11 nm thick film. The 11 nm grains show the angular dependence of the switching field that shows a Stoner-Wohlfarth like behaviour, see sub-chapter 5.2, where the angular dependence switching field first decreases from 0 degree and then starts to increase with further increase in the angle with 45 degree as its minimum switching field angle.

After increasing the thickness of the grain to 16 nm the switching field, the data measured (UoM) show a reduction in the angle from 45 degree to 42 degree at which the minimum occurs along with the decrease in the depth of the minimum of the normalized switching field curve [2]. Figure 5.8 shows the minimum switching

field and minimum angle as a function of temperature for the 16 nm grain as obtained in experiments. Whereas model shown the minimum switching at 45 degree for the 16 nm which is similar to what is observed for the 11 nm case. The discrepancy between the model and experiment is due the fact that the model is just a simplified one grain model and does not incorporate any contribution from the neighboring grains in the switching of the grain which might be present in the real media thin film.

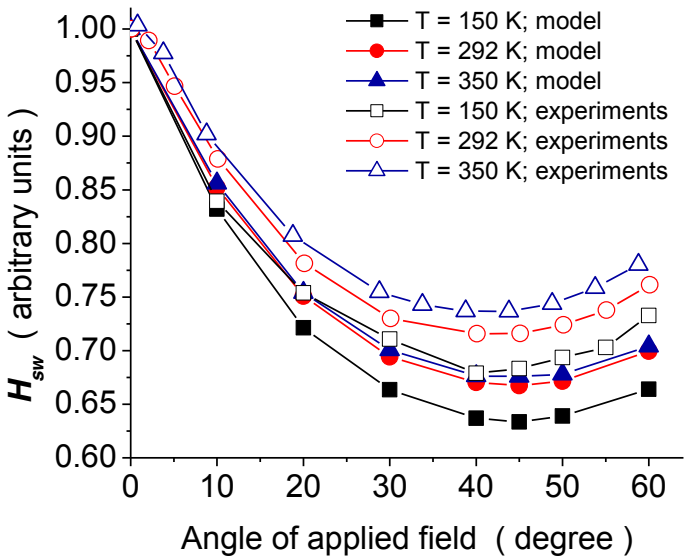

Figure 5.7: The normalized switching field $H_{sw}(\theta)/H_{sw}(0)$ for CoCrPt-oxide recording media layer with the thickness of16 nm, as a function of applied field angle. Bold and open symbols represent the simulations and experimental data measured by Prof. Thomson's group at the University of Manchester, respectively [2]. The different color of the curves represents the variable temperature: Black (150 K), red (292 K) and blue (350 K).

To further probe the variation in magnetization reversal behaviour the study was repeated at temperatures of 150 K and 350 K. As shown in figure 5.7) the magnitude of the minimum of the switching field measured experimentally (UoM) shows a clear shift with the change in the temperature for the grain with thickness 11 nm and 16 nm. For example for the 11 nm grain at 292 K the normalized switching field at 45 degree of applied field angle is 0.67 for the model system and for the experiments the minimum angle is at 44.68 degree with a normalized switching field at 0.68 whereas for the 16 nm thick grain at 292 K the normalized switching field at 45 degree applied field angle is 0.68 for model system and for the experiments the minimum angle is at 45.107 degree with a normalized switching field at 0.72. The error in the minimum angle in degree is 0.5 and minimum switching field error is 0.01. The percentage difference between the model and experiment normalized switching field for the 11 nm thick grain is 2 % and 16 nm thick grain is 5.5 %. Figure 5.4 (b) shows the position of the minimum angle remains constant within in the temperature range of 150 K – 350 K, measured by the Prof. Thomson group at the University of Manchester, within experimental error [2].

To explain the findings of the measurements (UoM) the experimental results were compared with the micromagnetic model as shown in Figure 5.7 [2]. While comparing the simulated results and experimental measured (UoM), one of the aim is to test the hypothesis regarding the change in the position of the minimum angle of the switching field that can take place through the inter/intra granular exchange coupling mechanism, whereas the change in the magnitude of the minimum of the switching field is a function of both the thermal activation as well as the coupling.

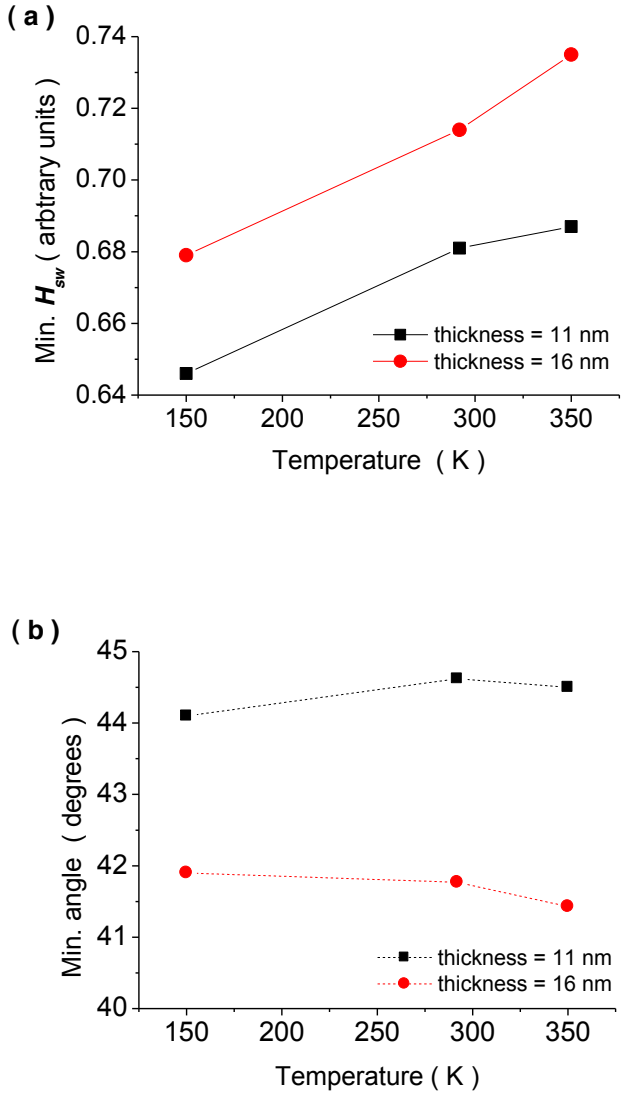

Figure 5.8: Minimum values of (a) normalized switching field and (b) the associated minimum applied field angle measured (UoM), as a function of temperature for 11 nm (black squares) and 16 nm (red dots) thick films of CoCrPt-Ox. The minimum switching angle is independent of temperature (thermal activation) and depends only on film thickness (inter/intra granular coupling). The error in the minimum angle in degree is 0.5 and minimum switching field error is 0.01. [2].

As can be seen in the figure 5.7 the simulated results of the grain with thickness 16 nm does not agree well with the experiments (UoM) in terms of magnitude of switching field, but the simulations has been successful in reproducing the trend of the switching field as a function of the applied field angle as well as a function of temperature over the range 150 K – 350 K [2]. The simulation also does not show any reduction in the minimum switching field angle as the grain considered in simulation is a simplified single grain model which is simulated at finite temperature only and does not account for any changes which might have due to the increase in the volume of the grain or influence from the nearest neighbor's.

The most important point to be taken into account here is that the micromagnetic model is a simplified model and does not include any intergranular exchange coupling from the neighboring grains present in the experimental thin film (UoM). By taking this into account, notice the deviation in the magnetization reversal behaviour can be explained by two mechanisms. Firstly, the simplified micromagnetic model accounts for the factors, which influence the switching behaviour in the single isolated grain. This indicates that increased thickness may results into intergranular exchange coupling as the quality of the segregation in the thin films degrades with the increased thickness. Secondly, the increased thickness may affect the atomic magnetic moment by reducing the coherence and permits the formation of the domain wall inside the very large grains.

To understand the effect of the variation in the strength of the exchange on the switching behaviour of the ferromagnetic grains further the simulation were repeated on a grain with thickness of 16 nm, for which the strength of the exchange constant A is varied to 0.25×10^{-11} J/m, 0.4×10^{-11} J/m, 0.7×10^{-11} J/m and 1.0×10^{-11} J/m.

Figure 5.9 show the angular dependence of switching field as function of the exchange coupling and demonstrates the decrease in the minimum switching field angle with the changing exchange constant from $A = 1.0 \times 10^{-11}$ J/m to 0.25×10^{-11} J/m inside the grain from angle 45 degree to 40 degree respectively also shown in figure 5.9 (a). Figure 5.9 (b) shows the shift in the minimum switching field curve while changing the $A = 1.0 \times 10^{-11}$ J/m to 0.25×10^{-11} J/m from 45 degree to 40 degree. These results indicates that in the real recording media thin film the change in the angle could be as a result of change in the exchange coupling either between the grains or from within the grains.

To say that the reduction in the minimum angle due to enhanced intergranular exchange coupling instead of the intragranular exchange coupling, the coupling inside the grains needs to be very high. The exchange length $l_{ex,}$ which is defined by the exchange constant A and uniaxial anisotropy K_u of the grain as follows $\sqrt{A/K_u}$, can be used to have an estimate of the length scale of intergranular incoherency, for our CoCrPt grains this exchange length is 5 nm. Meaning for grains that are larger than 5 nm some incoherency in the reversal mechanism can be expected.

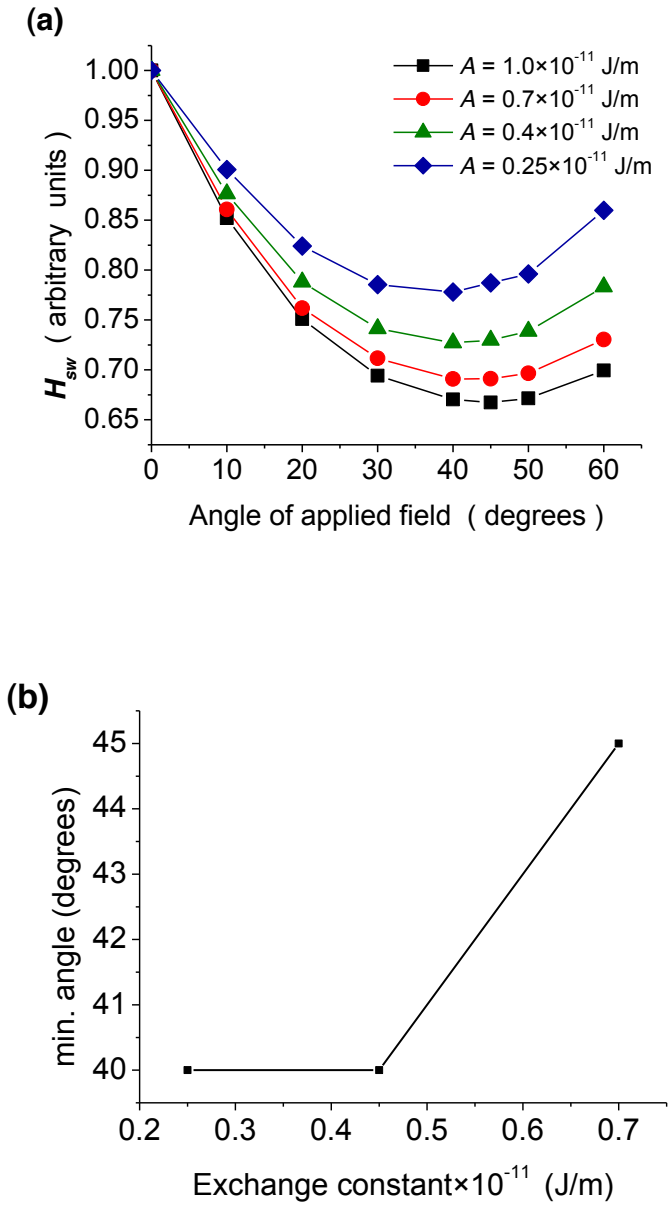

Figure 5.9: (a) Variation in the simulated angle dependent switching field loop of a 16 nm thick grain of CoCrPt as a function of exchange constant *A* values of 1×10^{-11} J/m (black squares), 0.7×10^{-11} J/m (red circles), 0.4×10^{-11} J/m (green triangles) and 0.25×10^{-11} J/m (blue diamonds). As the exchange coupling within the grain is reduced, the reversal mode of grain becomes less coherent, resulting in a reduction in both the minimum switching field and the angle at which this occurs. (b) Minimum switching field angle as a function of exchange constant.

5.3.3 Summary

In this chapter together with the experimental work done by Prof. Thomson's group at the University of Manchester it was shown by using a CoCrPt model grain system that the variation in the magnetization reversal in the recording media is determined by two effects: one is the intrinsic intra and inter granular exchange coupling and the other is the thermal activation. The presence of the too larger grains, which do not reverse like a single domain particle by coherent rotation results into a weaker intergranular exchange coupling inside the recording media and contributes to the incoherency in the magnetization reversal of the grain and also results into the decrease in the minimum switching field angle. In this chapter it was also shown that exchange coupling of either an inter or intra granular nature leads to a reduction in the switching minimum angle, whereas thermal activation leads to changes in the depth of the switching minimum but does not change the angle at which the minimum occurs. This reduction in the angle at which the minimum switching field occurs is a sign of localized incoherency that is associated with an increased intergranular coupling provided that individual grains can be considered coherent.

References

1. L. Saharan, C. Morrison, J. J. Miles, T. Thomson, T. Schrefl, J. Appl. Phys. **110**, 103906 (2011).
2. C. Morrison, L. Saharan, G. Hrkac, T. Schrefl, Y. Ikeda, K. Takano, J.J. Miles, and T. Thomson, App. Phys. Lett. **99,** 132507 (2011).
3. S. N. Piramanayagam, J. Appl. Phys. **102**, 011301 (2007).

4. Y. Hirayama, M. Futamoto, K. Kimoto, and K. Usami, IEEE Trans. Magn. **32**, 3807 (1996).
5. M. Futamoto, Y. Honda, H. Kakibayashi, and K. Yoshida, IEEE Trans. Magn. **21**, 1426 (1985).
6. T. Keitoku, J. Ariake, and N. Honda, J. Magn. Magn. Mater. **287**, 172 (2004).
7. A. K. Singh, Y. Jinhua, and T. Suzuki, IEEE Trans. Magn. **41**, 3205 (2005).
8. G. Sáfrán, T. Suzuki, K. Ouchi, P. B. Barna and G. Radnóczi, Thin Solid Films **496**, 580 (2006).
9. E. Goto, N. Hayashi, T. Miyashita, and K. Nakagawa, J. Appl. Phys. **36**, 2951 (1965).
10. T. Thomson, B. Lengsfield, H. Do, and B.D. Terris, J. Appl. Phys. **103**, 07F548 (2008).
11. S. J. Lister, M. P. Wismayer, V. Venkataramana, M. A. D. Vries, S. J. Ray, S. L. Lee, T. Thomson, J. Kohlberecher, H. Do, Y. Lkeda, K. Takano, and C. Dewhurst, J. Appl. Phys. **106**, 063908 (2009).
12. S. J. Lister, T. Thomson, J. Kohlbrecher, K. Takano, V. Venkataramana, S. J. Ray, M.P. Wismayer, M. A. de Vries, H. Do, Y. Ikeda, and S. L. Lee, Appl. Phys. Lett. **97**, 112503 (2010).
13. J. J. Miles, D. M. McKirdy, R. W. Chantrell, and R. Wood, IEEE Trans. Magn. **39**, 1876 (2003).
14. D. Suess, J. Lee, J. Fidler, H. S. Jung, E. M. T. Velu, W. Jiang, S. S. Malhotra, G. Betero, and T. Schrefl, IEEE Trans. Magn. **45**, 88 (2009).
15. A. V. Goncharov, T. Schrefl, G. Hrkac, and S. Bance, Physica B: Condensed Matter **403**, 278 (2008).
16. N. A. Usov, C. R. Chang, and Z.-H. Wei, Appl. Phys. Lett. **83**, 3749 (2003).

17. R. W. Chantrell, M. Wongsam, T. Schrefl, and J. Fidler, in Encyclopedia of Materials: Science and Technology, edited by K. H. J. Buschow, R. W. 424 Cahn, M. C. Flemings, B. Ilschner, E. J. Kramer, and S. Mahajan 425 Elsevier, New York, 5642 (2001).
18. T. Schrefl, G. Hrkac, G. Bance, D. Suess, O. Ertl, and J. Fidler, Handbook of Magn. and Advanced Magn. Mate, **2** 765 (Wiley, New York, 2007).
19. R. Dittrich, T. Schrefl, D. Suess, W. Scholz, H. Forster, and J. Fidler, J. Magn. Magn. Mater. **250**, L12 (2002).
20. E. C. Stoner and E. P. Wohlfarth, Philos. Trans. R. Soc. London, Ser. A **240**, 599 (1948).
21. T. Schrefl, H. Foster, D. Suess, W. Scholz, V. Tsiantos, and J. Fodler, Adv. Solid State Phys. **41**, 623 (2001)
22. W. F. Brown, Phys. Rev. **130**, 1677 (1963).
23. B. Braun, J. Appl. Phys. **76**, 6310 (1994).
24. A. Moser, K. Takano, D. T. Margulies, M. Albrecht, Y. Sonobe, Y. Ikeda, S. Sun, and E. E. Fullerton, J. Phys. D: Appl. Phys. **35**, R157 (2002).
25. G. Hrkac, T. G. Woodcock, C. Freeman, J.Dean, T. Schrefl, and O. Gutfleisch, Appl. Phys. Lett. **97**, 232511 (2010).
26. Y. Shinba, T. J. Konno, K. Ishikawa, K. Hiraga and M. Sagawa, J. Appl. Phys. **97**, 053504 (2005).
27. M. Matsuura, S. Sugimoto, R. Goto, and N. Tezuka, J. Appl. Phys. **105**, 07A741 (2009).
28. R. Dittrich, T. Schrefl, M. F. Kirschner, D. Suess, G. Hrkac, F. Dorfbauer, O. Ertl, and J. Fidler, IEEE Trans. Magn. **41**, 3592 (2005).
29. R .H. Victora and X. Shen, IEEE Trans. Magn. **41**, 2828 (2005).

30. E. Kondorsky, J. Phys. Moscow **2**, 161 (1940).

31. T. Schrefl, J. Fidler, R. Dittrich, D. Suess, W. Scholz, V. Tsiantos and H. Forster, Topics in Appl. Phys. **87**, 1 (2003).

Chapter 6: Parameter space mapping and magnetic grain structure study of exchange spring recording media at finite temperatures

6.1 Abstract

A combined numerical and experimental study done by Prof. Thomson's group at the University of Manchester (UoM) was carried out to investigate the effect of an intergranular interface layer between a magnetic soft and a magnetic hard phase, the exchange break layer. It was introduced to account for lattice deformations, defects and transition regions between two magnetic materials. The thickness of this layer, the magnetic properties (anisotropy and exchange) and its influence on the magnetization reversal process was studied at room temperature. It was found that the presence of an exchange break layer significantly influences the coupling between the two CoCrPt based hard and soft layers. The model was also used to study a complex exchange spring media grain in direct comparison with experiments (UoM). The effect of bulk material properties and the interaction of the ferromagnetic grain with the SiO_x matrix on the magnetization reversal were investigated. The overall study of magnetization distribution of the model structured modifies the Stoner-Wohlfarth angle dependency of the switching field by reducing the minimum switching angle that occurs at 45 degrees, highlighting the importance of the grain boundary phase on the quantitative value of the switching field.

6.2 Importance of intergranular interface in exchange spring media

Exchange spring magnets have been the subject of intensive research in the past two decades. In the beginning they were proven to be advantageous as permanent magnets with their novel properties of a high-energy product, high remanence and high isotropic remanence ratio $\boldsymbol{B_r/J_s}$ [1]. The large energy product $\boldsymbol{(BH)}_{max}$ arises from the high coercive field contribution from the hard magnetic material and high magnetization polarization from the soft magnet. Chang et. al. [2], and Goto et. al. [3] studied exchange coupled multi-layers with a focus on the coupling mechanism between the exchange spring thin films. Based on this study, Goto et. al. pointed out the potential of exchange coupled multi-layers in memory device applications. With the passage of time and improvement in the available resources it became possible to produce multilayer systems with controlled magnetic properties and dimensions. With the gain in the understanding of the physics behind the exchange spring effect and the understanding of the reversal mechanism, new research areas emerged for various technological applications, the most common of these being magnetic recording [4]. In the recording industry the soft and hard phases were used to decrease the switching field and increase the thermal stability. Various theoretical efforts were reported in the 1990s by research groups across the world to explain the exchange spring phenomenon. Goto et. al. and R.Skomski et. al. have performed analytical studies [5, 6], T. Scherfl et. al. and R.Fischer et. al. performed micromagnetic modelling [7-9], whereas R.F. Sabiryanov et. al. derived an expression from first principles to describe the coupling mechanism in soft/hard bi-layer systems [10]. Fullerton studied the bi-layer system of SmCo (hard phase) and Fe (soft phase) to demonstrate that exchange coupling is a robust and more general phenomenon.

Recently, when the recording industry began to approach the fundamental limits of scaling in existing perpendicular recording media, highly engineered magnetic exchange spring recording media, based on thin films of exchange spring magnets, emerged as a promising candidate. In data storage these materials are used to design magnetic media where the thermal stability and switching field can be tailored such that the thin films have a sufficient anisotropy to avoid thermally activated reversal but can still be reversed by fields deliverable by commercially available write heads.

In order to take full advantage of these materials there is a pressing need to address the exciting fundamental questions in thin film exchange spring magnets. Specifically, what are the optimum exchange spring material properties; how does the anisotropy of the soft phase affect the magnetization reversal; what role does an exchange break layer play in the structure to enhance the functionality of the media and in maintaining its thermal stability? The study performed here aims to develop our understanding of the role of the exchange break layer and soft phase on the reversal of exchange spring media in a quantitative way. So far micromagnetic studies have considered only exchange spring media with continuous hard/soft phase films. In this finite temperature micromagnetic study on the CoCrPt based exchange spring media the intergranular interface (the exchange break layer) between the soft and hard phase has been taken into account.

6.2.1 Micromagnetic model

To study the effect of the exchange break layer in a ferromagnetic multilayer system a cylindrical CoCrPt tri-layer system, which represents the hard/soft phase and the

exchange break layer is modeled. The cylindrical grain has a diameter of 8 nm and variable thickness. The thickness of the hard and soft phase is kept constant as 11 nm and 6 nm respectively. The thickness of the exchange break layer is varied from 0.5 nm to 2 nm and represents the lattice distortions present between the soft and hard layer. The material properties for the CoCrPt hard phase are taken from Morrison et. al. [11] and for the CoCrPt soft phase from Thomson et. al. [12]. The material properties of the hard phase are as follows: magnetocrystalline anisotropy constant K_h of 0.58 MJ/m^3, magnetic polarization $\boldsymbol{J_{s,\ h}}$ of 0.90 T and exchange constant A_h of 1×10^{-11} J/m. The soft phase has a magnetic polarization $\boldsymbol{J_{s,\ soft}}$ of 0.57 T and exchange constant A_s of 1×10^{-11} J/m. The soft phase magnetocrystalline anisotropy constant K_s is varied between 20% of 0.58 MJ/m^3 – 60 % of 0.58 MJ/m^3, as it is difficult to measure the exact value of magnetocrystalline anisotropy in this layer experimentally.

During the preparation of the multilayer system, sputtering of the soft phase onto the hard phase, an intermixing of the soft and hard phase takes place. The intermixing at the soft/hard interface leads to an intergranular interface (the exchange break layer) with magnetic properties that are in between the soft and hard phase material properties, the exchange break layer. To take this into account the material properties given to the exchange break layer are as follows: The magnetic polarization $\boldsymbol{J_{s,\ EBL}}$ is the same as in the soft layer i.e. 0.57 T. The magnetocrystalline anisotropy constant K_{EBL} is varied between the 20% - 60 % of 0.58 MJ/m^3 (hard layer magnetocrystalline anisotropy), and the exchange constant A_{EBL} is varied between 0.2×10^{-11} J/m - 1×10^{-11} J/m.

6.2.2 Results and discussion

In general, it is difficult to explore the effect of varying parameters experimentally in isolation. For example, anisotropy can vary by changing the crystal structure of a material, or by using different materials. In both these cases, other parameters such as the exchange constant *A* and magnetic polarization $\boldsymbol{J_s}$ will also vary in a non-systematic manner. Also, the nature of the interfacial exchange coupling between the layers is highly dependent on interfacial quality and is difficult to quantify experimentally. Therefore, micromagnetic modeling provides an ideal method for exploring the effect of varying individual parameters, as these constraints are not present.

6.2.2.1 Effect of soft phase anisotropy

The optimum value of the magnetocrystalline anisotropy for the different regions present in the multilayer system is very crucial in determining the magnetization reversal mechanism of the grain, but as it is challenging to measure the anisotropy of individual layers in the multilayer system, here it was determined via a comparison study of micromagnetic simulations and experimental measurements (UoM). Figures 6.1 and 6.2 show the quantitative and qualitative magnetization reversal for different magnetocrystalline anisotropy values of the soft phase of the multilayer system with two different exchange constant values 0.2×10^{-11} J/m and 0.8×10^{-11} J/m in the exchange break layer. The value of the exchange constant in the intergranular exchange break layer determines the coupling between the soft and hard phase resulting in the whole grain weakly or strongly coupled as shown in next section.

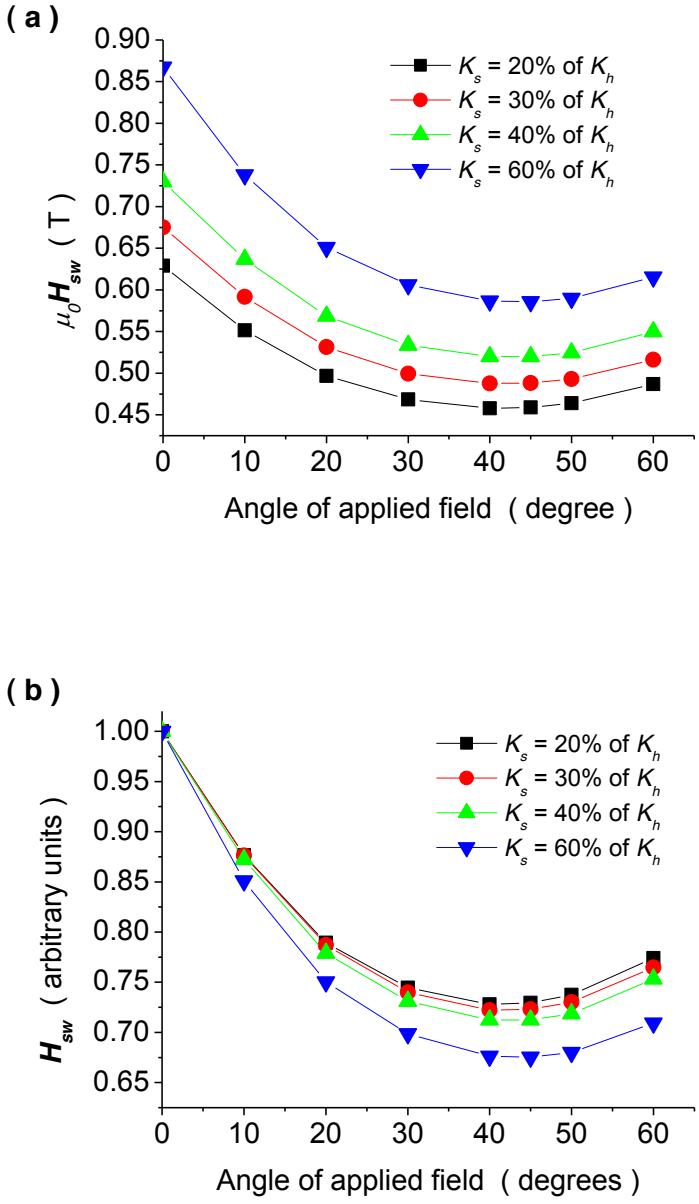

Figure 6.1: (a) The switching field and (b) normalized switching field as a function of angle of applied field with an f_0 of 10^{10} Hz for the CoCrPt based exchange spring grain with a diameter of 8 nm, a hard phase thickness of 11 nm, an exchange layer of 0.5 nm and a soft phase of 6 nm at 292 K. The measurement time is 10 seconds and the exchange constant of the intergranular exchange break layer is 0.2×10^{-11} J/m.

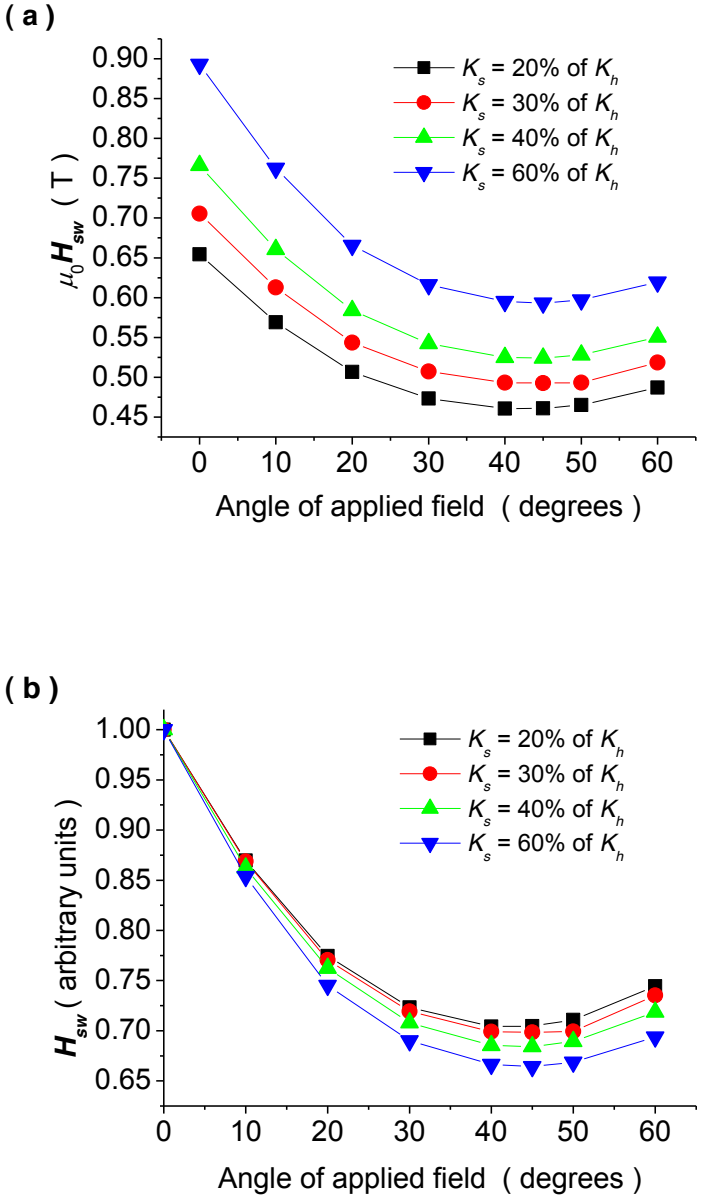

Figure 6.2: (a) The switching field and (b) normalized switching field as a function of angle of applied field with an attempt frequency of 10^{10} Hz for the CoCrPt based exchange spring grain with a diameter of 8 nm, a hard phase thickness of 11 nm, an exchange layer of 0.5 nm and a soft phase of 6 nm at 292 K. The measurement time is 10 seconds and the exchange constant of the intergranular exchange break layer is 0.8×10^{-11} J/m.

The anisotropy of the soft phase of the exchange spring media grain is other important factor which plays a determining role in defining the magnetization reversal and $\boldsymbol{H_{sw}}$ and leads to the exchange spring effect in these medias. The change in the soft phase anisotropy produces a clear shift in the reversal of the multilayer magnetic system. The reduction in the magnetocrystalline anisotropy (20% of K_h) leads to the shift in the minimum angle of the curve also shown in figure 6.3 (a), indicating a less stable grain. The exchange affects the magnetization reversal significantly more at lower soft phase anisotropy (20% of K_h) values; compared to higher anisotropy values (60% of K_h) of the grain, where the grains are highly coupled.

Figure 6.3 (b) shows the change in the switching field of the exchange spring recording media grain with the change in the anisotropy of the soft phase for two different intergranular exchange break layer exchange constant values 0.2×10^{-11} J/m and 0.8×10^{-11} J/m. The switching field increases with the increase in the soft phase anisotropy and intergranular exchange break layer exchange. While increasing the anisotropy of soft phase K_s from 20% K_h to 30% K_h the switching field has increased from 0.63 T to 0.67 T and $\mu_0\boldsymbol{H_{sw}}$ shows the overall increase of 6.8 % for the intergranular exchange break layer exchange constant A_{EBL} = 0.2×10^{-11} J/m Whereas for the case when the intergranular exchange break layer has A_{EBL} = 0.8×10^{-11} J/m the switching field for K_s = 20% K_h is 0.65 T and for K_s = 30% K_h is 0.70 T and shows the percentage increase of 7.2 %. The increase in the switching field is explained by the fact that by increasing the crystalline anisotropy value of the soft-phase the total anisotropy of the grain increases, which leads to a higher total energy of the system, leading to a higher energy barrier. A grain with a higher energy barrier is more stable and therefore needs a higher external field to change its magnetization, see chapter 4, figure 4.4

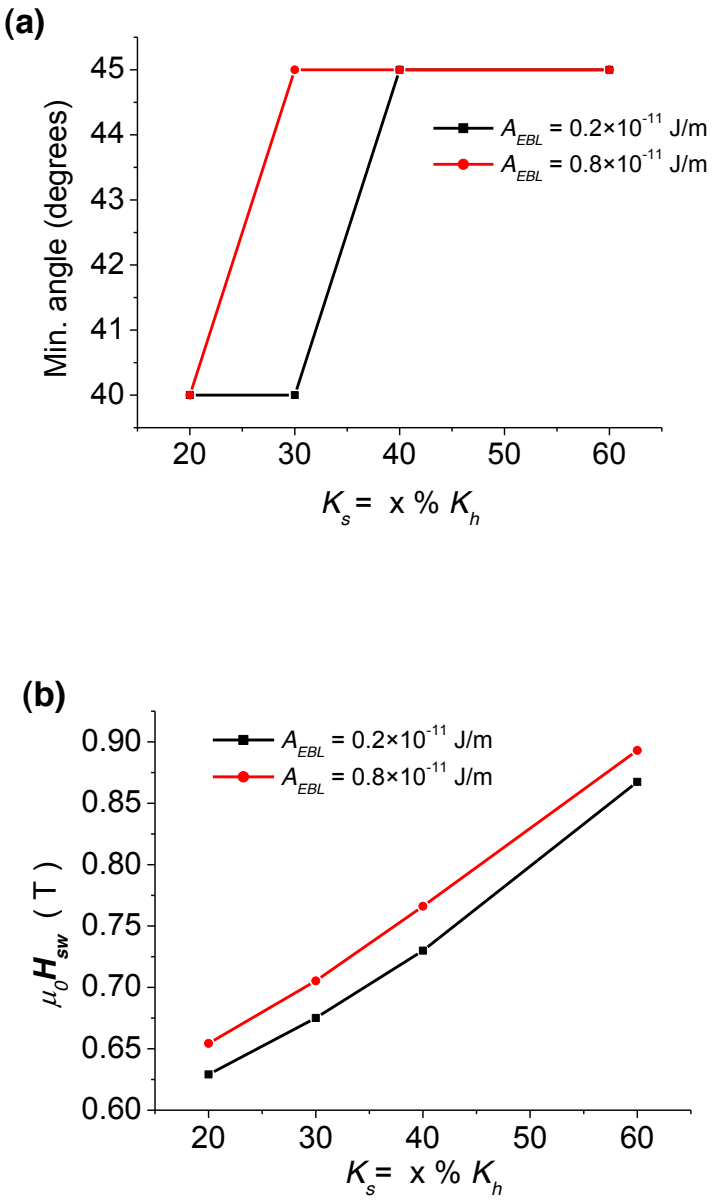

Figure 6.3: (a) Minimum switching field angle as a function of anisotropy of soft phase, (b) switching field for 0 degree of applied field as a function anisotropy of the soft phase K_s with an attempt frequency of 10^{10} Hz for the CoCrPt based exchange spring grain with a diameter of 8 nm, a hard phase thickness of 11 nm, an exchange layer of 0.5 nm and a soft phase of 6 nm at 292 K. The measurement time is 10 seconds and legend in black colour represents the exchange constant A_{EBL} of 0.2×10^{-11} J/m and red colour of 0.8×10^{-11} J/m in the intergranular exchange break layer.

6.2.2.2 Effect of the exchange break layer exchange constant

The strength of the exchange coupling in the exchange break layer is expected to affect the coupling between the hard and soft phase. In order to find the importance of the exchange of the exchange break layer exchange in the switching of the grain the exchange value is varied in the range of 0.2×10^{-11} J/m – 1×10^{-11} J/m. The study is done on two magnetocrystalline anisotropy values of the soft layer, 20% and 60% of K_h. Figure 6.4 and 6.5 shows the effect of the exchange constant of the exchange break layer on the multilayer system with a granular interface having different soft phase magnetocrystalline anisotropies. When the magnetocrystalline anisotropy of the soft phase is low i.e. 20% of K_h the normalized switching field curve shows a greater effect with the variation of the exchange break layer exchange constant and also shows a clear shift in the minimum angle indicative of a greater incoherency during the switching of the magnetization of the multi-layer system.

Whereas the normalized curve for the higher anisotropy of soft phase i.e. 60% of K_h are less dispersed as compared to the 20 % of K_h. In terms of the absolute switching field study the exchange spring media grain with low anisotropy has low switching field values approximately less by 0.25 T than grain with higher soft phase anisotropy at zero degree of angle of applied field.

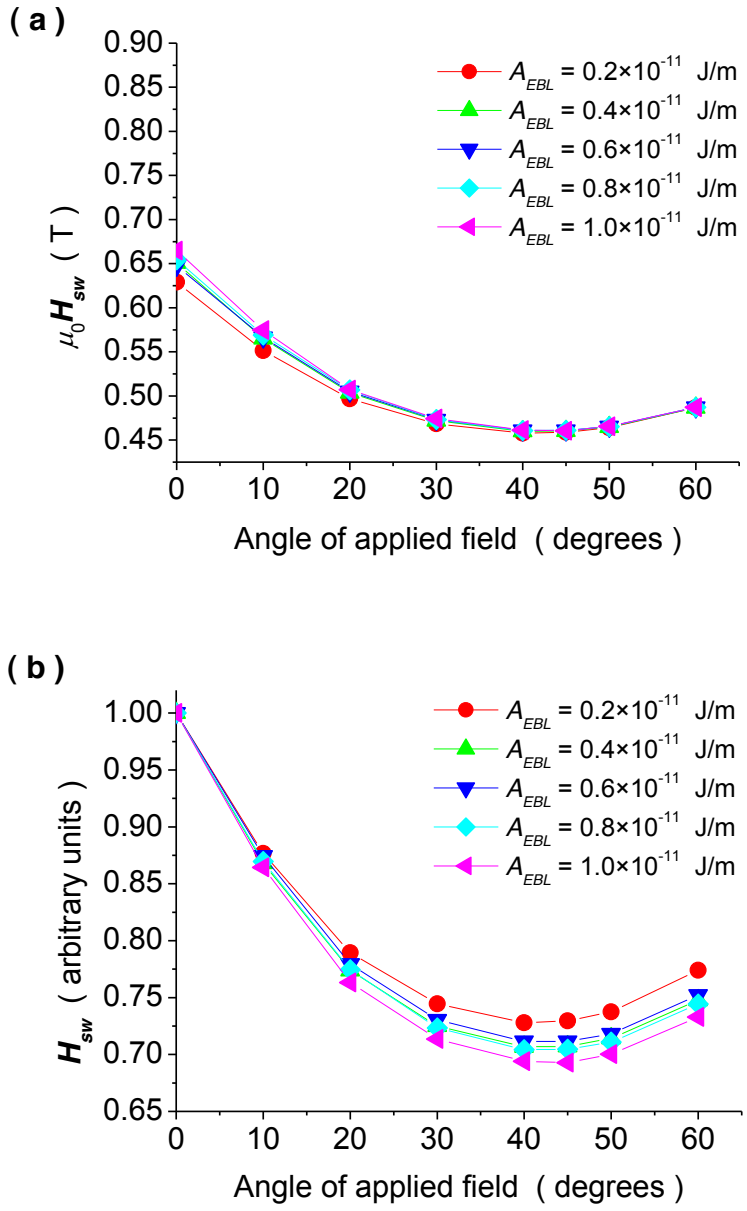

Figure 6.4: (a) The switching field and (b) normalized switching field as a function of angle of applied field with attempt and frequency of 10^{10} Hz for the CoCrPt based exchange spring grain with a diameter of 8 nm, a hard phase thickness of 11 nm, an exchange layer of 0.5 nm and a soft phase of 6 nm at 292 K. The measurement time is 10 seconds and the anisotropy of the soft phase is 20% of K_h.

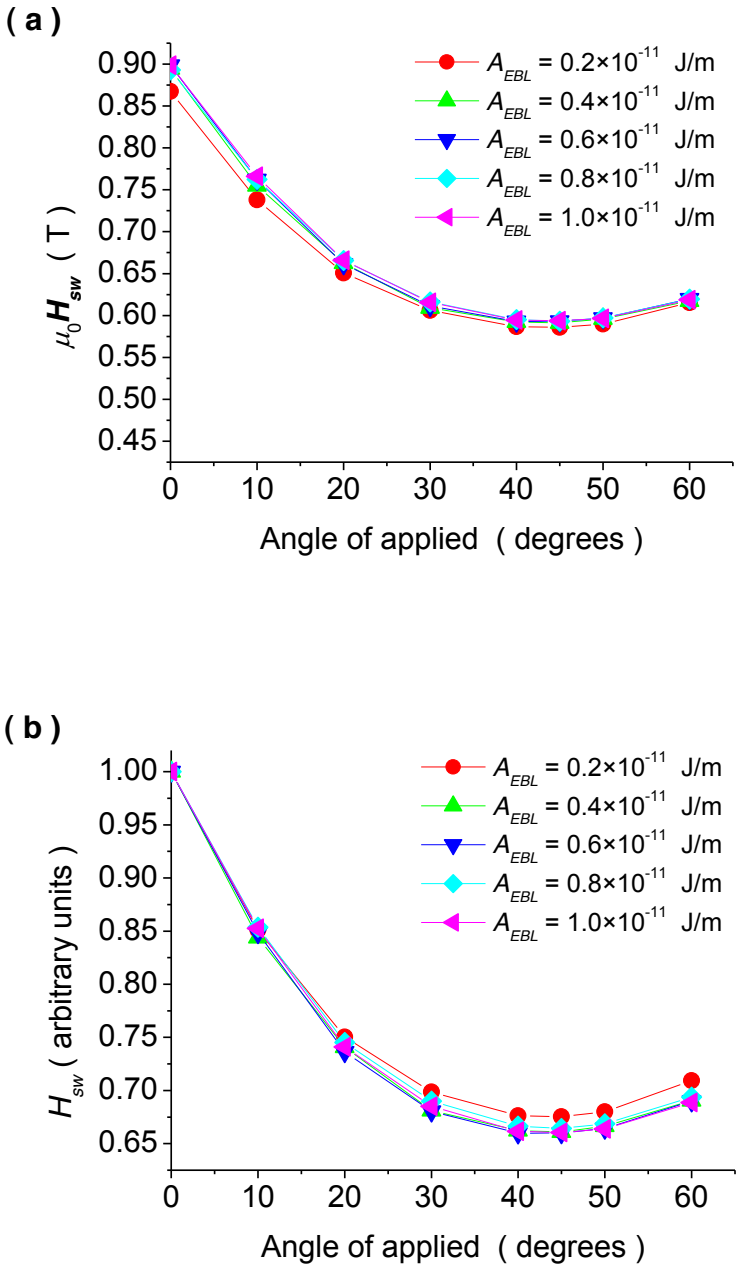

Figure 6.5: (a) The switching field and (b) normalized switching field as a function of angle of applied field with an attempt frequency of 10^{10} Hz for the CoCrPt based exchange spring grain with a diameter of 8 nm, a hard phase thickness of 11 nm, an exchange layer of 0.5 nm and a soft phase of 6 nm at 292 K. The measurement time is 10 seconds and the anisotropy of the soft phase is 60% of K_h.

6.2.2.3 Effect of the exchange break layer thickness

The thickness of the exchange break layer can vary the strength of the effect that its material properties have on the magnetization reversal of the multi-layer system. To study the affect of the thickness of the exchange break layer on exchange spring media grain the thickness of the intergranular exchange break layer is varied in the range of 0.5 nm to 2 nm. Figure 6.6 and 6.7 show the effect of exchange break layer thickness on the multilayer system with an interface exchange constant of 0.2×10^{-11} J/m and 0.8×10^{-11} J/m respectively.

The results show that the multilayer system is more strongly coupled at an exchange of 0.8×10^{-11} J/m as compared to the 0.4×10^{-11} J/m. The comparison in the exchange break layer thickness study indicates that with increasing thickness of the intergranular exchange break layer interface the hard and soft phase becomes weakly coupled, incorporating greater incoherency during the magnetization reversal. As shown in figure 6.8 the switching field of the grain decreases with the increase in the thickness and decrease in the exchange constant of the exchange break layer. It is explained by the fact that the two phases are getting more decoupled and therefore the stabilizing exchange coming from the hard layer is less pronounced in the soft layer, resulting in a smaller switching field. The minimum angle of the normalized curve shifts towards 40 degrees and this effect is more prominent at large thickness of 2 nm as compared to the smaller thickness of 0.5 nm. The minimum angle as a function of the exchange break layer thickness is also shown in figure 6.8 (b) for two exchange constants of 0.20×10^{-11} J/m and 0.8×10^{-11} J/m.

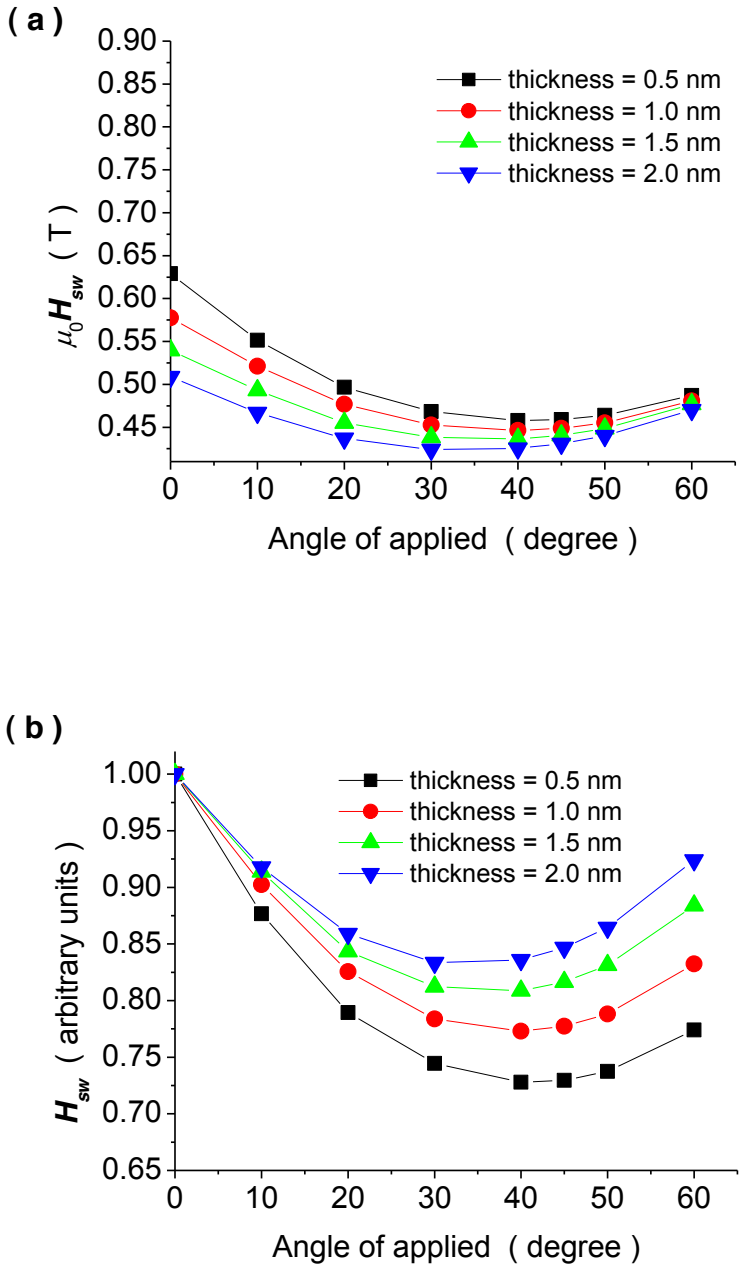

Figure 6.6: (a) The switching field and (b) normalized switching field as a function of angle of applied with an attempt frequency of 10^{10} Hz for the CoCrPt based exchange spring grain with a diameter of 8 nm, a hard phase thickness of 11 nm, an exchange layer of 0.5 nm and a soft phase of 6 nm at 292 K. The measurement time is 10 seconds. The soft phase anisotropy is 20% of K_h and the exchange of the intergranular interface is 0.2×10^{-11} J/m.

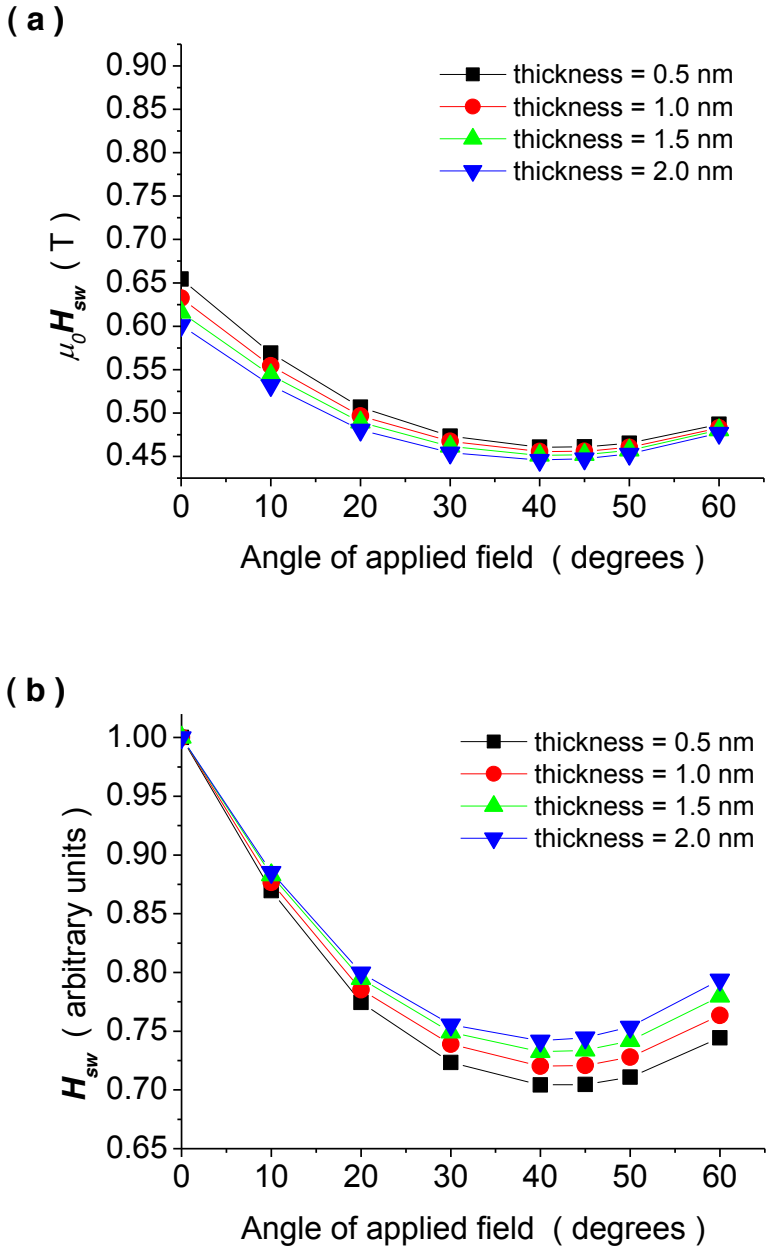

Figure 6.7: (a) The switching field and (b) normalized switching field as function of angle of applied field with an attempt frequency of 10^{10} Hz for the CoCrPt based exchange spring grain with a diameter of 8 nm, a hard phase thickness of 11 nm, an exchange layer of 0.5 nm and a soft phase of 6 nm at 292 K. The measurement time is 10 seconds. The soft phase anisotropy is 20% of K_h and the exchange of the intergranular interface is 0.8×10^{-11} J/m.

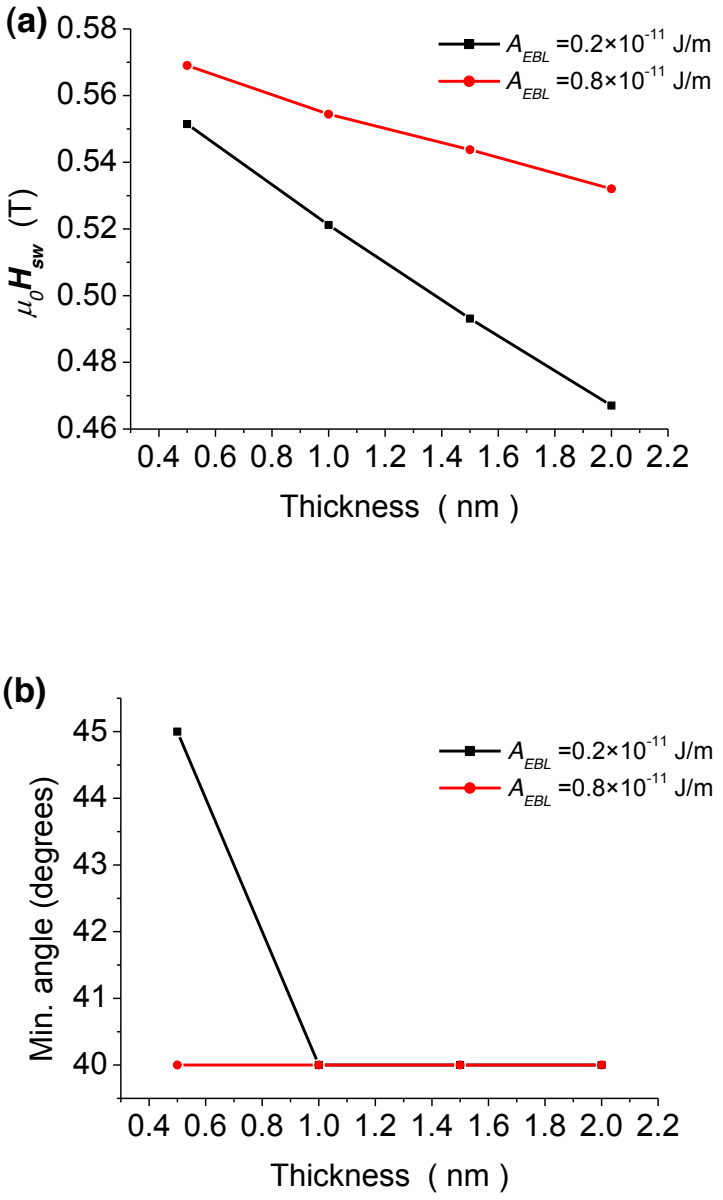

Figure 6.8: (a) The switching field for 10 degree of applied field angle as a function of grain thickness, (b) minimum switching field angle as a function of intergranular exchange break layer thickness with an attempt frequency of 10^{10} Hz for the CoCrPt based exchange spring grain with a diameter of 8 nm, a hard phase thickness of 11 nm, and a soft phase of 6 nm at 292 K. The measurement time is 10 seconds and legend in black colour represents the exchange constant A_{EBL} of 0.2×10^{-11} J/m and red colour of 0.8×10^{-11} J/m in the intergranular exchange break layer.

The comparison in the exchange break layer thickness study indicates that with increasing thickness of the intergranular exchange break layer interface the hard and soft phase becomes weakly coupled, incorporating greater incoherency during the magnetization reversal. The minimum angle of the normalized curve shifts towards 40 degrees and this effect is more prominent at large thickness of 2 nm as compared to the smaller thickness of 0.5 nm as shown in figure 6.7 (b) and figure 6.8(b).

6.2.3 Summary

Presented in the sub-chapter is the parameter space study on the effect of layer properties on the switching field strength and switching mechanism of exchange spring recording media. The effect of the exchange and thickness of the intergranular exchange break layer and anisotropy of the soft phase was studied on the switching field and the magnetization reversal of the CoCrPt based exchange spring media at 292 K.

The study conducted above suggests that the magnetization reversal mechanism depends on the material properties of the exchange break layer as well as the thickness of the layer. For high magnetic anisotropy values and low exchange break layer thickness the coupling between the soft/hard phases is stronger as compared to a low magnetic anisotropy value and high exchange break layer thickness. This means that for a strongly coupled system a shift in the minimum angle was not observed, while for a weaker couple system a clear shift in the minimum angle from 45 to 40 degree is observed. The change in the exchange constant of the exchange break layer leads to a shift in the minimum angle from 45 towards 40 degrees, as the exchange strength is lowered from 0.8×10^{-11} J/m to 0.2×10^{-11} J/m. In addition by

increasing the exchange break layer thickness from 0.5 to 2 nm a clear shift in the angular minimum, from 45 to 40 degrees was observed. In all the simulations the shift of the angular minimum can be attributed to increased incoherency of the magnetization reversal.

Based on the above findings of the parameter space mapping of the exchange spring media, further investigations was conducted to describe the magnetization reversal behaviour of real exchange spring recording media measurements (UoM) by including not only an exchange break layer but also a grain boundary based on the findings of Lister et al [13], see next sub-chapter.

6.3 Grain boundary interaction in exchange spring recording media

Recently Lister et al [13] performed a SANSpol study on CoCrPt-SiO_2 to understand the magnetic structure of the storage layer, which determines the characteristic switching behaviour of the recording layer. In his study Lister pointed out the importance of his findings from a micromagnetic modelling point of view. So far micromagnetic studies done on recording media (single-phase and exchange spring media) treat the magnetic grain as a bulk material and do not consider the irregularities that are present on the boundary of the grains, as mentioned in chapter 4 [14-22]. The grain boundary interaction study done on single-phase media was presented in an earlier chapter and the results show a large change in the switching field values of the grain with a deviation in the magnetization reversal from the bulk single-phase grain. For example the switching field is decreased i.e. for the bulk grain $\mu_0 \boldsymbol{H_{sw}}$ (5°) = 0.59 T, and for the core/shell grain $\mu_0 \boldsymbol{H_{sw}}$ (5°) = 0.51 T, which is a change of 13 %.

Here the focus is to understand the effect of those irregularities on the exchange spring recording media grain. This section of the chapter presents a micromagnetic study done on CoCrPt based exchange spring recording media at 292 K. The study focuses on the interaction between the core and the oxide present around the grain and their effect on the reversal process of the magnetization of the magnetic grains. In order to derive a fundamental understanding of the mechanism and its effects on the switching process, different magnetic structures were considered during the study. The simulations results were directly compared with VSM measurements (UoM).

6.3.1 Model setup

Experimentally, the data storage medium of the recording media used by Prof. Thomson's group at the University of Manchester is a complex multi-layered structure [12]. The complete structure constitute a protective overcoat and thin lubricant layer to prevent any damage from the flying head, onto the CoCrPt-based perpendicular exchange spring data storage layer of 17 nm thickness. The structure is grown with a dc magnetron sputtering on a glass substrate, which has a thickness of 65 mm. On top of the glass substrate a 100 nm thick CoFe based antiferromagnetically coupled soft under layer is grown followed by thin Ru seed layer. Figure 6.9 shows the schematic of the exchange spring media as seen in experiments.

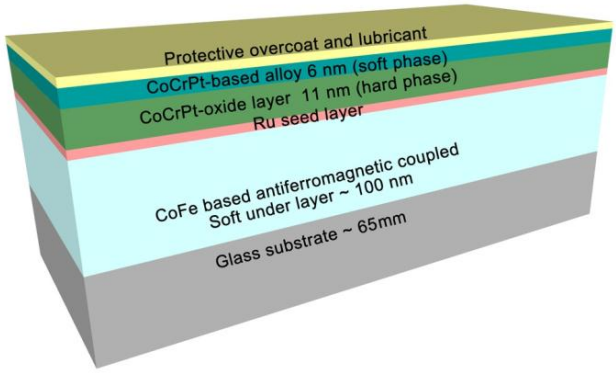

Figure 6.9: Schematic of the data storage layer as seen in experiments [11]. On the top of the magnetic recording media is a protective overcoat and lubricant layer, against oxidation and mechanical effects (friction from the head). Below that is the CoCrPt multilayer, which consists of a magnetically soft alloy layer ~6 nm and a magnetically hard layer of ~11 nm. Followed by a thin Ru seed layer that is on top of a ~100 nm thick CoFe based antiferromagnetic coupled soft under layer. All these layers are deposited on a ~65 mm glass substrate.

As pointed out earlier the data storage layer has ferromagnetic core regions embedded inside a non-magnetic SiO_2 matrix. Due to the intermixing of the ferromagnetic material with the SiO_2 the size of the ferromagnetic region is found to be smaller than the corresponding grain size. It was shown by experiments [13] that in the boundary region of the ferromagnetic grain, the magnetic properties show a step at the interface between the CoCrPt and the SiO_2. The step at the interface divides the grains into different regions based on magnetic properties: the magnetic core, shell and the grain boundary region. The magnetic core is concentrated in the centre of the grain and the less magnetic regions, shell and boundary surrounds the magnetic core [13].

Presented here is a micromagnetic study to understand the influence of the boundary phase on the switching behaviour of the exchange spring recording media magnetic grains. The study has been divided into three cases, based on the way material parameters are assigned to the columnar exchange spring magnetic grains. Cylindrical grain with the following lateral parameters was considered for the study: total diameter of 8 nm, hard and soft phase thickness of 11 nm and 6 nm and the thickness of the intergranular exchange break layer is varied from 0.5 nm to 1 nm.

Soft phase	K_s (MJ/m^3)	$J_{s,soft}$ (T)	A_s (J/m)
	0.17	0.57	1×10^{-11}
Exchange break layer	K_{EBL} (MJ/m^3)	$J_{s,EBL}$ (T)	A_{EBL} (J/m)
	0.17	0.57	0.2×10^{-11}-0.8×10^{-11}
Hard phase	K_h (MJ/m^3)	$J_{s,h}$ (T)	A_h (J/m)
	0.58	0.90	1×10^{-11}

Table 6.1: The material parameters at temperature 292 K experimentally derived by Prof Thomson's group at the University of Manchester University [1], have been used for the modelling of the simplified CoCrPt based one-grain exchange spring recording media cylindrical model [11, 12].

Case1: A CoCrPt based two-phase material with with the intergranular exchange break layer between the hard and soft phase was used as exchange spring recording media grain similar to the one studied in the sub-chapter 6.2. The diameter of the grain is kept constant as 8 nm and the thickness of the hard phase; intergranular exchange break layer and soft phase are as follows 11 nm, 0.5 nm and

6 nm. The grain has the bulk material properties. The material parameters given to the grain are given in the table 6.1.

The material properties for the hard phase were taken from Morrison et. al. [11] and for the soft phase from Thomson et. al [12]. The material properties like the magnetocrystalline anisotropy of the soft phase and intergranular exchange break layer of the grain were chosen based on the finding of the above explained parameter space study and the value of the magnetic polarization was taken from Morrison et. al. [11].

Case 2: The volume of the grain is divided into three parts: core, shell and boundary. All three of them have different material properties as shown in figure 6.10. The inner volume represents the magnetic core with the same material parameters as in case 1 for the hard/ soft phase and exchange break layer, except for the exchange in the exchange break layer, which was set to be either 0.2×10^{-11} J/m or 0.4×10^{-11} J/m. These two values have been selected based on previous studies where the values have been varied between 0.2×10^{-11} J/m - 0.8×10^{-11} J/m. It was shown that lower exchange values in the exchange break layer are more likely to give a shift in the angular dependency.

The complete list of material parameters given to all the three volumes of the designated by different colours in Figure 6.10, the core, shell and boundary of the soft phase, exchange break layer and the hard phase are given in the table 6.2 [11-13].

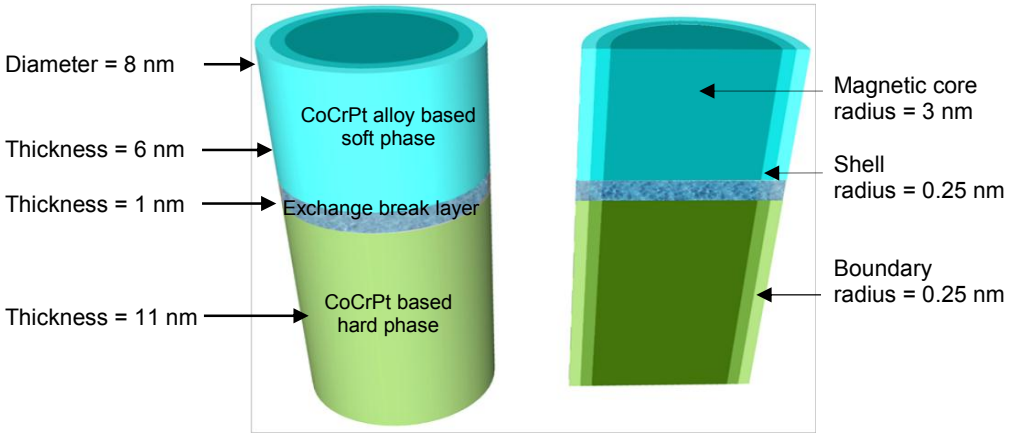

Figure 6.10: Schematic of the CoCrPt based exchange spring recording media used in case 2. The two-phase grain consists of a CoCrPt based hard phase, intergranular exchange break layer and CoCrPt based alloy as soft phase. The grain is divided into three parts by volume: core, shell and boundary. The radius of the core/ shell/ boundary is 3.5 nm/ 0.25 nm/ 0.25 nm. The thickness of the hard phase, intergranular exchange break layer and soft phase is 11 nm, 1 nm and 6 nm. The magnetocrystalline anisotropy and magnetic polarization of the core is the same as in case1, the shell is 20% of that of the core, and the boundary is 10% of that of the core. The exchange of the core, shell and boundary for the hard/ soft phase is 1×10^{-11} J/m whereas for the exchange break layer the value is either 0.2×10^{-11} J/m or 0.4×10^{-11} J/m.

Case 3: In order to understand the angular dependence of the exchange spring recording media as a function of a more coherent magnetic soft phase and its effect on the switching field, we have constructed a grain that reflects a granular hard phase, covered by a soft magnetic film. Here the soft and intergranular exchange break layer region are considered each as one whole volume and only the volume of the hard phase is divided into two parts: core and shell with variable material properties as shown in figure 6.11. The material properties of the soft phase and the

exchange break layer region are the same as in case 1. The core and shell region of the hard phase have the same the material properties as in case 2. The material parameter considered for case 3 are given in table 6.2.

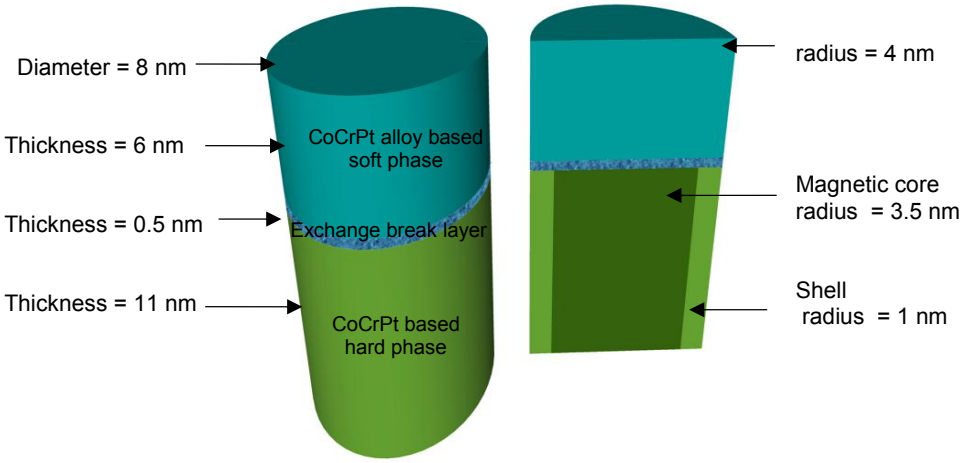

Figure 6.11: Schematic of the CoCrPt based exchange spring recording media used in case 3. The grain consists of a hard phase, intergranular exchange break layer and a soft phase. The soft phase and the exchange break layer are considered as bulk in terms of volume and material properties with radius 4 nm. The thickness of the hard phase, intergranular exchange break layer and soft phase are 11 nm, 1 nm and 6 nm. The hard phase is divided into two parts by volume: core/shell with radius 3 nm/ 1 nm. The magnetocrystalline anisotropy, magnetic polarization and exchange for the core region of the hard phase are the same as in case 1, whereas the shell is 20% of that of the core region with an exchange constant of 1×10^{-11} J/m.

Soft phase	K_s (MJ/m^3)	$J_{s,soft}$ (T)	A_s (J/m)
	0.17	0.57	1×10^{-11}
	$K_{s,shell}$ (MJ/m^3)	$J_{s,soft,shell}$ (T)	A_s (J/m)
	0.038	0.114	1×10^{-11}
	$K_{s,boundary}$ (MJ/m^3)	$J_{s,soft,boundary}$ (T)	A_s (J/m)
	0.017	0.057	1×10^{-11}
Exchange break layer	K_{EBL} (MJ/m^3)	$J_{s,EBL}$ (T)	A_{EBL} (J/m)
	0.17	0.57	0.2×10^{-11} -0.4×10^{-11}
	$K_{EBL,shell}$ (MJ/m^3)	$J_{s,EBL,shell}$ (T)	A_{EBL} (J/m)
	0.038	0.114	0.2×10^{-11} -0.4×10^{-11}
	$K_{EBL,boundary}$ (MJ/m^3)	$J_{s,EBL,boundary}$ (T)	A_{EBL} (J/m)
	0.038	0.057	0.2×10^{-11} -0.4×10^{-11}
Hard phase	K_h (MJ/m^3)	$J_{s,h}$ (T)	A_h (J/m)
	0.58	0.90	1×10^{-11}
	$K_{h,shell}$ (MJ/m^3)	$J_{s,h,shell}$ (T)	A_h (J/m)
	0.116	0.18	1×10^{-11}
	$K_{h,boundary}$ (MJ/m^3)	$J_{s,h,boundary}$ (T)	A_h (J/m)
	0.058	0.09	1×10^{-11}

Table 6.2: The material parameters at temperature 292 K experimentally derived by Prof Thomson's group at the University of Manchester University [1], have been used for the modelling of the simplified CoCrPt based one-grain exchange spring recording media cylindrical model of case 2 [11-13].

6.3.2 Experiments and simulations

As mentioned before the aim of this study is to explore the magnetic structure and magnetization reversal of the exchange spring recording media in line with experiments carried out by Prof. Thomson's group at the University of Manchester. To get a better understanding how interfaces and grain boundaries change the

magnetic reversal behaviour we choose a systematic approach to explore the impact of these effects. In case 1 a homogenous magnetic grain structure is chosen for the exchange spring recording media. Choosing this kind of setup not only gives simulation results that can be compared with models from other groups, but also gives an idea how a perfect interface and grain structure would behave. This will be a reference structure where all our other results will be compared against, in terms of chemical and morphological variations, case 2 and 3.

6.3.2.1 Case1: homogenous magnetic structures

The material parameters for the grain in case 1 are based on the previous study done in sub-chapter: section 6.2 (the importance of intergranular interface in exchange spring recording media). Figure 6.12 shows a comparison of the switching field and normalized switching field for the exchange spring media grain of case 1 with experiments at 292 K. The attempt frequency f_o and measurement time τ for the calculations of the switching field are 10^{11} Hz and 10 seconds. The measurement time of seconds is the minimum time that can be achieved with the help of VSM.

In order to compare normalized switching field with experiments the presence of an easy axis distribution in the experimental grains has been taken into account, which is sigma 3. To do so, first the switching field at zero degree applied field angle with the help of a gauss normalization that considers the grain distribution of sigma (σ) equal to 3 degree as reported by Thomson et. al. [12] was calculated.

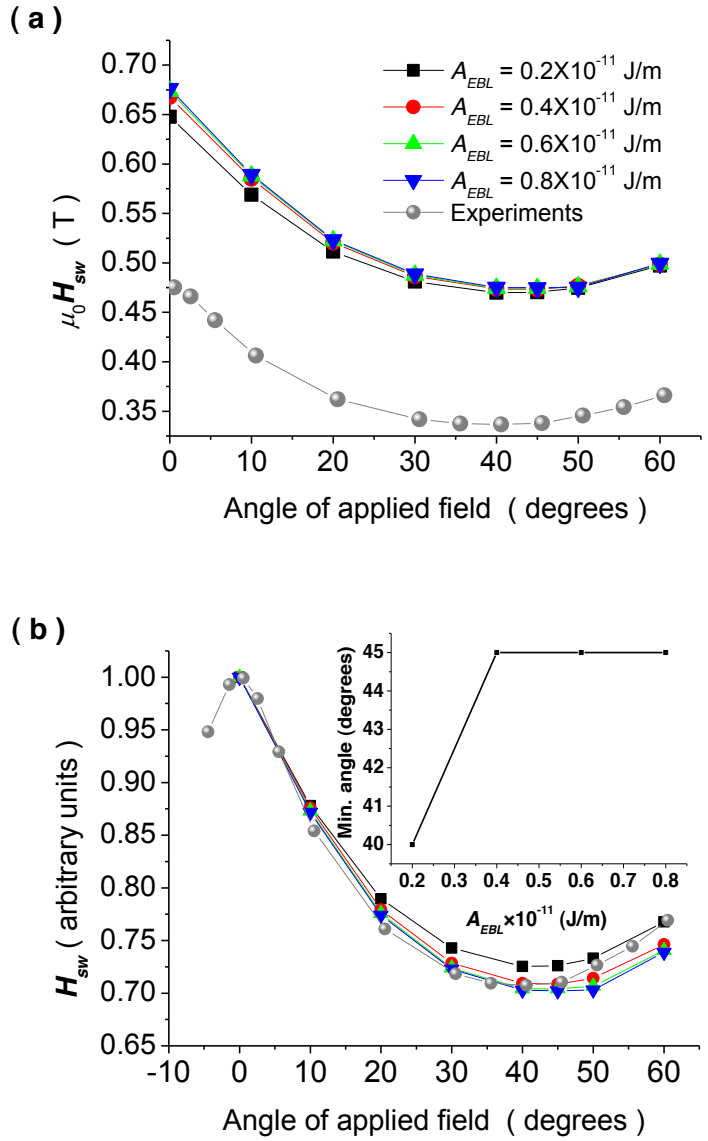

Figure 6.12: Comparison of (a) the switching field and (b) the normalized switching field as a function of angle for the CoCrPt based exchange spring recording media grain at 292 K with experiments. The value of the attempt frequency is 10^{11} Hz and the measurement time is 10 seconds. The different colours of the curve represent the different values of the exchange in the exchange break layer in the range of 0.2×10^{-11} J/m - 0.8×10^{-11}J/m. The grey curve represents the experimental values (UoM). Inset shows the minimum angle as a function of exchange constant in the exchange break layer for model.

The comparison of the switching field in the figure 6.12 (a) with different intergranular exchange break layer exchange constants shows that the calculated switching field values are higher than the experimental values by approximately 0.2 T, at an applied field angle of zero degrees. The other important thing to note here is that apart from the discrepancy in the switching field magnitude, the trend of the switching field of the model is similar to that of the experimental measurements (UoM).

The minimum switching field angle for the experimental curves measured (UoM) is 40 degree and deviates from the Stoner-Wohlfarth behaviour where the minimum angle lies on 45 degree. In the simulations the minimum switching field angle exits on 45 degree for a high exchange values in the intergranular exchange break layer ranging from 0.4×10^{-11} J/m to 0.8×10^{-11} J/m**,** whereas for the exchange of 0.2×10^{-11} J/m the minimum switching field angle is 40 degree with an absolute switching field of 0.487 T, which is less than the switching field at 45 degree by 0.000476 T as shown in inset in figure 6.12 (b). On the other hand the exchange value of 0.2×10^{-11} J/m is too small to be considered physical.

The normalized switching field as a function of applied field angle for the model does not agree well with the experimental measurements (UoM) as shown in Figure 6.12 (b). For example for model $\mu_0 \boldsymbol{H_{sw}}$ (0°) = 0.68 T when A_{EBL} = 0.8×10^{-11} J/m and for experiments $\mu_0 \boldsymbol{H_{sw}}$ (0.55°) = 0.48 T which is 29 % lower than the one predicted by model. The model predicts a different magnetization reversal for the grain as compared to the experiments (UoM). The experimental normalized curve clearly shows the minimum at 40 degree where as the model indicates the minimum at 45 degree except at an exchange value of 0.2×10^{-11} J/m where the minimum is at 40 degree. Apart from all these discrepancies, a good agreement between simulations and experiments for the gradient of the normalized curve and the absolute switching

field values at smaller applied field angles from 0 degree to 30 degree can be observed.

6.3.2.2 Case 2: heterogeneous grain (core/shell/boundary)

In the second case, the magnetic structure of the exchange spring media grain was varied. Based on the publications of Lister, the gradual transition of the magnetic composition across the grain boundary was taken into account. To approximate such a transition the volume of the grain was divided into three parts and different material properties to each of these sub volumes were allocated, as outlined above. It is expected that the variation in the magnetic properties over the volume of the grains will redefine the switching dynamics of the recording media.

Figure 6.13 (a) shows the comparison of the switching field as function of angle with experiments. The absolute value of the switching field predicted by the model is 0.009 T higher than that of the experiments at an applied field angle of zero degree. The switching field values of the core shell model of case 2 are closer to the experiments than the ones from case1. For example for model $\mu_0 \boldsymbol{H_{sw}}$ (0°) = 0.48 T when A_{EBL} = 0.2×10^{-11} J/m and for experiments $\mu_0 \boldsymbol{H_{sw}}$ (0.55°) = 0.48 T. Concerning the minimum angle of the angular dependency trend is same as observed earlier as in case 1, the minimum is at 45 degree except for an exchange value of 0.2×10^{-11} J/m where the minimum is at 40 degree. In figure 6.13 (b), the comparison of the magnetization reversal i.e. the normalized switching field for the core/shell/boundary grain between the experiments (UoM) and the model with the two different exchange break layer's exchange 0.2×10^{-11} J/m and 0.4×10^{-11} J/m is done.

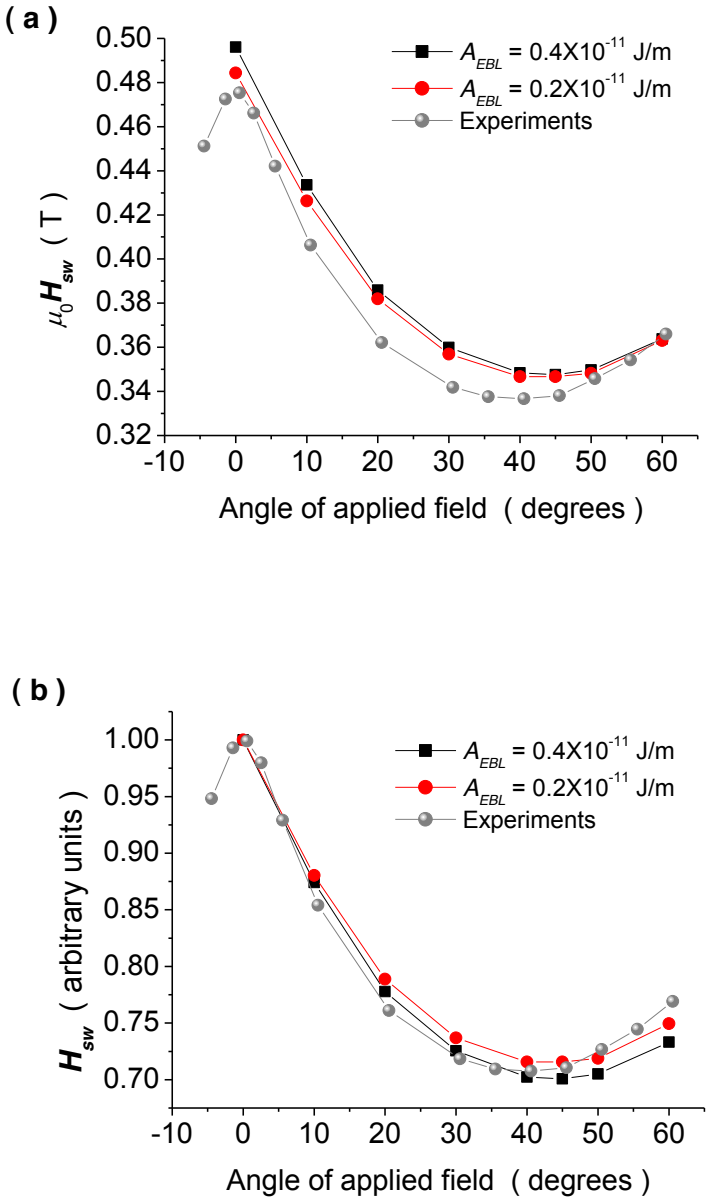

Figure 6.13: Comparison of (a) the switching field and (b) normalized switching field as a function of angle for the CoCrPt exchange spring recording media grain at 292 K with experiments. The attempt frequency and measurement time for the calculation are 10^{11} Hz and 10 seconds. The black curve represents the simulation values for an exchange value of the exchange break layer of 0.4×10^{-11} J/m and the red curve the ones for 0.2×10^{-11} J/m. The grey curve represents the experimental measurements (UoM).

The model shows a Stoner-Wohlfarth like behaviour for the 0.4×10^{-11} J/m value with its minimum switching field angle at 45 degree and deviates from the experiments where the minimum switching angle lies at 40 degree, which is moving towards a Kondorsky (1/cosθ) type of magnetization reversal behaviour [14]. But here the model shows better agreement with experiment, if an exchange constant value of 0.2×10^{-11} J/m is considered. As at the exchange of 0.2×10^{-11} J/m has the switching field values lower than the switching field values at of 0.4×10^{-11} J/m as shown in figure 6.13 (a). For example for model for A_{EBL} = 0.2×10^{-11} J/m, $\mu_0 \boldsymbol{H_{sw}}$ (0°) = 0.48 T and for A_{EBL} = 0.4×10^{-11} J/m, $\mu_0 \boldsymbol{H_{sw}}$ (0°) = 0.50 T.

These findings indicate the importance and support the existence of the core/shell region within in the grain as proposed by Lister et. al. [13].

6.3.2.3 Case 3: bulk: soft, EBL and core/shell: hard phase

The fact that the model in case 2 predicts the switching field in the range of experimental values but fails to fully capture the normalized switching field trend suggests the complexity of the magnetic structure of the real recording layer structure. For example for model $\mu_0 \boldsymbol{H_{sw}}$ (10°) = 0.40 T when A_{EBL} = 0.8×10^{-11} J/m and for experiments $\mu_0 \boldsymbol{H_{sw}}$ (10.55°) = 0.40 T, which is same as predicted by the model. In order to understand the anomaly in the minimum switching field angle further the magnetic structure of the exchange spring grain was changed as explained in the case 3 above. Figure 6.14 compares the results of case 3 with experiments (UoM).Figure 6.14 (a) shows the switching field as a function of applied field angle for different exchange values of the exchange break layer ranging from 0.4×10^{-11} J/m - 0.8×10^{-11}J/m with experiments.

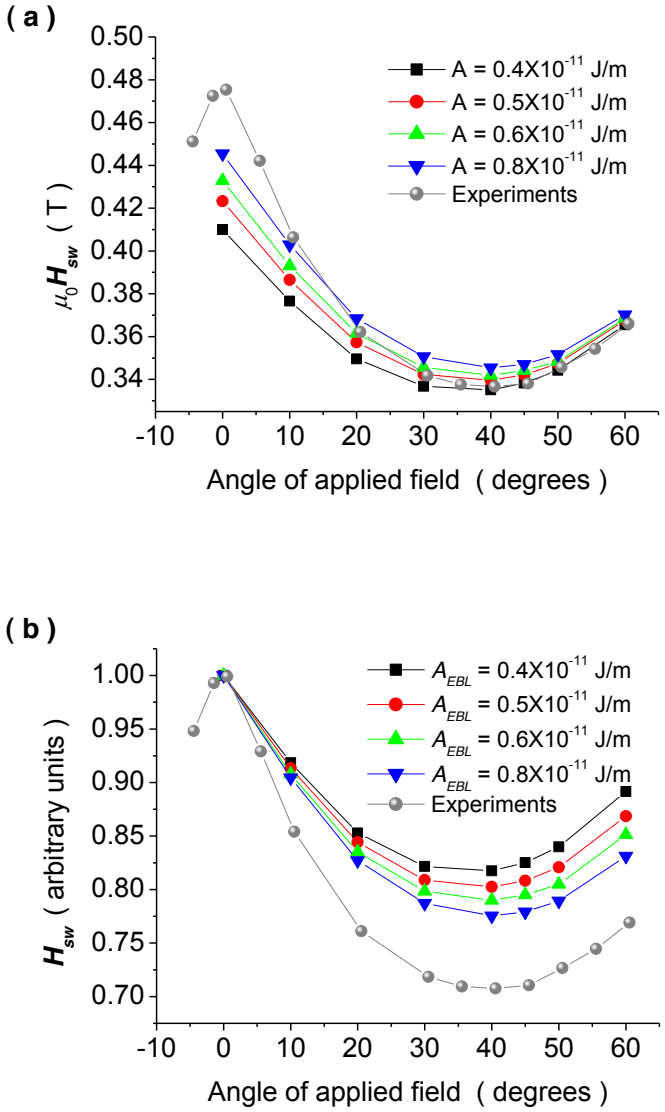

Figure 6.14: Comparison of (a) the switching field and (b) normalized switching field as a function of angle for the CoCrPt exchange spring recording media grain at 292 K with experiments. The attempt frequency and measurement time for the calculation are 10^{11} Hz and 10 seconds. The black curve represents the simulation values for an exchange value of the exchange break layer of 0.4×10^{-11} J/m, the red curve for 0.5×10^{-11} J/m, the green curve for 0.6×10^{-11} J/m, the blue curve for 0.8×10^{-11} J/m, and the grey curve represents the experiments (UoM).

Here it can be seen that the model predicts the switching field well at intermediate angles (40 to 60 degree) but deviates slightly for small angles (0 to 30 degree). Furthermore the model also predicts the minimum switching field angle, which is 40 degree in accordance with experiments done by Prof. Thomson's group.

As previously described this shift in minimum angle and absolute switching field values can be attributed to an incoherency originating from the grain boundaries, where weaker coupled spins pose an intrinsic weak spot for nucleation.

From figure 6.14 (b) it is observed that the model shows a clear shift from the Stoner-Wohlfarth towards the Kondorsky model. The model successfully captures a similar trend as in the experiments done by Prof. Thomson's group along with the minimum switching field angle at 40 degree. Albeit of all the agreement in trend and minimum switching field angle the model shows higher absolute normalized switching field values. For experiments the change in the normalized switching field values while changing the angle from 0.5 to 40.5 degree is 0.29, which is larger than the changes shown by the simulation data where normalized switching field changes by 0.18 while changing angle form 0 to 40 degree for A_{EBL} = 0.4x10-11J/m. The reason for this disagreement in the absolute value at small angles in the switching field and higher absolute normalized switching field values in figure 6.14 (b) can be understood by the fact that the model may not be able to capture the exact material structure and properties as it exists in the real data storage film. In addition the model is a simplified one grain exchange spring media structure, which is a very simple approximation and might not have all the complexity which exists in a real magnetic recording layer, like the exchange from neighbouring grains and the extended film layer on top of the hard layer.

6.3.3 Summary

A micromagnetic study of the grain boundary interaction and the influence of the intergranular exchange break layer on the exchange spring recording media at 292 K were performed to explain qualitative and quantitative measured switching fields which are essential in the design of magnetic recording heads. The comparison of the simulations with VSM measurements done by Prof. Thomson's group at the University of Manchester clearly emphasize on the importance of the core/shell in micromagnetic studies and validates the findings of Lister et. al. shown by the fact that the core/shell model is successful in replicating the trend in the magnetization reversal of the two-phase media. The material and lateral properties of the intergranular exchange break layer were investigated and it was shown that a variation in these parameters can be used to design and control switching field values and the magnetization reversal of these grains. The model captures the trend in the magnetization reversal as observed in experiments done by Prof. Thomson's group although the magnitude of the switching field value shows some discrepancies for low angles (close to zero).

The simulations point out the importance of the core/shell model for micromagnetic studies and also the mapping of the parameter space of the magnetic properties of the magnetic structure. The latter is important because the material properties of the soft phase and intergranular exchange break layer are very difficult to measure experimentally. Today with the continuous focus on scaling of magnetic grains to a diameter less than 6 nm with the purpose to increase the areal density of the hard disk drives, the presence of a core/shell in the grains might pose a fundamental limit on the diameter that can be achieved.

References

1. E. F. Kneller, and R. Hawing, IEEE Trans. Magn. **27**, 4 (1991).
2. H. Chang, J. Appl. Phys. **35**, 770 (1964).
3. E. Goto, N. Hayashi, T. Miyashita and K. Nakagawa, J. App. Phys. **36**, 9-2951(1965).
4. E. E. Fullerton, J.S. Jiang, M. Grimsditch, C.H. Sowers and S.D. Badar Phys. Rev. B **58**, 12193 (1998).]
5. S.N. Piramanayagam, Appl. Phys. Lett. **102**, 011301 (2007).
6. R.Skomski, and J.M.D Coey, Phys. Rev. B **48**, 15812 (1993).
7. T. Schrefl, J.Fidler, and H. Kronmuller, Phys. Rev. B **49**, 6100 (1994).
8. R. Fischer, T. Schrefl, H. Kronmuller, and J.Fidler,J. Magn. Magn. Mater.**150**, 329 (1995).
9. R.Fischer, T. Schrefl, and H. Kronmuller, Phys. Rev. B **57**, 10723 (1998).
10. E. E. Fullerton, J.S. Jiang, S.D. Badar, J. Magn. Magn. Mater. **200**, 392 (1999).
11. C. Morrison, L. Saharan, G. Hrkac, T. Schrefl, Y. Ikeda, K. Takano, J. J. Miles and T. Thomson, Appl. Phys. Lett. **99,** (2011).
12. T. Thomson, B. Lengsfield, H. Do, and B. Terris, J. Appl. Phys. **103,** 07F548 (2008).

13. S. J. Lister, M. P. Wismayer, V. Venkataramana, M. A. De Vries, S.J. Ray, S.L. Lee, T. Thomson, J. Kohlberecher, H. D, Y. Lkeda, K. Takano, and C. Dewhurst," J. Appl. Phys. **106**, 063908 (2009)**.**

14. M. Benakli, A. F. Torabi, M. L. Mallary, H. Zhou, and H. Neal Bertram, IEEE Trans. Magn. **34**, 4 (2001).

15. N. Honda*,* K. Ouchi*,* and S. Iwasaki*,* IEEE Trans. Magn. **38**, 4 (2002).

16. Kai-Zhong Gao and H. Neal Bertram*,* IEEE Trans. Magn. **38**, 6 (2002).

17. R. Wood, M. Williams*,* A. Kavcic, and J. Miles, IEEE Trans. Magn. **45**, 2 (2009).

18. T. Tanaka, A. Kato, Y. Furomoto, A. F. Md Nor, Y. Kanai, and K. Matsuyama, J. Appl. Phys. **111**, 07B711 (2012).

19. Y. Nozaki, A. Kato, K. Noda, Y. Kanai, T. Tanaka, and K. Matsuyama, J. Appl. Phys. **109**, 123912 (2011)

20. D. Suess, J. Magn. Magn. Mater. **308**, 2 (2007).

21. R. H. Victora*,* and Xiao Shen*,* IEEE Trans. Magn. **41**, 2 (2005).

22. J. Zhang, Y. Liu, F. Wang, J. Zhang, R. Zhang, Z. Wang, and X. Xu, J. Appl. Phys. **111**, 073910 (2012).

Chapter 7: Conclusion and outlook

7.1 Conclusion

This thesis has shown that a simplified grain model with adequate granular structure can be used to study the magnetization reversal behaviour of the real media thin films at finite temperatures. The study conducted here bridges the gap between the simulations and experiments, by study the magnetization reversal dynamics of the real media in the regime which has not been studied before.

Today or in the close future when the recording industry has reached its fundamental limit of scaling (trilemma), any technology is welcome to further increase the areal density in hard disk drives. The most promising writing and recording techniques proposed to postpone the trilemma of recording are: HAMR [1], MAMR [2], BPMR [3, 4], TDMR [5] technology and exchange spring recording medias [6]. Before these options could be successfully adopted for HDDs by the industry, there are technological challenges that need to be addressed. Meanwhile it is important to concentrate on improving the current possible conventional recording media, while exploring new options in parallel.

Despite of the experimental and modelling efforts the magnetization reversal dynamics of the grains in the data storage medium are not well understood at finite temperature regimes [7-10]. Presented here is a micromagnetic study conducted on the magnetization dynamics and the optimization of CoCrPt–based single and exchange spring perpendicular magnetic recording media in close collaboration with experiments, done by Prof Thomson's group at the University of Manchester (UoM).

One of the aims of the project was to investigate the possibility to use a simplified single-phase media and exchange spring media to explain the magnetization dynamics of real recording media films. By the direct comparison of our results of the simplified single grain model with the vector vibrating sample magnetometer measurements (UoM) on well-segregated, single layer CoCrPt-SiO_x recording media and demonstrate that the thermal activation modifies the Stoner-Wohlfarth angle dependency of the switching field by reducing the depth of the minimum that occurs at 45 degrees [11]. Although results could capture the reduction of the switching field as function of applied field angle there are still a few features that could not be explained, such as the shift away from the 45-angle minimum.

Therefore the effect of inter/intra granular exchange coupling and thermal activation on the switching behavior of the single-phase media was studied. It was shown that for larger grains the switching field as a function of angle of the applied field shows a shift in the minimum angle, which arises solely due to incoherent reversal induced by inter/intra granular exchange coupling or incoherency, rather than thermal activation [12, 13].

For multi-layer systems an in-depth study was conducted on exchange spring recording media to understand the importance of the intergranular exchange break layer interface present between the soft/hard phases was included in the model, in contrary to previously studies which did not consider the intergranular exchange break layer interface. Our results show that the intergranular exchange break layer interface plays a vital role in the magnetization reversal of the exchange spring grains. The purpose of this study was to model an optimized exchange spring media in line with experiments (UoM). Hence the effect of the material properties of the exchange break and soft phase were studied intensively. All this progress in model

systems could explain most effects like angular shift that originates from incoherency and coupling effects at the interface layer, but for the multi-layer systems only a poor agreement with experiments (UoM) especially the quantitative values of the switching field was achieved. To deal with this problem it was decided to investigate the chemical and morphological structure of the grains.

Past studies treated the magnetic grain as a bulk material. The main aim of this study is to bridge the gap between the experimental and theoretical studies by considering more realistic grain structures, which are based on experimental findings of Lister et. al. where a deviation in the magnetic structure of the grains, from the centre to the boundary of the grain, has been observed and it is indicated that the magnetization reversal of the magnetic grain depends critically on the magnetic structure of the grains [14].

Therefore, a grain boundary study was conducted representing the variation in the magnetic structure of the overall grain, on the single-phase media and exchange spring recording media based on Lister et. al. findings. The simulation results show the impact of the grain boundary interaction and the importance of the core/shell model on the quantitative and qualitative switching field and the magnetization reversal in the recording media.

7.2 Outlook

The work presented here has direct impact on the theoretical and experimental studies being done. The theoretical investigation carried out laid foundation for the future studies; it was shown that the real media thin film can be model with the

simplified micromagnetic models. Meaning that in future more complex real systems are possible to model with simplified model and could also be useful to find out the material properties of the grains where they are difficult to determine through experiments. The study plays important role in bridging the gap between the theoretical and the experimental work. Together with the experimental measurements and theoretical study the effect of thermal activation and exchange coupling on the switching behaviour of the magnetic grains is shown for the first time.

The past study based on the magnetization of the magnetic grain has ignored the dependence of the exchange on the switching of grains and has considered the theoretical value of the exchange constant of 1×10^{-11} J/m for the CoCrPt material. This work for the first time has shown that the exchange plays determining role in the switching of such grains and stress further in-depth study of the exchange which has been ignored in the past. The consideration of exchange coupling ensures deeper understanding of the magnetization reversal of magnetic grains.

Based on the work presented in the thesis, one can hypothesis that the presence of a core/shell in the grains might pose a fundamental limit on the diameter that could be achieved in future. To reduce the effect of grain boundaries, a refinement of the fabrication process would be necessary or the inclusion of certain doping materials or different embedding matrices than SiO_2. Any fabrication error during the sputtering process of the grain directly affects the efficiency and areal density of the media that can be achieved. On the other hand the presence of the core/shell could also be used to an advantage to initiate magnetization reversal at low field values where the high anisotropy materials are used in the data storage layer. Overall the grain boundary effect is expected to play vital role in the future recording media like HAMR and BPMR to achieve higher areal densities 4Tb/in^2 and above.

References:

1. M. H. Kryder, E. C. Gage, T. W. McDaniel, W.A. Challener, R. E. Rottmayer, G. Ju, Y. T. Hsia, and M. F. Erde, IEEE Trans. Magn. **96**, 1810 (2008).
2. J. G. Zhu, X. Zhu, and Y. Tang, IEEE Trans. Magn. **44**, 1(2008).
3. B. D. Terris and T. Thomson, J. Phys. D: Appl. Phys. **38**, R199 (2005).
4. Y. Shiroishi, K. Fukuda, I. Tagawa, H. Iwasaki, S. Takenoiri, H. Tanaka, H. Mutoh, and N. Yoshikawa, IEEE Trans. Magn. **45**, 10 (2009).
5. T. Thomson, B. Lengsfield, H. Do, and B.D. Terris, J. Appl. Phys. **103**, 07F54 (2008).
6. E. E. Fullerton, J.S. Jiang, M. Grimsditch, C.H. Sowers and S.D. Badar Phys. Rev. B **58**, 12193 (1998).
7. R. Dittrich, T. Schrefl, D. Suess, W. Scholz, H. Forster, and J. Fidler, J. Magn. Magn. Mater. **250**, L12 (2002).
8. D. V. Berkov, J. Magn. Magn. Mater. **186**, 199 (1998).
9. W. Scholz, T. Schrefl, and J. Fidler, J. Magn. Magn. Mater. **233**, 296 (2001).
10. G. Hrkac, T. Schrefl, J. Dean, A. Goncharov, S. Bance, D. Suess, and J. Fidler, J. Appl. Phys. **105**, 053901 (2009).
11. E.C. Stoner, and E.P. Wohlfarth, Phil. Trans. R. Soc. Lond. A **240,** 599 (1948).
12. S. J. Lister, T. Thomson, J. Kohlbrecher, K. Takano, V. Venkataramana, S. J. Ray, M.P. Wismayer, M. A. de Vries, H. Do, Y. Ikeda, and S. L. Lee, Appl. Phys. Lett. **97**, 112503 (2010).
13. J. J. Miles, D. M. McKirdy, R. W. Chantrell, and R. Wood, IEEE Trans. Magn. **39**, 1876 (2003).

14. S. J. Lister, M. P. Wismayer, V. Venkataramana, M. A. De Vries, S.J. Ray, S.L. Lee, T. Thomson, J. Kohlberecher, H. D, Y. Lkeda, K. Takano, and C. Dewhurst," J. Appl. Phys. **106**, 063908 (2009)**.**